

DISSERTATION

WEAK GALERKIN FINITE ELEMENT METHODS FOR ELASTICITY AND COUPLED
FLOW PROBLEMS

Submitted by

Graham Bennett Harper

Department of Mathematics

In partial fulfillment of the requirements

For the Degree of Doctor of Philosophy

Colorado State University

Fort Collins, Colorado

Summer 2020

Doctoral Committee:

Advisor: Jianguo (James) Liu

Wolfgang Bangerth

Stephen Guzik

Simon Tavener

Yongcheng Zhou

Copyright by Graham Bennett Harper 2020

All Rights Reserved

ABSTRACT

WEAK GALERKIN FINITE ELEMENT METHODS FOR ELASTICITY AND COUPLED FLOW PROBLEMS

We present novel stabilizer-free weak Galerkin finite element methods for linear elasticity and coupled Stokes-Darcy flow with a comprehensive treatment of theoretical results and the numerical methods for each.

Weak Galerkin finite element methods take a discontinuous approximation space and bind degrees of freedom together through the discrete weak gradient, which involves solving a small symmetric positive-definite linear system on every element of the mesh. We introduce notation and analysis using a general framework that highlights properties that unify many existing weak Galerkin methods. This framework makes analysis for the methods much more straightforward.

The method for linear elasticity on quadrilateral and hexahedral meshes uses piecewise constant vectors to approximate the displacement on each cell, and it uses the Raviart-Thomas space for the discrete weak gradient. We use the Schur complement to simplify the solution of the global linear system and increase computational efficiency further. We prove first-order convergence in the L^2 norm, verify our analysis with numerical experiments, and compare to another weak Galerkin approach for this problem.

The method for coupled Stokes-Darcy flow uses an extensible multinumerics approach on quadrilateral meshes. The Darcy flow discretization uses a weak Galerkin finite element method with piecewise constants approximating pressure and the Arbogast-Correa space for the weak gradient. The Stokes domain discretization uses the classical Bernardi-Raugel pair. We prove first-order convergence in the energy norm and verify our analysis with numerical experiments.

All algorithms implemented in this dissertation are publicly available as part of James Liu's `DarcyLite` and `Darcy+` packages and as part of the `deal.II` library.

DEDICATION

I would like to dedicate this thesis to my fiancée Catherine, my parents Clint and Rochelle, my brother Brentan, my advisor and committee members, and my friends and coworkers for their unconditional love and support.

TABLE OF CONTENTS

	ABSTRACT	ii
	DEDICATION	iii
	LIST OF TABLES	vi
	LIST OF FIGURES	vii
Chapter 1	Introduction	1
1.1	Background	1
1.2	Existing Methods	3
1.2.1	Linear Elasticity	4
1.2.2	Stokes-Darcy Coupling	4
1.3	Contribution of This Thesis	5
Chapter 2	Weak Galerkin Finite Element Methods	7
2.1	Definitions and Notation	7
2.1.1	Sobolev Spaces and Meshes	7
2.1.2	Weak Functions and Discrete Weak Functions	8
2.1.3	Discrete Weak Differential Operators	9
2.1.4	A WG Finite Element Scheme for a General Elliptic Problem	13
2.2	Properties for WGFEMs	14
2.3	Choices for Discrete Weak Gradient Space	19
2.3.1	The Raviart-Thomas Space on Quadrilaterals and Hexahedra	19
2.3.2	The Arbogast-Correa Space on Quadrilaterals	21
2.4	Software Implementation	23
2.5	Assumptions for Mesh Quality	24
Chapter 3	Linear Elasticity	26
3.1	Introduction	26
3.2	Weak Galerkin Finite Element Scheme	31
3.3	A Priori Error Analysis	32
3.4	Implementation	42
3.4.1	Calculation of Numerical Stress on a Quadrilateral	42
3.4.2	Calculation of Numerical Stress on a Hexahedron	44
3.4.3	Block Diagonal Schur Complement	46
3.5	A Related Method: $WG(P_1^2, P_{rm}; P_0^{2 \times 2}, P_0)$ With Stabilization	47
3.6	Numerical Results	48
3.7	Summary	57
Chapter 4	Stokes-Darcy Coupling	58
4.1	Introduction and Notation	58
4.2	Dimensional Analysis	60
4.3	Weak Formulation	61

4.4	The Bernardi-Raugel Space on Quadrilateral Meshes	64
4.4.1	Properties of the (BR_1, Q_0) Element Pair for Stokes Flow	66
4.4.2	Implementation Details	67
4.5	A Priori Error Analysis	69
4.5.1	Properties of Operators and Subspaces	69
4.5.2	Existence and Uniqueness	70
4.5.3	Error Equations	71
4.5.4	Error Estimation	75
4.6	Numerical Results	79
4.7	Summary	83
Chapter 5	Conclusion	85
5.1	Locking-Free WGFEMs for Linear Elasticity	85
5.2	Efficient Quadrilateral Solver for Stokes-Darcy Coupling	85
5.3	Extensions and Future Work	86
Bibliography	88

LIST OF TABLES

3.1	Example 3.1 Case I ($\lambda = 1.6644 \times 10^2$): $\text{WG}(Q_0^2, Q_0^2; RT_{[0]}, Q_0)$ on rectangular meshes	49
3.2	Example 3.1 Case II ($\lambda = 1.667 \times 10^8$): $\text{WG}(Q_0^2, Q_0^2; RT_{[0]}, Q_0)$ on rectangular meshes	50
3.3	Example 3.2 Case I ($\nu = 0.3$): Lowest-order WG on uniform rectangular meshes . . .	51
3.4	Example 3.2 Case II ($\nu = 0.49999$): Lowest-order WG on graded rectangular meshes .	52
3.5	Example 3.3: Results of $\text{WG}(Q_0^2, Q_0^2; RT_{[0]}^2, Q_0)$ on rectangular meshes and asymptotically parallelogram trapezoidal meshes adopted from [1]	53
3.6	Example 3.4: Results of two WG methods on rectangular meshes	54
3.7	Example 3.5: Lowest-order WG solver on hexahedral meshes: Single-matrix approach	54
3.8	Example 3.5: Lowest-order WG on hexahedral meshes: Schur-complement approach .	55
4.1	Example 4.1: Errors and convergence rates	82

LIST OF FIGURES

2.1	Degrees of freedom for some choices of $\text{WG}(Q_{k_1}, Q_{k_2})$	9
2.2	Commuting diagram for $\text{WG}(P_{k_1}, P_{k_2}; W_{\text{grad}})$	16
3.1	Some meshes used in numerical experiments: <i>Left</i> : An initial graded mesh used in Example 3.2 Case II; <i>Right</i> : An initial trapezoidal mesh used in Example 3.3 (see [1] also).	49
3.2	Example 3.2 Case I ($\nu = 0.3$): Low-regularity captured by the lowest-order WG method on rectangular meshes	52
3.3	Example 3.6: A nearly incompressible block under compression. <i>Left</i> : An illustration for the problem; <i>Right</i> : A profile of the vertical displacement (z -component) obtained from using $\text{WG}(Q_0^3, Q_0^3; RT_{[0]}^3, Q_0)$ with $h = 1/8$	56
3.4	Example 3.6: $\text{WG}(Q_0^3, Q_0^3; RT_{[0]}^3, Q_0)$ applied with $h = 1/8$. <i>Left</i> : Profile of elementwise normal stress σ_{zz} ; <i>Right</i> : Elementwise dilation and deformation magnified 100 times. Plots were produced using <code>visIt</code> [2]. Note the positive and negative scales are not equal.	56
4.1	An example of the Stokes-Darcy configuration for $d = 2$	58
4.2	Four edge-based bubble functions used in the BR_1 space.	65
4.3	Degrees of freedom for the coupled $\text{WG}(Q_0, Q_0; AC_0)$ (light green), BR_1 (blue), Q_0 (dark red) method for Stokes-Darcy flow.	67
4.4	Example 4.2: Numerical velocity and pressure obtained from using $\text{CG}(BR_1, Q_0) + \text{WG}(P_0, P_0; AC_0)$ on a rectangular mesh with $h = 1/20$. (Velocity is plotted at element centers and the magnitude is doubled for better visual effect.)	83

Chapter 1

Introduction

1.1 Background

Many physical problems are expensive or difficult to simulate multiple times. For those reasons we often rely on mathematical models of physical phenomena as a cheap surrogate for experimentation. When appropriate and possible we desire models that satisfy properties such as conservation of mass, force, and energy. For our purposes, these mathematical models are transformed from partial differential equations (PDEs) into variational models and then into finite element schemes which may be solved on a computer.

Variational problems are defined on the Sobolev spaces; however, these spaces are infinite-dimensional, and therefore pose difficulties for numerical computations. Instead, finite element methods (FEMs) rely on finite-dimensional discretizations of these infinite-dimensional spaces in order to develop computationally feasible algorithms. These discretizations may be continuous, as with continuous Galerkin (CG) FEMs, or they may be discontinuous, as with discontinuous Galerkin (DG), hybridizable discontinuous Galerkin (HDG), and weak Galerkin (WG) FEMs. HDG and WG FEMs are DG methods that additionally place degrees of freedom on the mesh skeleton, but WGFEMs are unique in their use of a weak gradient.

As nearly ten years have passed since the first WG preprint was posted in April 2011 [3], WGFEMs have been used to tackle a broad spectrum of problems ranging from fluids [4–9], continuum mechanics [10–15], electricity and magnetism [16], interface problems [17], and even stock pricing [18]. This list is not complete, but highlights some of the more prominent works. Some other work has been done to analyze the computational advantages of WGFEMs. Mu, Wang, Wang, and Ye analyze the computational aspects of WGFEMs in [19] and describe how to write many of the discrete operators as matrices.

There are several reasons that WGFEMs gained popularity in the past decade. The main attraction of WGFEMs is the reconstruction of differential operators from discontinuous functions whose values live on a mesh and its skeleton. More importantly, these weak differential operators are consistent with classical differential operators for continuous functions. These reconstructed derivatives tie discontinuous degrees of freedom together and also provide desirable conservation properties for mass and flux in fluid problems [3, 4].

Some approaches for discretizations with WGFEMs include stabilizers to limit the jumps across the mesh skeleton [5, 12, 13, 20], but there are many stabilizer-free methods as well [4, 10, 17, 21, 22]. WGFEMs are flexible and use any degree $k \geq 0$ approximations, and they are even used on polygonal meshes [20, 22] and hybrid meshes [23]. Some work has also been done combining WGFEMs with other finite element discretizations [24], and Chapter 4 provides rigorous analysis for a combination of WG and mixed CG discretizations.

From a computational standpoint, there are many other benefits to using WGFEMs. Due to the local nature of these weak differential operators, much of the assembly of a FEM problem involves large amounts of computation on a small amount of data. This makes parallel computing and even computations on a graphics processing unit (GPU) an excellent fit. Other computational advantages include performing a Schur complement elimination on some degrees of freedom in the global linear system. Recently Liu and Wang provided a framework in [25] for performing this elimination before the linear system is even constructed.

One interesting test for numerical PDE solvers is simulating the behavior of linear elastic materials. Linear elasticity is a simplification of models for resolving forces inside of materials. More specifically, the linear elasticity equation describes the behavior of a material within the linear region of the stress-strain relationship. This arises most importantly in structural analysis, as plastic deformations to permanent structures tend to be undesirable, and it also appears in biomechanical and geophysical applications. The main interest in developing solvers for linear elasticity is developing a solver which is robust for nearly incompressible materials. Such a solver may also serve as a key building block for nonlinear elasticity.

Flow problems are another interesting target for FEMs because there are many different types of flow. Darcy flow is characterized by a fluid in a porous medium where flow is driven exclusively by pressure. Darcy flow arises in models for groundwater flow and models for oil reservoirs in petroleum engineering, and it also appears in many fluid filtration problems. The goal with Darcy flow is to construct a mass conservative FEM without paying for additional, expensive computations. For laminar incompressible flows, flow is modeled by the incompressible Stokes equations. The Stokes equations are a simplification of the Navier-Stokes equations when the Reynolds number is small, i.e., when viscous forces dominate inertial forces. These flows require careful choice of discretization due to the divergence condition. Discretizations that satisfy the Ladyzhenskaya–Babuška–Brezzi condition [26–28] are required for studying Stokes flows.

Stokes-Darcy coupling, as the name implies, involves the coupling of Stokes and Darcy flows along an interface. It often arises in applications where a fluid passes from a regime of laminar flow into a porous medium. Some applications include flow of fluid in a karst aquifer, filtration of fluid in a river through the riverbed, filtration of oil in a filter, filtration of blood through capillaries, or filtration of exhaust in a catalytic converter [29–34]. We consider Stokes-Darcy coupling with three conditions posed along the fluid interface: conservation of mass, balance of forces, and the Beavers-Joseph-Saffman boundary condition [35, 36]. The problem of developing FEMs for Stokes-Darcy flow is interesting because we now require two discretizations, and we would like each discretization to satisfy their respective desirable properties. However, naively combining two independent discretizations does not guarantee the pair converges, so there is a lot of recent literature focusing on developing compatible discretizations for this [37–42].

1.2 Existing Methods

There are many existing methods for simulating the behavior of elastic materials and fluids coupled on an interface. This section will provide an overview of some relevant, but certainly not all existing methods that have been used to tackle these problems.

1.2.1 Linear Elasticity

The development of FEMs for linear elasticity has been studied for at least six decades [43,44], and particular emphasis has been placed on locking-free FEMs due to their value for problems involving nearly incompressible materials. We will take a closer look at some more recent and relevant FEMs for linear elasticity.

One method for the linear elasticity equation on polygonal meshes was developed in [20]. It develops WGFEMs using vector-valued polynomials where each component has degree $k \geq 1$ on element interiors and degree $k - 1$ on the mesh skeleton. It uses a stabilizer, but order $k + 1$ convergence is proven for displacement and order k convergence is obtained for stress and dilation. We provide a comparison against this method in Chapter 3.

Other recent work for locking-free FEMs is found in [45, 46], where the authors consider nonconforming mixed finite element methods (MFEMs) on rectangular meshes in two and three dimensions. Their method is based on the Hellinger-Reissner variational principle for the pure traction problem and it converges with optimal order.

More efficient methods for this may be found in [47] where the authors present a nonconforming dimension-independent method on rectangular meshes. This approach uses the least degrees of freedom per element in one, two, and three dimensions. Locking-free nonconforming finite elements for linear elasticity on general quadrilaterals can be found in [48, 49], and mixed finite elements on quadrilaterals can be found in [50] and references therein.

1.2.2 Stokes-Darcy Coupling

One of the most popular methods for solving coupled Stokes-Darcy flow recently has been a domain decomposition FEM approach with Lagrange multipliers, which are also referred to as mortar elements [51–53]. These methods tend to proliferate degrees of freedom as they require mortar elements that exist only on the interface in addition to the degrees of freedom on the Stokes and Darcy meshes along the interface, but allow for the flexibility of a meshes on each domain that do not match along the interface.

There is an existing approach for steady-state Stokes-Darcy coupling in [54] that uses WGFEMs on both the Stokes domain and the Darcy domain. They use a stabilized approach on a polygonal mesh with degree k polynomials on element interiors, degree $k - 1$ polynomials on element boundaries, and 2×2 matrices of degree k polynomials for the discrete weak gradient.

The authors in [55] also apply stabilized WGFEMs to steady-state Stokes-Darcy coupling. They use arbitrary polynomial order for all polynomial spaces on a polygonal mesh and then determine suitable choices for the spaces based on their analysis. Neither of the aforementioned WGFEMs approaches utilize an $H(\text{div})$ conforming space for the velocity.

Some other approaches develop conforming mixed finite element methods [51, 56, 57], stabilized mixed approaches [42], virtual elements [58], iterative coupling schemes [52, 59], and an HDG Stokes with mixed Darcy discretization [60].

1.3 Contribution of This Thesis

This dissertation presents lowest-order WGFEMs for linear elasticity and a multinumerics approach involving WGFEMs and MFEMs for Stokes-Darcy coupling. These finite element methods are computationally inexpensive and stabilizer-free.

Besides the definitions and notation in Chapter 2, we also prove lemmas which are not stated in generality in literature. These lemmas describe properties of the projection operators for WGFEMs, tools for expanding terms in analysis for the lowest-order WGFEMs, and properties of the discrete weak gradient. These are commonly reproven in each paper for WGFEMs but we prove them once and in more generality.

In Chapter 3 we perform analysis for the lowest-order WGFEM for linear elasticity on rectangular and brick meshes in the primal formulation following our work in [10]. This method solves for the displacement field using piecewise constants on each element and on the mesh skeleton. The approach is stabilizer-free and obtains first-order convergence in displacement, stress, and dilation. We perform Schur complement reduction to further reduce the size of the global linear system and increase computational benefit, as shown in the numerical examples. Additionally,

we show numerically that this method may capture solutions for low regularity problems and it extends to the more general quadrilateral and hexahedral meshes.

In Chapter 4 we develop an efficient FEM for steady-state Stokes-Darcy coupling. For Stokes flow we use the classical Bernardi-Raugel pair (BR_1, Q_0) [61] for the mixed problem and for Darcy flow we use the $WG(P_0, P_0; AC_0)$ space [62] in the primal formulation. This approach utilizes the novel Arbogast-Correa space for quadrilaterals [63]. One advantage of this method is that we do not use mortar elements as others do in [51–53, 64]; however, the WG degrees of freedom on the mesh skeleton behave similarly to mortar elements and we use some techniques from the analysis of mortar methods to analyze this method. We present rigorous analysis for the method and show first-order convergence in the energy norm for Stokes velocity and Darcy pressure and first-order convergence in the L^2 norm for Stokes pressure. A numerical example is also provided to suggest that all variables converge with optimal order with respect to the L^2 norm, although it is not proven.

Chapter 5 concludes the dissertation and provides insight for further extensions. It discusses higher-order and higher dimensional extensions of these methods as well as applications to other multiphysics problems. Further implementations and improvements in software are also discussed.

Chapter 2

Weak Galerkin Finite Element Methods

WGFEMs were first introduced by Wang and Ye [3] for solving the second-order elliptic PDE on an open polygonal (polyhedral when $d = 3$) domain Ω

$$\begin{aligned} -\nabla \cdot (a\nabla u) + \nabla \cdot (bu) + cu &= f \quad \text{in } \Omega, \\ u &= g \quad \text{on } \partial\Omega. \end{aligned} \tag{2.1}$$

In order to discuss how to write WGFEMs for this problem, we must first introduce some definitions and notation in Section 2.1.

2.1 Definitions and Notation

2.1.1 Sobolev Spaces and Meshes

We adopt the following notation for the remainder of this dissertation. For an open polygonal (polyhedral when $d = 3$) domain $\Omega \subset \mathbb{R}^d$ ($d = 2, 3$), let $W^{k,p}(\Omega)$ (also sometimes denoted by $W_p^k(\Omega)$) be the space of functions on Ω whose weak derivatives up to order k are in $L^p(\Omega)$. In the case where $p = 2$, we will write $H^k(\Omega) := W^{k,2}(\Omega)$. We use $L^2(\Omega)$, $H^1(\Omega)$ as notation for scalar-valued functions and $\mathbf{L}^2(\Omega)$, $\mathbf{H}^1(\Omega)$ for functions where each component is in $L^2(\Omega)$ or $H^1(\Omega)$, respectively. A function lies in $L^p(\Omega)$ if its norm is finite

$$\|f\|_{L^p(\Omega)} := \left(\int_{\Omega} f^p d\mu \right)^{1/p}, \tag{2.2}$$

where μ is the Lebesgue measure on Ω . All integrals in this dissertation will be taken with respect to a Lebesgue measure. The norm on $H^1(\Omega)$ is defined similarly, by

$$\|f\|_{H^1(\Omega)} := \left(\|f\|_{L^2(\Omega)}^2 + \sum_{|\alpha|=1} \int_{\Omega} (\partial^\alpha f)^2 d\mu \right)^{1/2}, \tag{2.3}$$

where α is a multi-index that accounts for all spatial partial derivatives of f , and similarly we say $f \in H^1(\Omega)$ if $\|f\|_{H^1(\Omega)} < \infty$. For vector-valued functions, we define these norms similarly, except instead acting on the l^2 norm of the vector.

On $\Omega \subset \mathbb{R}^d$, we refer to a polygonal (polyhedral when $d = 3$) mesh \mathcal{E}_h as a set of subdomains $\mathcal{E}_h = \{E_i : i = 1, \dots, n\}$ which satisfy the conditions given in [65] in addition to two other conditions:

1. $\text{int}(E_i) \cap \text{int}(E_j) = \emptyset$ if $i \neq j$.
2. $\bigcup_{i=1}^n E_i = \bar{\Omega}$.
3. E_i is a nondegenerate convex polygon (polyhedron when $d = 3$) for $i = 1, \dots, n$.
4. $E_i \cap E_j$, is an entire vertex, edge, or face of E_i and of E_j when it is not empty and $i \neq j$.

We refer to the subdomains E_i as elements of the mesh, and we remark that part 4. of this definition excludes the possibility of hanging vertices in the mesh. A triangular mesh is a polygonal mesh consisting of only triangles, and similarly for quadrilateral, tetrahedral, and hexahedral meshes. We will refer to the mesh skeleton as the set of edges (faces when $d = 3$) of the elements of the mesh. The size of the mesh, h , is defined as roughly the largest element diameter of the mesh

$$h := \frac{1}{\sqrt{d}} \max\{\text{diam}(E) : E \in \mathcal{E}_h\}. \quad (2.4)$$

We include the factor of $d^{-1/2}$ for ease of presentation for results later, but we remark that it does not change any of the analysis.

2.1.2 Weak Functions and Discrete Weak Functions

A *weak function* on an element $E \in \mathcal{E}_h$ is defined by Wang and Ye in [3] as a function whose values on the interior and boundary of the element may disagree. More precisely, the space of weak functions, $W(E)$, is defined by

$$W(E) := \{v = \{v^\circ, v^\partial\} : v^\circ \in L^2(E), v^\partial|_\gamma \in H^{1/2}(\gamma), \gamma \text{ is an edge of } E\}. \quad (2.5)$$

Here $H^{1/2}(\gamma)$ is the trace space for $L^2(E)$ functions. If E is a three-dimensional domain, then γ is instead a face of E . A dimension-independent approach is to say every v^∂ is defined on the mesh skeleton. From a computational standpoint, this isn't very useful since $W(E)$ is infinite-dimensional; however, there is a discrete analogue of $W(E)$ that is defined by replacing $L^2(E)$ with the space of polynomials of d variables of total degree at most $k_1 \geq 0$, $P_{k_1}(E)$, and replacing $H^{1/2}(\gamma)$ with the a similar space $P_{k_2}(\gamma)$ ($k_2 \geq 0$) on each face. These polynomials need not be continuous from face to face. The weak Galerkin discrete space $\text{WG}(P_{k_1}, P_{k_2})$ is the space of *discrete weak functions* defined on \mathcal{E}_h by

$$\text{WG}(P_{k_1}, P_{k_2}) := \{v_h = \{v_h^\circ, v_h^\partial\} : v_h^\circ|_E \in P_{k_1}(E), v_h^\partial|_\gamma \in P_{k_2}(\gamma), \gamma \text{ is a face of } E \in \mathcal{E}_h\}. \quad (2.6)$$

On quadrilaterals and hexahedra we will use the space $\text{WG}(Q_{k_1}, Q_{k_2})$ for polynomials whose degree in each variable does not exceed k_1 on element interiors and does not exceed k_2 on the mesh skeleton. For example, on the reference element $\hat{E} = [0, 1]^2$, $f(\hat{x}, \hat{y}) = 1 + \hat{x}\hat{y} + \hat{x}^2\hat{y}$ satisfies $f \notin P_2(\hat{E})$, $f \in P_3(\hat{E})$, and $f \in Q_2(\hat{E})$. Figure 2.1 shows how local degrees of freedom are distributed on a general quadrilateral for some choices of k_1, k_2 .

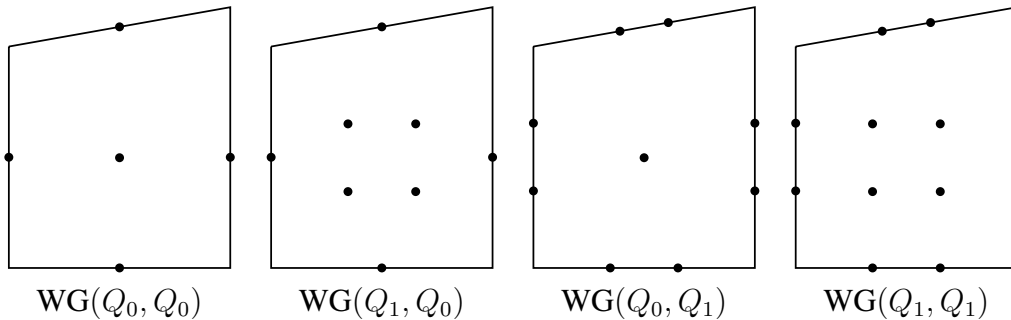


Figure 2.1: Degrees of freedom for some choices of $\text{WG}(Q_{k_1}, Q_{k_2})$

2.1.3 Discrete Weak Differential Operators

We may now define the *discrete weak gradient* by combining the degrees of freedom on an element and its boundary through integration by parts. Let $W_{\text{grad}}(E) = \text{span}\{\mathbf{w}_1, \mathbf{w}_2, \dots, \mathbf{w}_{n_g}\}$

be an n_g -dimensional subspace of $\mathbf{L}^2(E)$ for $E \in \mathcal{E}_h$. We may also refer to this local space by W_{grad} for ease of notation, but since there is no concept of continuity across elements in the definition of W_{grad} it behaves like a broken finite element space across all of \mathcal{E}_h . Then the discrete weak gradient, denoted by $\nabla_w : \mathbf{WG}(P_{k_1}, P_{k_2}) \rightarrow W_{\text{grad}}(E)$, is a local map defined by its action and by utilizing both v_h° and v_h^∂ so that

$$\int_E \nabla_w v_h \cdot \mathbf{q} \, dA = - \int_E v_h^\circ \nabla \cdot \mathbf{q} \, dA + \int_{\partial E} v_h^\partial \mathbf{q} \cdot \mathbf{n} \, ds, \quad \forall \mathbf{q} \in W_{\text{grad}}. \quad (2.7)$$

The notation \mathbf{n} will always refer to the unit outward normal when it is unambiguous, and we use bold lower-case characters such as \mathbf{q} to represent vector-valued functions.

It's not difficult to see from Equation (2.7) that if the values for v_h° and v_h^∂ are continuous across elements and their faces then v_h and its discrete weak gradient behave like a continuous function and the L^2 projection of its gradient into W_{grad} . The definition of the discrete weak gradient is a statement about solving linear systems on an element E since $\nabla_w v_h \in W_{\text{grad}}$ implies it is a linear combination $\nabla_w v_h = \sum_i c_i \mathbf{w}_i$. Plugging this in and writing the $L^2(E)$ inner product on the left-hand side using inner product notation yields

$$\left(\sum_i c_i \mathbf{w}_i, \mathbf{w}_j \right)_E = - \int_E v_h^\circ \nabla \cdot \mathbf{w}_j \, dA + \int_{\partial E} v_h^\partial \mathbf{w}_j \cdot \mathbf{n} \, ds, \quad \forall j = 1, \dots, n_g. \quad (2.8)$$

This equation may be expanded additionally into a linear system that now involves the mass matrix of the space W_{grad} . Since the mass matrix is also a Gram matrix with respect to the $L^2(E)$ inner product, let $G_{W_{\text{grad}}}$ be the $n_g \times n_g$ Gram matrix of W_{grad} , defined by

$$G_{W_{\text{grad}}} := \left[\int_E \mathbf{w}_i \cdot \mathbf{w}_j \, dA \right]_{i,j=1}^{n_g}.$$

Then Equation (2.7) may be rewritten using this matrix as

$$G_{W_{\text{grad}}} \begin{bmatrix} c_1 \\ c_2 \\ \vdots \\ c_{n_g} \end{bmatrix} = \begin{bmatrix} - \int_E v_h^\circ \nabla \cdot \mathbf{w}_1 dA + \int_{\partial E} v_h^\partial \mathbf{w}_1 \cdot \mathbf{n} ds \\ - \int_E v_h^\circ \nabla \cdot \mathbf{w}_2 dA + \int_{\partial E} v_h^\partial \mathbf{w}_2 \cdot \mathbf{n} ds \\ \vdots \\ - \int_E v_h^\circ \nabla \cdot \mathbf{w}_{n_g} dA + \int_{\partial E} v_h^\partial \mathbf{w}_{n_g} \cdot \mathbf{n} ds \end{bmatrix}. \quad (2.9)$$

Horn & Johnson show that a Gram matrix of an inner product space is always symmetric positive-semidefinite (SPSD) and is further symmetric positive-definite (SPD) if the elements are linearly independent [66]. In particular, since this Gram matrix uses basis functions from W_{grad} , the Gram matrix for discrete weak gradient computations is necessarily SPD. Computationally, solving this system becomes more complex as $n_g = \dim(W_{\text{grad}})$ increases, so it is important to develop numerically efficient ways to compute this. A conjugate gradient solver may be unnecessary for solving an SPD system for each element in the mesh, but carefully choosing the basis for W_{grad} may improve the computation time. Section 2.3 discusses some of those choices in more detail. From a computational standpoint, computing the weak Gradient of a discrete weak function may be done independently from other elements in the mesh and is therefore an easy target for exploiting parallelism in software. It requires little information other than the cell's vertices and orientation, a numerical quadrature, and the shape function information. For the numerical quadrature, we use the lowest-order Gaussian quadrature that still provides an exact integral on an affine mesh.

The discrete weak gradient is also defined for vector-valued functions, but it then acts as a map $\nabla_w : \text{WG}(P_{k_1}^d, P_{k_2}^d) \rightarrow W_{\text{grad}}^d$. All of the remarks made above hold for this vector-valued version, but now the gradient is computed componentwise, yielding a tensor-product structure in the Gram matrix computations. When referring to WG FEMs, we will also use the notation $\text{WG}(P_{k_1}, P_{k_2}; W_{\text{grad}})$ if there is a weak gradient structure. Patching together these spaces yields the global finite element space, which is typically denoted by V_h .

The *discrete weak divergence*, denoted by ∇_{w^\cdot} , of a discrete weak function is defined similarly to the discrete weak gradient. The discrete weak divergence is defined on vector-valued polynomials $\nabla_{w^\cdot} : \text{WG}(P_{k_1}^d, P_{k_2}^d) \rightarrow W_{\text{div}}$, but similarly to Equation (2.7), it is defined by its action,

$$(\nabla_w \cdot \mathbf{v}_h, q)_E = - \int_E \mathbf{v}_h^\circ \cdot \nabla q \, dA + \int_{\partial E} (\mathbf{v}_h^\partial \cdot \mathbf{n}) q \, ds \quad \forall q \in W_{\text{div}}. \quad (2.10)$$

As with (2.9), this requires solving a linear system which depends on $n_d := \dim(W_{\text{div}})$. The linear system is

$$G_{W_{\text{div}}} \begin{bmatrix} c_1 \\ c_2 \\ \vdots \\ c_{n_d} \end{bmatrix} = \begin{bmatrix} - \int_E \mathbf{v}_h^\circ \cdot \nabla q_1 \, dA + \int_{\partial E} (\mathbf{v}_h^\partial \cdot \mathbf{n}) q_1 \, ds \\ - \int_E \mathbf{v}_h^\circ \cdot \nabla q_2 \, dA + \int_{\partial E} (\mathbf{v}_h^\partial \cdot \mathbf{n}) q_2 \, ds \\ \vdots \\ - \int_E \mathbf{v}_h^\circ \cdot \nabla q_{n_d} \, dA + \int_{\partial E} (\mathbf{v}_h^\partial \cdot \mathbf{n}) q_{n_d} \, ds \end{bmatrix}. \quad (2.11)$$

There is a discrete weak curl as well; however, the work in this dissertation does not rely on a curl operator, so we will omit further discussion and instead refer the interested reader to [16] for more information.

This treatment is different for the discrete weak strain, denoted by ε_w . Instead, it is simply defined in terms of the discrete weak gradients

$$\varepsilon_w(\mathbf{v}_h) = (\nabla_w \mathbf{v}_h + (\nabla_w \mathbf{v}_h)^T)/2. \quad (2.12)$$

Therefore, the discrete weak strain does not live in W_{grad} , but rather a new space spanned by the averages of each basis function with its transpose. This makes computations involving the discrete weak strain slightly simpler because

$$\begin{aligned} \varepsilon_w(\mathbf{v}_h) &= \frac{1}{2} \left(\sum_{i=1}^{n_g} c_i W_i + \sum_{i=1}^{n_g} c_i W_i^T \right) \\ &= \sum_{i=1}^{n_g} c_i (W_i + W_i^T)/2. \end{aligned}$$

We will discuss this in more detail with the appropriate context in Chapter 3.

2.1.4 A WG Finite Element Scheme for a General Elliptic Problem

We now revisit the task of writing a WG finite element scheme for Equation (2.1). First, we test Equation (2.1) by $v \in H_0^1(\Omega)$ to obtain

$$\int_{\Omega} (-\nabla \cdot (a\nabla u) + \nabla \cdot (bu) + cu)v \, dA = \int_{\Omega} f v \, dA, \quad \forall v \in H_0^1(\Omega),$$

where $H_0^1(\Omega)$ denotes functions that are compactly supported on $H^1(\Omega)$. Applying integration by parts, which is sometimes referred to as Green's first identity, to the divergence terms yields

$$\int_{\Omega} (a\nabla u \cdot \nabla v) - bu \cdot \nabla v + cuv \, dA = \int_{\Omega} f v \, dA, \quad \forall v \in H_0^1(\Omega).$$

This yields the variational form of Equation (2.1), which we write with L^2 inner product notation as: Seek $u \in H_{g,D}^1(\Omega)$ so that

$$(a\nabla u, \nabla v)_{\Omega} - (bu, \nabla v)_{\Omega} + (cu, v)_{\Omega} = (f, v)_{\Omega}, \quad \forall v \in H_0^1(\Omega). \quad (2.13)$$

A WGFEM is now developed by taking a mesh \mathcal{E}_h of the domain Ω , setting the finite element space $V_h := \text{WG}(P_{k_1}, P_{k_2}; W_{\text{grad}})$, and replacing the differential operators with their corresponding discrete weak differential operators. Let V_h^0 is the subspace of V_h whose boundary components are 0 on the Dirichlet boundary, and let Q_h^{∂} be the L^2 projection onto P_{k_2} of the mesh skeleton. The finite element scheme for problem is: Seek $u_h \in V_h$ satisfying $u_h|_{\partial\Omega} = Q_h^{\partial}g$ and

$$\sum_{E \in \mathcal{E}_h} ((a\nabla_w u_h, \nabla_w v)_E - (bu_h, \nabla_w v)_E + (cu_h, v)_E) = \sum_{E \in \mathcal{E}_h} (f, v)_E, \quad \forall v \in V_h^0. \quad (2.14)$$

For more details on the analysis for this problem, we refer the interested reader to continue reading [3]. In the next section we more carefully examine the discrete weak differential operators and projection operators to give an overview of tools for analysis of WGFEMs with an emphasis on the lowest-order approximations.

2.2 Properties for WGFEMs

This section contains lemmas for WGFEMs that will be referenced in later sections. These are re-proven often in literature for each specific problem, but this section aims to establish them in a more general form so they may be simply applied to each problem. First we introduce notation specific to reading these lemmas.

For scalar-valued function spaces, let $V_h := \text{WG}(P_{k_1}, P_{k_2}; W_{\text{grad}})$ be any weak Galerkin finite element space with no assumption on the structure of W_{grad} . Let $Q_h = \{Q_h^\circ, Q_h^\partial\}$, be the local L^2 projection into the finite element space consisting of $Q_h^\circ : L^2(E) \rightarrow V_h$ and $Q_h^\partial : L^2(\gamma) \rightarrow V_h$, where γ is a face in the mesh. Let $\mathbf{Q}_h : L^2(E)^d \rightarrow W_{\text{grad}}$ be the local L^2 projection associated with the gradient space. These projections satisfy

$$\int_E f v^\circ dA = \int_E (Q_h^\circ f) v^\circ dA, \quad \forall f \in L^2(E), v^\circ \in P_{k_1}(E), \quad (2.15)$$

$$\int_\gamma g v^\partial ds = \int_\gamma (Q_h^\partial g) v^\partial ds, \quad \forall g \in L^2(\gamma), v^\partial \in P_{k_2}(\gamma), \quad (2.16)$$

$$\int_E \mathbf{f} \cdot \mathbf{v} dA = \int_E (\mathbf{Q}_h \mathbf{f}) \cdot \mathbf{v} dA, \quad \forall \mathbf{f} \in L^2(E)^d, \mathbf{v} \in W_{\text{grad}}. \quad (2.17)$$

We remark that if we choose to apply both Q_h° and Q_h^∂ to the same function, we need enough regularity that the function's trace to element boundaries is still in $L^2(\gamma)$. This is possible when the function lives in $H^1(E)$, and is also possible when the function lives in $H^{1/2+\epsilon}(E)$ for $\epsilon > 0$.

When a global interpolation into W_{grad} is defined, we will denote it by $\mathbf{\Pi}_h$. For vector-valued function spaces, let $\mathbf{V}_h := \text{WG}(P_{k_1}^d, P_{k_2}^d; W_{\text{grad}}, W_{\text{div}})$ be any weak Galerkin finite element space of vector-valued functions with d components and with no assumptions on W_{grad} or W_{div} . Let $Q_h : L^2(E) \rightarrow W_{\text{div}}$, $\mathbf{Q}_h = \{\mathbf{Q}_h^\circ, \mathbf{Q}_h^\partial\} : L^2(E)^d \rightarrow \mathbf{V}_h$, and $\mathbb{Q}_h : L^2(E)^{d \times d}$ be the local L^2 projections associated with the finite element space.

Lemma 2.1. (Commuting identities) [4, 67] For $E \in \mathcal{E}_h$, the following hold in the $L^2(E)$ sense:

1. For $f \in H^1(E)$, we have $\nabla_w(Q_h f) = \mathbf{Q}_h(\nabla f)$;
2. For $\mathbf{f} \in H^1(E)^d$, we have $\nabla_w(\mathbf{Q}_h \mathbf{f}) = \mathbb{Q}_h(\nabla \mathbf{f})$;

3. For $\mathbf{f} \in H^1(E)^d$, we have $\nabla_w \cdot (\mathbf{Q}_h \mathbf{f}) = Q_h(\nabla \cdot \mathbf{f})$.

Proof. 1. Let $\mathbf{w} \in W_{\text{grad}}$. Then

$$\begin{aligned}
\int_E \mathbf{Q}_h(\nabla f) \cdot \mathbf{w} &= \int_E \nabla f \cdot \mathbf{w} \\
&= \int_{\partial E} f(\mathbf{w} \cdot \mathbf{n}) - \int_E f(\nabla \cdot \mathbf{w}) \\
&= \int_{\partial E} Q_h^\partial f(\mathbf{w} \cdot \mathbf{n}) - \int_E Q_h^\circ f(\nabla \cdot \mathbf{w}) \\
&= \int_E \nabla_w f \cdot \mathbf{w}
\end{aligned}$$

2. Let $W \in W_{\text{grad}}$. Then

$$\begin{aligned}
\int_E \mathbf{Q}_h(\nabla \mathbf{f}) : W &= \int_E \nabla \mathbf{f} : W \\
&= \int_{\partial E} \mathbf{f} \cdot (W \mathbf{n}) - \int_E \mathbf{f} \cdot (\nabla \cdot W) \\
&= \int_{\partial E} \mathbf{Q}_h^\partial \mathbf{f}(W \mathbf{n}) - \int_E \mathbf{Q}_h^\circ \mathbf{f}(\nabla \cdot W) \\
&= \int_E \nabla_w \mathbf{f} : W
\end{aligned}$$

3. Let $q \in W_{\text{div}}$. Then

$$\begin{aligned}
\int_E Q_h(\nabla \cdot \mathbf{f})q &= \int_E (\nabla \cdot \mathbf{f})q \\
&= \int_{\partial E} (\mathbf{f} \cdot \mathbf{n})q - \int_E \mathbf{f} \cdot \nabla q \\
&= \int_{\partial E} (\mathbf{Q}_h^\partial \mathbf{f} \cdot \mathbf{n})q - \int_E (\mathbf{Q}_h^\circ \mathbf{f}) \cdot \nabla q \\
&= \int_E (\nabla_w \cdot \mathbf{f})q
\end{aligned}$$

□

Often in the literature this lemma is shown alongside a commuting diagram for scalar-valued functions in $H^1(E)$, as shown in Figure 2.2.

$$\begin{array}{ccc}
H^1(E) & \xrightarrow{\nabla} & L^2(E) \\
\downarrow Q_h & & \downarrow \mathbf{Q}_h \\
WG(P_{k_1}, P_{k_2}) & \xrightarrow{\nabla_w} & V_h
\end{array}$$

Figure 2.2: Commuting diagram for $WG(P_{k_1}, P_{k_2}; W_{\text{grad}})$

Lemma 2.2. (Conversion to trace) Let $E \in \mathcal{E}_h$ and $k_1 = k_2 = 0$ for the lowest-order weak Galerkin finite element space.

1. For $v \in V_h$, $\mathbf{w} \in W_{\text{grad}}$, there holds $(\mathbf{w}, \nabla_w v)_E = (\mathbf{w} \cdot \mathbf{n}, v^\partial - v^\circ)_{\partial E}$;
2. For $\mathbf{v} \in \mathbf{V}_h$, $W \in W_{\text{grad}}$, there holds $(W, \nabla_w \mathbf{v})_E = (W \mathbf{n}, \mathbf{v}^\partial - \mathbf{v}^\circ)_{\partial E}$;
3. For $\mathbf{v} \in \mathbf{V}_h$, $w \in W_{\text{div}}$, there holds $(w, \nabla_w \cdot \mathbf{v})_E = (w \mathbf{n}, \mathbf{v}^\partial - \mathbf{v}^\circ)_{\partial E}$.

Here the value of v° on ∂E is taken as the extension of v° to the boundary of the element. In some cases it is written as $\text{tr}(v^\circ)$ to be more precise. This mild abuse of notation will appear frequently throughout this dissertation.

Proof. Each of the proofs follows from applying the definition of weak gradient or weak divergence and then a divergence theorem.

1. Let $E \in \mathcal{E}_h$, $v \in V_h^{(0)}$, and $\mathbf{w} \in W_{\text{grad}}$. Then

$$\begin{aligned}
(\mathbf{w}, \nabla_w v)_E &= -(\nabla \cdot \mathbf{w}, v^\circ)_E + (\mathbf{w} \cdot \mathbf{n}, v^\partial)_{\partial E} \\
&= -(\mathbf{w} \cdot \mathbf{n}, v^\circ)_{\partial E} + (\mathbf{w} \cdot \mathbf{n}, v^\partial)_{\partial E} \\
&= (\mathbf{w} \cdot \mathbf{n}, v^\partial - v^\circ)_{\partial E}.
\end{aligned}$$

2. Let $E \in \mathcal{E}_h$, $\mathbf{v} \in \mathbf{V}_h^{(0)}$, and $W \in W_{\text{grad}}$. Then

$$\begin{aligned}
(W, \nabla_w \mathbf{v})_E &= -(\nabla \cdot W, \mathbf{v}^\circ)_E + (W \mathbf{n}, \mathbf{v}^\partial)_{\partial E} \\
&= -(W \mathbf{n}, \mathbf{v}^\circ)_{\partial E} + (W \mathbf{n}, \mathbf{v}^\partial)_{\partial E} \\
&= (W \mathbf{n}, \mathbf{v}^\partial - \mathbf{v}^\circ)_{\partial E}.
\end{aligned}$$

3. Let $E \in \mathcal{E}_h$, $\mathbf{v} \in V_h$, and $w \in W_{\text{div}}$. Then

$$\begin{aligned}
(w, \nabla_w \cdot \mathbf{v})_E &= -(\nabla w, \mathbf{v}^\circ)_E + (w \mathbf{n}, \mathbf{v}^\partial)_{\partial E} \\
&= -(w \mathbf{n}, \mathbf{v}^\circ)_{\partial E} + (w \mathbf{n}, \mathbf{v}^\partial)_{\partial E} \\
&= (w \mathbf{n}, \mathbf{v}^\partial - \mathbf{v}^\circ)_{\partial E}.
\end{aligned}$$

□

Lemma 2.2 reflects one of the nice properties of the lowest-order weak Galerkin finite element methods. In the L^2 sense on an element, the weak gradient acts as a sort of jump measurement from one element to the next. This is also one of the many ways to show that the L^2 norm of the weak gradient induces a norm on a weak Galerkin finite element test space. When $k_1, k_2 > 0$, similar ideas may be used, but the details become more intricate.

Lemma 2.3. (Coercivity of weak gradient) Suppose that W_{grad} is a space that satisfies the following conditions:

1. For any $E \in \mathcal{E}_h$, $q_h \in V_h$, there exists $\mathbf{w} \in W_{\text{grad}}$ so that $\mathbf{w} \cdot \mathbf{n}|_{E^\partial} = q_h^\partial - q_h^\circ$.
2. For any $\mathbf{w} \in W_{\text{grad}}$, the trace bound $\|\mathbf{w}\|_E \lesssim h^{1/2} \|\mathbf{w} \cdot \mathbf{n}\|_{\partial E}$ holds.

Then for the lowest-order weak Galerkin space $k_1 = k_2 = 0$, there holds

$$h^{-1/2} \|q_h^\partial - q_h^\circ\|_{\partial E} \lesssim \|\nabla_w q_h\|_E, \quad \forall q_h \in V_h. \quad (2.18)$$

For convenience, we have introduced the notation $A \lesssim B$ to simplify an inequality $A \leq CB$ when $C > 0$ is a constant independent of h .

Proof. Choose $\mathbf{w} \in W_{\text{grad}}$ so that $\mathbf{w} \cdot \mathbf{n}|_{E\partial} = q_h^\partial - q_h^\circ$. Then the choice of \mathbf{w} , lemma 2.2, a Cauchy-Schwarz inequality, and the trace bound for W_{grad} , yield

$$\begin{aligned}
\|q_h^\partial - q_h^\circ\|_{\partial E}^2 &= \langle \mathbf{w} \cdot \mathbf{n}, q_h^\partial - q_h^\circ \rangle_{\partial E} \\
&= (\mathbf{w}, \nabla_w q_h)_E \\
&\leq \|\mathbf{w}\|_E \|\nabla_w q_h\|_E \\
&\lesssim h^{1/2} \|\mathbf{w} \cdot \mathbf{n}\|_{\partial E} \|\nabla_w q_h\|_{\partial E} \\
&= h^{1/2} \|q_h^\partial - q_h^\circ\|_{\partial E} \|\nabla_w q_h\|_{\partial E}.
\end{aligned}$$

Dividing by $h^{1/2} \|q_h^\partial - q_h^\circ\|_{\partial E}$ finishes the proof. \square

We remark that while the assumptions for this lemma appear strict, all finite element spaces with degrees of freedom defined in terms of bulk normal fluxes are applicable. This extends to vector-valued finite element spaces where the gradient of each component belongs to W_{grad} .

Lemma 2.4. (Norm property of weak gradient) Let V_h be the lowest-order weak Galerkin finite element space corresponding to $k_1 = k_2 = 0$. Let V_h^0 be subspace of V_h whose functions are zero on any subset of edges of a connected mesh \mathcal{E}_h . Suppose that W_{grad} satisfies the conditions stated in Lemma 2.3. Then

$$\|\nabla_w v\|_{L^2(\mathcal{E}_h)} := \left(\sum_{E \in \mathcal{E}_h} \|\nabla_w v\|_{L^2(E)}^2 \right)^{1/2} \quad (2.19)$$

is a norm on V_h^0 .

Proof. Checking the triangle equality and scalability by a constant are trivial. The only thing that remains is to show that $\|\nabla_w v\|_{L^2(\mathcal{E}_h)} = 0$ implies $v \equiv 0$. First, $\|\nabla_w v\|_{L^2(\mathcal{E}_h)} = 0$ implies $\|\nabla_w v\|_{L^2(E)} = 0 \forall E \in \mathcal{E}_h$. Since v is 0 on some edge in the mesh, consider a cell E adjacent to such an edge. Then by Lemma 2.3, it must be the jump on the entire cell is 0, so the interior value is 0. The value on the remaining edges of the element are also 0 by the same logic. Propagating this information through the connected mesh implies that every value must be 0, and therefore we conclude $v \equiv 0$. \square

We remark this also extends to vector-valued functions just as Lemma 2.3. To summarize, lowest-order WGFEMs equipped with a suitable choice of W_{grad} have a nice structure associated with them, but these properties are just a small number of applicable properties for WGFEMs since this dissertation focuses primarily on the lowest-order methods.

2.3 Choices for Discrete Weak Gradient Space

This section presents a discussion on finite element spaces that will be used for W_{grad} in later analysis, their Gram matrices, and how they relate to the lemmas presented in the previous section. In particular, we will focus on the lowest-order spaces so that we may match them with the lowest-order methods discussed in the lemmas in the previous section. Since these are local spaces, we will work with normalized coordinates $X = x - x_c$, $Y = y - y_c$, and $Z = z - z_c$, where (x_c, y_c) is the center of the element E when $d = 2$ and (x_c, y_c, z_c) is the center of the element when $d = 3$ [68]. The center is computed by taking the arithmetic average of the vertices of the element E .

2.3.1 The Raviart-Thomas Space on Quadrilaterals and Hexahedra

Some of the most popular finite element spaces are the Raviart-Thomas spaces for quadrilaterals and hexahedra, $RT_{[k]}$, $k \geq 0$ [69]. The unmapped Raviart-Thomas space on a quadrilateral is the space of vector-valued functions

$$RT_{[k]}(E) = P_{k+1,k}(E) \times P_{k,k+1}(E), \quad (2.20)$$

where $P_{k+1,k}(E)$ denotes polynomials of degree $k + 1$ in x and degree k in y . The unmapped Raviart-Thomas space on a hexahedron is

$$RT_{[k]}(E) = P_{k+1,k,k}(E) \times P_{k,k+1,k}(E) \times P_{k,k,k+1}(E), \quad (2.21)$$

where $P_{k+1,k,k}(E)$ denotes polynomials of degree $k + 1$ in x , degree k in y , and degree k in z . The increase of polynomial degree in a variable for its respective component accounts for approximation of a vector field's divergence. That is, the increase in order is necessary so that the operator $\nabla \cdot$ maps $RT_{[k]}$ onto $P_k(E)$. In this dissertation we will focus on the lowest-order space, $RT_{[0]}$, and when approximating a displacement vector field in Chapter 3, we will use the $\text{WG}(P_0^d, P_0^d; RT_{[0]}^d, P_0)$ space. Therefore we have $W_{\text{grad}} = RT_{[0]}^d$, which are tensors where each row is a function in the unmapped $RT_{[0]}$ space. We write the Raviart-Thomas space using the following basis

$$RT_{[0]} = \text{span} \left\{ \begin{bmatrix} 1 \\ 0 \end{bmatrix}, \begin{bmatrix} 0 \\ 1 \end{bmatrix}, \begin{bmatrix} X \\ 0 \end{bmatrix}, \begin{bmatrix} 0 \\ Y \end{bmatrix} \right\} \quad (2.22)$$

for a quadrilateral and

$$RT_{[0]} = \text{span} \left\{ \begin{bmatrix} 1 \\ 0 \\ 0 \end{bmatrix}, \begin{bmatrix} 0 \\ 1 \\ 0 \end{bmatrix}, \begin{bmatrix} 0 \\ 0 \\ 1 \end{bmatrix}, \begin{bmatrix} X \\ 0 \\ 0 \end{bmatrix}, \begin{bmatrix} 0 \\ Y \\ 0 \end{bmatrix}, \begin{bmatrix} 0 \\ 0 \\ Z \end{bmatrix} \right\} \quad (2.23)$$

for a hexahedron. The Gram matrix for the hexahedral element is

$$G_{RT_{[0]}} = \begin{bmatrix} |E| & 0 & 0 & \int_E X & 0 & 0 \\ 0 & |E| & 0 & 0 & \int_E Y & 0 \\ 0 & 0 & |E| & 0 & 0 & \int_E Z \\ \int_E X & 0 & 0 & \int_E X^2 & 0 & 0 \\ 0 & \int_E Y & 0 & 0 & \int_E Y^2 & 0 \\ 0 & 0 & \int_E Z & 0 & 0 & \int_E Z^2 \end{bmatrix}, \quad (2.24)$$

where the area of E , denoted by $|E|$, is given by $|E| = \int_E 1$.

When the hexahedron is a parallelepiped, the off-diagonal entries of the Gram matrix vanish, making weak gradient computations trivial. In the more general case, it is not guaranteed that the off-diagonal entries vanish. One approach we briefly considered to combat this is to define

(x_c, y_c, z_c) as the hexahedron's center of mass. This would ensure the off-diagonal entries vanish at the cost of computing the barycenter for a general hexahedron; however, it is not clear that this provides a significant advantage, so we refrain from doing so.

Extending this information allows us to define the tensor-valued space

$$RT_{[0]}^2 = \text{span} \{W_i : 1 \leq i \leq 8\}, \quad (2.25)$$

where

$$\begin{aligned} W_1 &= \begin{bmatrix} 1 & 0 \\ 0 & 0 \end{bmatrix}, W_2 = \begin{bmatrix} 0 & 1 \\ 0 & 0 \end{bmatrix}, W_3 = \begin{bmatrix} X & 0 \\ 0 & 0 \end{bmatrix}, W_4 = \begin{bmatrix} 0 & Y \\ 0 & 0 \end{bmatrix}, \\ W_5 &= \begin{bmatrix} 0 & 0 \\ 1 & 0 \end{bmatrix}, W_6 = \begin{bmatrix} 0 & 0 \\ 0 & 1 \end{bmatrix}, W_7 = \begin{bmatrix} 0 & 0 \\ X & 0 \end{bmatrix}, W_8 = \begin{bmatrix} 0 & 0 \\ 0 & Y \end{bmatrix}. \end{aligned} \quad (2.26)$$

The space $RT_{[0]}^3$ is defined in the same fashion, but we refrain from writing all 18 members explicitly. Due to the natural tensor product nature of this space, the Gram matrix for the weak gradient is a block-diagonal version of the Gram matrix in Equation (2.24)

$$G_{RT_{[0]}^3} = \begin{bmatrix} G_{RT_{[0]}} & 0 & 0 \\ 0 & G_{RT_{[0]}} & 0 \\ 0 & 0 & G_{RT_{[0]}} \end{bmatrix}. \quad (2.27)$$

Aside from the simplicity that this basis provides, this space also satisfies the necessary conditions for Lemmas 2.3 and 2.4, making it a prime candidate for use with lowest-order WGFEMs.

2.3.2 The Arbogast-Correa Space on Quadrilaterals

We now turn our attention to a similar space named the Arbogast-Correa space. Compared to the classical Raviart-Thomas space [28] or the Arnold-Boffi-Falk space [70], the Arbogast-Correa space constructed recently in [63] for convex quadrilaterals has better approximation properties

and less degrees of freedom. The $AC_k(k \geq 0)$ spaces are constructed using both unmapped vector-valued polynomials and rational functions obtained via the Piola transformation. The local Arbogast-Correa space is defined by

$$AC_k(E) = P_k^2(E) + \mathbf{x}\tilde{P}_k(E) + \mathbb{S}_k(E), \quad (2.28)$$

where $P_k^2(E)$ is the space of vector-valued polynomials of two variables with total degree at most k , $\tilde{P}_k(E)$ is the space of homogeneous scalar-valued polynomials of two variables with degree exactly k , and $\mathbb{S}_k(E)$ is a supplementary space of vector-valued rational functions obtained via the Piola transformation.

For convenience, we write $\mathbb{S}_k = \mathcal{P}_E \hat{\mathbb{S}}_k$, where \mathcal{P}_E is the Piola transformation. Let (\hat{x}, \hat{y}) be the coordinates in the reference element $[0, 1]^2$. According to [63], for $k = 0$,

$$\hat{\mathbb{S}}_0 = \text{span}\{\mathbf{curl}(\hat{x}\hat{y})\}, \quad (2.29)$$

and $k \geq 1$,

$$\hat{\mathbb{S}}_k = \text{span}\{\mathbf{curl}((1 - \hat{x}^2)\hat{x}^{k-1}\hat{y}), \mathbf{curl}(\hat{x}^{k-1}\hat{y}(1 - \hat{y}^2))\}. \quad (2.30)$$

Roughly speaking, $P_k^2(E)$ accounts for the approximation of a vector field on a convex quadrilateral, $\mathbf{x}\tilde{P}_k(E)$ accounts for the approximation of divergence, and \mathbb{S}_k offers a divergence-free supplement. Their motivation for \mathbb{S}_k comes from approaching a vector field approximation by looking at the Helmholtz decomposition.

For these discrete spaces, we have

$$\dim(P_k^2) = (k + 1)(k + 2), \quad \dim(\tilde{P}_k) = k + 1,$$

and

$$\dim(\mathbb{S}_k) = 1 \text{ if } k = 0, \quad \dim(\mathbb{S}_k) = 2 \text{ if } k > 0.$$

If we set $s_k = \dim(\mathbb{S}_k)$, then

$$\dim(AC_k(E)) = (k+1)(k+3) + s_k. \quad (2.31)$$

Note that $(k+1)(k+3) = \dim(RT_k)$, which is the dimension of the k -th order Raviart-Thomas space on a triangle [69]. Thus, s_k acts similarly to the additional degrees of freedom needed for augmenting the Raviart-Thomas space on a quadrilateral [63].

However, in Chapter 4 of this dissertation, we will use the $WG(Q_0, Q_0; AC_0)$ discretization. Therefore we will focus on the lowest-order space AC_0 . We may write this space as

$$AC_0 := \text{span} \left\{ \begin{bmatrix} 1 \\ 0 \end{bmatrix}, \begin{bmatrix} 0 \\ 1 \end{bmatrix}, \begin{bmatrix} X \\ Y \end{bmatrix}, \mathcal{P}_E \begin{bmatrix} \hat{x} \\ -\hat{y} \end{bmatrix} \right\}. \quad (2.32)$$

In addition to the local projection operators discussed in Lemma 2.1, we also need the global interpolation operator $\mathbf{\Pi}_h$. For any edge e in the mesh $\mathcal{E}_h^{\mathcal{D}}$, this operators satisfies

$$\langle (\mathbf{\Pi}_h \mathbf{v}) \cdot \mathbf{n}, 1 \rangle_e = \langle \mathbf{v} \cdot \mathbf{n}, 1 \rangle_e, \quad \forall \mathbf{v} \in H(\text{div}, \Omega^{\mathcal{D}}). \quad (2.33)$$

This flux-capturing property is extremely important for the analysis in Chapter 4. Since the $\mathbb{S}_0(E)$ portion of the space yields a more difficult basis function, we will not dive into a discussion of the discrete weak gradient computation for this space as we did with the Raviart-Thomas space.

2.4 Software Implementation

While there are not many publicly available software packages for WGFEMs, all of the computations in this chapter are publicly available as part of the `DarcyLite` and `Darcy+` software packages written in Matlab and C++, respectively [71]. These may be found on James Liu's website. Between `DarcyLite` and `Darcy+`, one may solve WGFEMs for Darcy flow, Stokes flow, Stokes-Darcy coupling, linear elasticity, and poroelasticity on varying meshes and spatial dimen-

sions. These packages output errors and figures for postprocessed quantities such as the discrete weak gradient as well as the primary variables.

There is also a WG tutorial available in the `deal.II` library, which is publicly available on Github. The step-47 tutorial added in version 9.1 uses the $WG(P_k, P_k; RT_{[k]})$ space ($k = 0, 1, 2$) on quadrilaterals to solve Darcy flow [72]. We have also used a `deal.II` implementation of WGFEMs to solve Darcy flow on a hexahedral mesh using the SPE10 dataset, which is a permeability profile available in the `Matlab Reservoir Simulation Toolbox` [73, 74].

Since `deal.II` supports physics coupling along an interface (see step-46), and since we implemented the Bernardi-Raugel element in `deal.II` as part of version 9.1 [72], the only finite element space missing from `deal.II` to construct our Stokes-Darcy solver from Chapter 4 is the AC_k space. Instead, the results in Chapter 3 are derived from a three-dimensional implementation in `Darcy+` and a two-dimensional implementation in `DarcyLite`. The results in Chapter 4 are all written and available in `DarcyLite`.

2.5 Assumptions for Mesh Quality

In this section we will present some related material for meshes to clarify and simplify later analysis.

We will refer to a mesh as a rectangle mesh if every element has a clear tensor product structure. That is, if $E \in \mathcal{E}_h$ may be written as $E = [x_1, x_2] \times [y_1, y_2]$. We will refer to its three-dimensional analogue as a brick mesh, where $E \in \mathcal{E}_h$ may be written as $E = [x_1, x_2] \times [y_1, y_2] \times [z_1, z_2]$.

Following other weak Galerkin literature [75], we present some regularity assumptions for a mesh, which we will refer to as a shape-regular mesh (not to be confused with a shape regular family of meshes). In two dimensions, we say a mesh \mathcal{E}_h with diameter $h = \max_{E \in \mathcal{E}_h} h_E$ is shape-regular if there are constants $C_1, C_2, C_3, C_4 > 0$ so that

1. $|e| \geq C_1 h_E$ for all $E \in \mathcal{E}_h$, e an edge of E .
2. $|E| \geq C_2 h_E^2$ for all $E \in \mathcal{E}_h$.

3. There exists a triangle with base e inside E whose height exceeds $C_3 h_E$ for all $E \in \mathcal{E}_h$, e an edge of E .
4. There exists a triangle containing E whose diameter does not exceed $C_4 h_E$ for all $E \in \mathcal{E}_h$.

The definitions are similar for the three-dimensional case. A simple summary of the shape-regular requirement, which was stated in [22], is that the following should hold for a mesh:

1. Edges are not too short.
2. Polygons are not too small.
3. Interior triangles are not too short.
4. Circumscribed triangles are not too tall.

For a quadrilateral E , let θ_1 be the angle between the outward unit normal vectors on two opposite edges, θ_2 be the angle for the other two edges. Let $\sigma_E = \max\{|\pi - \theta_1|, |\pi - \theta_2|\}$ and h_E be the diameter of E . A quadrilateral mesh \mathcal{E}_h is asymptotically parallelogram [1], provided that there exists a positive constant C such that $\sigma_E/h_E \leq C$ for all $E \in \mathcal{E}_h$. This definition is similar for an asymptotically parallelepiped mesh.

Quadrilateral and hexahedral meshes are more suitable than rectangular and brick meshes for handling complicated domain geometry, and since WGFEMs place variables on the mesh skeleton, quadrilateral and hexahedral meshes are also more efficient than triangular and tetrahedral meshes for the same mesh size. Our numerical results in Chapter 3 show that asymptotically parallelogram quadrilateral and asymptotically parallelepiped hexahedral meshes provide satisfactory results for linear elasticity.

Chapter 3

Linear Elasticity

3.1 Introduction

To discuss forces for elastic materials in d -dimensions, we introduce the second-order $d \times d$ tensors, σ and ε . σ is the Cauchy stress tensor describing stresses experienced by a material in a deformed state, and ε is the strain tensor describing the deformation of the material. For infinitesimally small displacements \mathbf{u} of particles in the material, the strain tensor is defined by the symmetric gradient of the displacement of the material. This relation takes the form

$$\varepsilon = (\nabla \mathbf{u} + \nabla \mathbf{u}^T)/2.$$

Because strain acts like a first-order differential operator for displacement, we may also notate it like a differential operator with $\varepsilon(\mathbf{u})$. The stress and strain tensors are related by the fourth-order stiffness tensor C . For our model, we assume the elastic material is isotropic and homogeneous so that the stiffness tensor is constant. Hooke's law for continuous media therefore states

$$\sigma = C\varepsilon = 2\mu\varepsilon + \lambda\text{tr}(\varepsilon)\mathbf{I},$$

where μ and λ denote the Lamé constants. The trace of the strain tensor is equal to

$$\text{tr}(\varepsilon(\mathbf{u})) = \sum_{i=1}^d \varepsilon_{ii} = \sum_{i=1}^d \frac{\partial \mathbf{u}_i}{\partial x_i} = \nabla \cdot \mathbf{u},$$

so we also may refer to $\nabla \cdot \mathbf{u}$ as the dilation of the material. Since the Lamé constants relate a dimensionless quantity ($[\varepsilon] = 1$) to a quantity with units for pressure ($[\sigma] = \text{ML}^{-1}\text{T}^{-2}$), these constants also have units for pressure $[\lambda] = [\mu] = \text{ML}^{-1}\text{T}^{-2}$, where M, L, T are general units for mass, length, and time. The Lamé parameters are additionally related to the commonly used

Young's modulus E and Poisson ratio ν by

$$\lambda = \frac{E\nu}{(1+\nu)(1-2\nu)}, \quad \mu = \frac{E}{2(1+\nu)}. \quad (3.1)$$

From a physical standpoint, as λ becomes arbitrarily large, or as ν approaches 0.5 from the left, a small compressive strain requires an arbitrarily large stress in a material, which may not be physically possible. For that reason, a material is often referred to as incompressible when $\lambda \rightarrow \infty$ or when $\nu \rightarrow 0.5$. When the material experiences internal forces given by \mathbf{f} , the forces are related to the stress by

$$\nabla \cdot \sigma = \mathbf{f}.$$

Combining these relations yields a system of PDEs governing the displacement of particles within the isotropic linear elastic material in an open bounded polygonal domain $\Omega \subset \mathbb{R}^d$

$$\left\{ \begin{array}{ll} -\nabla \cdot \sigma = \mathbf{f}, & \text{in } \Omega, \\ \sigma = 2\mu\varepsilon(\mathbf{u}) + \lambda \operatorname{tr}(\varepsilon(\mathbf{u}))\mathbf{I}, & \text{in } \Omega, \\ \varepsilon(\mathbf{u}) = (\nabla\mathbf{u} + \nabla\mathbf{u}^T)/2, & \text{in } \Omega, \\ \mathbf{u} = \mathbf{u}_D, & \text{on } \Gamma^D, \\ -\sigma\mathbf{n} = \mathbf{t}_N, & \text{on } \Gamma^N, \end{array} \right. \quad (3.2)$$

where $\partial\Omega$ may be partitioned into $\partial\Omega = \Gamma^D \cup \Gamma^N$, $\mathbf{u} \in H^1(\Omega)^d$ is the unknown displacement function and $\mathbf{f} \in L^2(\Omega)^d$ is the given body force. \mathbf{u}_D and \mathbf{t}_N are Dirichlet and Neumann boundary data for the corresponding boundaries. \mathbf{u}_D is referred to as the displacement boundary condition and \mathbf{t}_N is referred to as a traction boundary condition. We solve this problem in the primal formulation, meaning we discretize only \mathbf{u} . The stress and strain in (3.2) are computed from \mathbf{u} .

We proceed to derive the variational form of the linear elasticity equation by testing against a function $\mathbf{v} \in H_{0,D}^1(\Omega)^d$, which is the space of $H^1(\Omega)$ functions whose extension to the Dirichlet boundary is 0. Integration by parts, splitting the integrals, and applying the traction boundary

condition yields

$$\begin{aligned}
\int_{\Omega} \mathbf{f} \cdot \mathbf{v} &= \int_{\Omega} \nabla \cdot \boldsymbol{\sigma} \cdot \mathbf{v} \\
&= \int_{\Omega} \boldsymbol{\sigma} : \nabla \mathbf{v} - \int_{\Gamma^N} \boldsymbol{\sigma} \mathbf{n} \cdot \mathbf{v} \\
&= \int_{\Omega} (2\mu \boldsymbol{\varepsilon}(\mathbf{u}) + \lambda \text{tr}(\boldsymbol{\varepsilon}(\mathbf{u})) \mathbf{I}) : \nabla \mathbf{v} + \int_{\Gamma^N} \mathbf{t}_N \cdot \mathbf{v} \\
&= 2\mu \int_{\Omega} \boldsymbol{\varepsilon}(\mathbf{u}) : \nabla \mathbf{v} + \lambda \int_{\Omega} (\text{tr}(\boldsymbol{\varepsilon}(\mathbf{u})) \mathbf{I}) : \nabla \mathbf{v} + \int_{\Gamma^N} \mathbf{t}_N \cdot \mathbf{v}.
\end{aligned} \tag{3.3}$$

We observe

$$\begin{aligned}
(\text{tr}(\boldsymbol{\varepsilon}(\mathbf{u})) \mathbf{I}) : \nabla \mathbf{v} &= (\nabla \cdot \mathbf{u}) \mathbf{I} : \nabla \mathbf{v} \\
&= (\nabla \cdot \mathbf{u}) \text{tr}(\nabla \mathbf{v}) \\
&= (\nabla \cdot \mathbf{u}) \left(\sum_{i=1}^d \frac{\partial v_i}{\partial x_i} \right) \\
&= (\nabla \cdot \mathbf{u}) (\nabla \cdot \mathbf{v}).
\end{aligned}$$

For the $\boldsymbol{\varepsilon}(\mathbf{u}) : \nabla \mathbf{v}$ term, we have

$$\begin{aligned}
\boldsymbol{\varepsilon}(\mathbf{u}) : \nabla \mathbf{v} &= (\nabla \mathbf{u} + \nabla \mathbf{u}^T) / 2 : \nabla \mathbf{v} \\
&= (\nabla \mathbf{u} + \nabla \mathbf{u}^T) / 2 : (\nabla \mathbf{v} + \nabla \mathbf{v}) / 2 \\
&= \frac{1}{4} (\nabla \mathbf{u} : \nabla \mathbf{v} + \nabla \mathbf{u}^T : \nabla \mathbf{v} + \nabla \mathbf{u}^T : \nabla \mathbf{v} + \nabla \mathbf{u} : \nabla \mathbf{v}) \\
&= \frac{1}{4} (\nabla \mathbf{u} : \nabla \mathbf{v} + \nabla \mathbf{u} : \nabla \mathbf{v}^T + \nabla \mathbf{u}^T : \nabla \mathbf{v} + \nabla \mathbf{u}^T : \nabla \mathbf{v}^T) \\
&= \boldsymbol{\varepsilon}(\mathbf{u}) : \boldsymbol{\varepsilon}(\mathbf{v}).
\end{aligned}$$

Substituting these results back into Equation (3.3) yields

$$\begin{aligned}
\int_{\Omega} \mathbf{f} \cdot \mathbf{v} - \int_{\Gamma^N} \mathbf{t}_N \cdot \mathbf{v} &= 2\mu \int_{\Omega} \varepsilon(\mathbf{u}) : \nabla \mathbf{v} + \lambda \int_{\Omega} (\text{tr}(\varepsilon(\mathbf{u}))\mathbf{I}) : \nabla \mathbf{v} \\
&= 2\mu \int_{\Omega} \varepsilon(\mathbf{u}) : \varepsilon(\mathbf{v}) + \lambda \int_{\Omega} (\nabla \cdot \mathbf{u})(\nabla \cdot \mathbf{v}).
\end{aligned}$$

The variational form for the displacement form of the linear elasticity problem is now stated as follows: Seek $\mathbf{u} \in H_{\mathbf{u}_D, D}^1(\Omega)^d$ so that

$$2\mu(\varepsilon(\mathbf{u}), \varepsilon(\mathbf{v}))_{\Omega} + \lambda(\nabla \cdot \mathbf{u}, \nabla \cdot \mathbf{v})_{\Omega} = (\mathbf{f}, \mathbf{v})_{\Omega} - (\mathbf{t}_N, \mathbf{v})_{\Gamma^N}, \quad \forall \mathbf{v} \in H_{0, D}^1(\Omega)^d. \quad (3.4)$$

It has been known for decades that traditional CGFEMs suffer from loss in convergence rates when tackling Equation (3.4) as λ becomes unbounded [65, 76, 77]. An elegant explanation for why this occurs may be found in [65, 77], where a bound for the exact solution is given by

$$\|\mathbf{u}\|_{H^2} + \lambda\|\nabla \cdot \mathbf{u}\|_{H^1} \leq C(\|\mathbf{f}\|_{L^2} + \|\mathbf{u}_D\|_{H^2} + \|\mathbf{t}_N\|_{H^1}). \quad (3.5)$$

This bound now drives a much more exciting discussion of the interplay between physics and numerical discretization. For large values of λ , the H^1 norm of $\nabla \cdot \mathbf{u}$ must decrease at a rate proportional to λ^{-1} or faster. $\nabla \cdot \mathbf{u}$ is also referred to as the dilation of the material. This means as $\lambda \rightarrow \infty$, the dilation must satisfy $\nabla \cdot \mathbf{u} \rightarrow 0$, which is equivalent to saying the material must be incompressible. For that reason, the case of $\lambda \rightarrow \infty$ is also referred to as the incompressible limit. A finite element method for solving linear elasticity is said to experience locking if the finite element solution deteriorates as λ increases [65]. The reason for a loss of convergence is often because the finite element space cannot approximate a nonzero dilation-free displacement field.

To examine the incompressible limit more closely, consider the artificial pressure variable

$$p = \lambda \nabla \cdot \mathbf{u}.$$

This allows the variational form for linear elasticity to be written in an equivalent mixed formulation: Seek $\mathbf{u} \in H_{\mathbf{u}_D, D}^1(\Omega)^d$, $p \in L^2(\Omega)$ satisfying

$$\begin{aligned}
2\mu(\varepsilon(\mathbf{u}), \varepsilon(\mathbf{v}))_\Omega + (\nabla \cdot \mathbf{v}, p)_\Omega &= (\mathbf{f}, \mathbf{v})_\Omega - (\mathbf{t}_N, \mathbf{v})_{\Gamma_N}, & \forall \mathbf{v} \in H_{0,D}^1(\Omega)^d, \\
(\nabla \cdot \mathbf{u}, q)_\Omega - \lambda^{-1}(p, q)_\Omega &= 0, & \forall q \in L_0^2(\Omega).
\end{aligned}$$

As $\lambda \rightarrow \infty$, and assuming $|\Gamma_N| = 0$, this equation looks similar to the saddle-point problem for Stokes flow

$$\begin{aligned}
2\mu(\varepsilon(\mathbf{u}), \varepsilon(\mathbf{v}))_\Omega + (\nabla \cdot \mathbf{v}, p)_\Omega &= (\mathbf{f}, \mathbf{v})_\Omega, & \forall \mathbf{v} \in H_0^1(\Omega)^d, \\
(\nabla \cdot \mathbf{u}, q)_\Omega &= 0, & \forall q \in L_0^2(\Omega).
\end{aligned}$$

However, the case with no Neumann boundary conditions for Stokes flow is equivalent to the variational form with $(\nabla \mathbf{u}, \nabla \mathbf{v})_\Omega$ because a calculus exercise shows $\nabla \cdot \varepsilon(\mathbf{u}) = \frac{1}{2} \nabla^2 \mathbf{u}$ when $\nabla \cdot \mathbf{u} = 0$. This means solving Equation (3.2) is similar to solving the problem

$$\begin{cases} -\mu \Delta \mathbf{u} - (\mu + \lambda) \nabla (\nabla \cdot \mathbf{u}) = \mathbf{f}, \\ \mathbf{u}|_{\partial\Omega} = \mathbf{u}_D. \end{cases} \quad (3.6)$$

We now make some modifications to Equation (3.4) in light of these insights. Assuming there is no traction condition, we consider the variational formulation of the primal problem to find $\mathbf{u} \in H_{\mathbf{u}_D, D}^1(\Omega)^d$ satisfying

$$\mu(\nabla \mathbf{u}, \nabla \mathbf{v}) + (\mu + \lambda)(\nabla \cdot \mathbf{u}, \nabla \cdot \mathbf{v}) = (\mathbf{f}, \mathbf{v}), \quad \forall \mathbf{v} \in H^1(\Omega)^d. \quad (3.7)$$

We refer to the formulation in Equation (3.4) as the strain-div formulation for linear elasticity, and we refer to the formulation in Equation (3.7) as the grad-div formulation for linear elasticity. We will introduce finite element schemes for both but only rigorously prove convergence of the solution for the grad-div formulation.

3.2 Weak Galerkin Finite Element Scheme

To develop the lowest-order WGFEMs for linear elasticity, we consider a mesh \mathcal{E}_h of Ω containing quadrilaterals or hexahedra which are shape-regular (from Section 2.5) and a finite element space of the form $\text{WG}(Q_0^d, Q_0^d; W_{\text{grad}}, W_{\text{div}})$. In light of the properties discussed in Chapter 2, we consider $W_{\text{grad}} = RT_{[0]}^3$ to be the unmapped Raviart-Thomas space on quadrilaterals. In the next section we will prove Lemma 3.1 to show the discrete weak gradient for each component of the shape functions satisfies Lemma 2.4. Additionally, to reduce computational complexity, we take $W_{\text{div}} = Q_0$. This may be viewed as a projection of dilation into piecewise constants, which is a form of reduced integration.

Let $V_h := \text{WG}(Q_0^d, Q_0^d; RT_{[0]}^d, Q_0)$. The finite element scheme in the strain-div formulation for the linear elasticity problem (3.2) is formulated as: Seek $\mathbf{u}_h \in V_h$ such that $\mathbf{u}_h|_{\Gamma_h^D} = \mathbf{Q}_h^\partial(\mathbf{u}_D)$ and

$$\mathcal{A}_h^{SD}(\mathbf{u}_h, \mathbf{v}) = \mathcal{F}_h^{SD}(\mathbf{v}), \quad \forall \mathbf{v} \in V_h^0, \quad (3.8)$$

where

$$\mathcal{A}_h^{SD}(\mathbf{u}_h, \mathbf{v}) = 2\mu \sum_{E \in \mathcal{E}_h} (\varepsilon_{w,d}(\mathbf{u}_h), \varepsilon_w(\mathbf{v}))_E \quad (3.9)$$

$$+ \lambda \sum_{E \in \mathcal{E}_h} (\nabla_w \cdot \mathbf{u}_h, \nabla_w \cdot \mathbf{v})_E, \quad (3.10)$$

and

$$\mathcal{F}_h^{SD}(\mathbf{v}) = \sum_{E \in \mathcal{E}_h} (\mathbf{f}, \mathbf{v}^\circ)_E - \sum_{\gamma \in \Gamma_h^N} \langle \mathbf{t}_N, \mathbf{v}^\partial \rangle_\gamma. \quad (3.11)$$

The finite element scheme in the grad-div formulation for the linear elasticity problem (3.6) is formulated as follows: Seek $\mathbf{u}_h \in V_h$ such that $\mathbf{u}_h|_{\Gamma_h^D} = \mathbf{Q}_h^\partial(\mathbf{u}_D)$ and

$$\mathcal{A}_h^{GD}(\mathbf{u}_h, \mathbf{v}) = \mathcal{F}_h^{GD}(\mathbf{v}), \quad \forall \mathbf{v} \in V_h^0, \quad (3.12)$$

where

$$\mathcal{A}_h^{GD}(\mathbf{u}_h, \mathbf{v}) = \mu \sum_{E \in \mathcal{E}_h} (\nabla_w \mathbf{u}_h, \nabla_w \mathbf{v})_E \quad (3.13)$$

$$+ (\mu + \lambda) \sum_{E \in \mathcal{E}_h} (\nabla_w \cdot \mathbf{u}_h, \nabla_w \cdot \mathbf{v})_E, \quad (3.14)$$

and

$$\mathcal{F}_h^{GD}(\mathbf{v}) = \sum_{E \in \mathcal{E}_h} (\mathbf{f}, \mathbf{v}^\circ)_E. \quad (3.15)$$

Using the framework developed in Chapter 2, we now proceed to perform analysis of the convergence for this finite element scheme.

3.3 A Priori Error Analysis

The error analysis in this section focuses on the finite element scheme (3.12) for problem (3.6) with homogeneous Dirichlet boundary conditions. We consider the grad-div formulation on a rectangular mesh. We now use $A \lesssim B$ to simplify an inequality $A \leq CB$ when $C > 0$ is a constant independent of h and λ .

Definition 3.1. (Semi-norm on V_h) For $\mathbf{v} \in V_h$, we define

$$\|\mathbf{v}\|^2 = \sum_{E \in \mathcal{E}_h} h_E^{-1} \|\mathbf{v}^\partial - \mathbf{v}^\circ\|_{E^\partial}^2. \quad (3.16)$$

Due to Lemma 2.3, this is essentially the same as the discrete weak gradient. Additionally, if a higher order WG space $\text{WG}(Q_k^d, Q_k^d)$ ($k \geq 1$) is used, we must add another term to (3.16), $\nabla \mathbf{v}^\circ$, for the classical gradient of its interior part. To see how this changes analysis, one may refer to [20].

Lemma 3.1. (Trace equivalence for $RT_{[0]}^d$) For $E \in \mathcal{E}_h$, there holds

$$\|W \mathbf{n}\|_{E^\partial}^2 \approx h_E^{-1} \|W\|_E^2, \quad \forall W \in RT_{[0]}^2(E). \quad (3.17)$$

Proof. It can be proved using the techniques in [28] that

$$\|\mathbf{w} \cdot \mathbf{n}\|_{E^\partial}^2 \approx h_E^{-1} \|\mathbf{w}\|_E^2, \quad \forall \mathbf{w} \in RT_{[0]}(E),$$

where the equivalence holds with absolute constants that are independent of the mesh size. The result in (3.17) is a matrix version of this equivalence. \square

Based on Lemma 3.1, we have a finite element space that satisfies Lemmas 2.1, 2.2, 2.3, and 2.4. Thus, the energy norm defined on the mesh satisfies the coercivity relation

$$\|\mathbf{v}\| \lesssim \|\nabla_w \mathbf{v}\|, \quad \forall \mathbf{v} \in V_h^0. \quad (3.18)$$

Lemma 3.2. (Boundedness) Assume $\mathbf{v} \in V_h$ and $E \in \mathcal{E}_h$. Then

$$\|\nabla_w \mathbf{v}\|_E^2 \lesssim h_E^{-1} \|\mathbf{v}^\partial - \mathbf{v}^\circ\|_{E^\partial}^2. \quad (3.19)$$

and

$$\|\nabla_w \cdot \mathbf{v}\|_E^2 \lesssim h_E^{-1} \|\mathbf{v}^\partial - \mathbf{v}^\circ\|_{E^\partial}^2. \quad (3.20)$$

Proof. For the first inequality, we take $W = \nabla_w \mathbf{v}$ in Lemma 2.2, then apply the Cauchy-Schwarz inequality, trace equivalence, and Young's inequality to obtain

$$\begin{aligned} \|\nabla_w \mathbf{v}\|_E^2 &= \langle (\nabla_w \mathbf{v}) \mathbf{n}, \mathbf{v}^\partial - \mathbf{v}^\circ \rangle_{E^\partial} \\ &\leq \|(\nabla_w \mathbf{v}) \mathbf{n}\|_{E^\partial} \|\mathbf{v}^\partial - \mathbf{v}^\circ\|_{E^\partial} \\ &\leq Ch_E^{-\frac{1}{2}} \|\nabla_w \mathbf{v}\|_E \|\mathbf{v}^\partial - \mathbf{v}^\circ\|_{E^\partial} \end{aligned}$$

Dividing by $\|\nabla_w \mathbf{v}\|_E$ and squaring both sides completes the proof. The inequality for discrete weak divergence can be proven in a similar way using the shape-regularity of the mesh, which we require so that $|E|/|E^\partial| \approx h$. \square

Lemma 3.3. (Error equation) Let \mathbf{u}_h be the numerical solution from the lowest-order finite element scheme in (3.12) with a homogeneous Dirichlet boundary condition. Let \mathbf{u} be the exact solution of (3.6). There holds

$$\mathcal{A}_h^{GD}(\mathbf{u}_h - \mathbf{Q}_h \mathbf{u}, \mathbf{v}) = \mu \mathcal{G}_1(\mathbf{u}, \mathbf{v}) + (\mu + \lambda) \mathcal{G}_2(\mathbf{u}, \mathbf{v}), \quad (3.21)$$

where

$$\mathcal{G}_1(\mathbf{u}, \mathbf{v}) = \sum_{E \in \mathcal{E}_h} \langle (\nabla \mathbf{u} - \mathbf{Q}_h(\nabla \mathbf{u})) \mathbf{n}, \mathbf{v}^\partial - \mathbf{v}^\circ \rangle_{E^\partial}, \quad (3.22)$$

and

$$\mathcal{G}_2(\mathbf{u}, \mathbf{v}) = \sum_{E \in \mathcal{E}_h} \langle (\nabla \cdot \mathbf{u} - Q_h(\nabla \cdot \mathbf{u})) \mathbf{n}, \mathbf{v}^\partial - \mathbf{v}^\circ \rangle_{E^\partial}. \quad (3.23)$$

Proof. Let $\mathbf{v} = \{\mathbf{v}^\circ, \mathbf{v}^\partial\} \in V_h$ and $E \in \mathcal{E}_h$. Using the differential equation in (3.6) and integration by parts, we have

$$\begin{aligned} (\mathbf{f}, \mathbf{v}^\circ)_E &= -\mu(\Delta \mathbf{u}, \mathbf{v}^\circ)_E - (\mu + \lambda)(\nabla(\nabla \cdot \mathbf{u}), \mathbf{v}^\circ)_E \\ &= -\mu \langle (\nabla \mathbf{u}) \mathbf{n}, \mathbf{v}^\circ \rangle_{E^\partial} + \mu(\nabla \mathbf{u}, \nabla \mathbf{v}^\circ)_E \\ &\quad - (\mu + \lambda) \langle (\nabla \cdot \mathbf{u}) \mathbf{n}, \mathbf{v}^\circ \rangle_{E^\partial} + (\mu + \lambda)(\nabla \cdot \mathbf{u}, \nabla \cdot \mathbf{v}^\circ)_E. \end{aligned}$$

Since \mathbf{v}° is an elementwise constant vector, $\nabla \mathbf{v}^\circ = \mathbf{0}$ and $\nabla \cdot \mathbf{v}^\circ = 0$. Therefore, the previous expression can be simplified as

$$(\mathbf{f}, \mathbf{v}^\circ)_E = -\mu \langle (\nabla \mathbf{u}) \mathbf{n}, \mathbf{v}^\circ \rangle_{E^\partial} - (\mu + \lambda) \langle (\nabla \cdot \mathbf{u}) \mathbf{n}, \mathbf{v}^\circ \rangle_{E^\partial}. \quad (3.24)$$

Under the assumptions of normal continuity of the exact solution and homogeneous boundary conditions, we have

$$\sum_{E \in \mathcal{E}_h} \langle (\nabla \mathbf{u}) \mathbf{n}, \mathbf{v}^\circ \rangle_{E^\partial} = 0, \quad \sum_{E \in \mathcal{E}_h} \langle (\nabla \cdot \mathbf{u}) \mathbf{n}, \mathbf{v}^\circ \rangle_{E^\partial} = 0. \quad (3.25)$$

Combining these with (3.24) and the finite element scheme (3.12) gives

$$\mathcal{A}_h^{GD}(\mathbf{u}_h, \mathbf{v}) = \sum_{E \in \mathcal{E}_h} (\mathbf{f}, \mathbf{v}^\circ)_E \quad (3.26)$$

$$= \mu \sum_{E \in \mathcal{E}_h} \langle (\nabla \mathbf{u}) \mathbf{n}, \mathbf{v}^\partial - \mathbf{v}^\circ \rangle_{E^\partial} \quad (3.27)$$

$$+ (\mu + \lambda) \sum_{E \in \mathcal{E}_h} \langle (\nabla \cdot \mathbf{u}) \mathbf{n}, \mathbf{v}^\partial - \mathbf{v}^\circ \rangle_{E^\partial}. \quad (3.28)$$

On the other hand, by the commuting identities in Lemma 1 and the conversion formulas in Lemma 2, we have

$$(\nabla_w(\mathbf{Q}_h \mathbf{u}), \nabla_w \mathbf{v})_E = (\mathbf{Q}_h \nabla \mathbf{u}, \nabla_w \mathbf{v})_E = \langle (\mathbf{Q}_h \nabla \mathbf{u}) \mathbf{n}, \mathbf{v}^\partial - \mathbf{v}^\circ \rangle_{E^\partial},$$

and

$$(\nabla_w \cdot (\mathbf{Q}_h \mathbf{u}), \nabla_w \cdot \mathbf{v})_E = (\mathbf{Q}_h(\nabla \cdot \mathbf{u}), \nabla_w \cdot \mathbf{v})_E = \langle \mathbf{Q}_h(\nabla \cdot \mathbf{u}) \mathbf{n}, \mathbf{v}^\partial - \mathbf{v}^\circ \rangle_{E^\partial}.$$

Thus we have, by summing over the entire mesh,

$$\mathcal{A}_h^{GD}(\mathbf{Q}_h \mathbf{u}, \mathbf{v}) = \mu \sum_{E \in \mathcal{E}_h} \langle (\mathbf{Q}_h \nabla \mathbf{u}) \mathbf{n}, \mathbf{v}^\partial - \mathbf{v}^\circ \rangle_{E^\partial} \quad (3.29)$$

$$+ (\mu + \lambda) \sum_{E \in \mathcal{E}_h} \langle \mathbf{Q}_h(\nabla \cdot \mathbf{u}) \mathbf{n}, \mathbf{v}^\partial - \mathbf{v}^\circ \rangle_{E^\partial}. \quad (3.30)$$

Subtracting (3.30) from (3.28) yields the error equation claimed in (3.21). \square

Lemma 3.4. (Estimates on linear functionals) Under the same assumptions as Lemma 3.3 and additionally assuming the exact solution of (3.6) has regularity $\mathbf{u} \in \mathbf{H}^2(\Omega)$, for any $\mathbf{v} \in V_h$, there hold

$$|\mathcal{G}_1(\mathbf{u}, \mathbf{v})| \lesssim h \|\mathbf{u}\|_{\mathbf{H}^2(\Omega)} \|\mathbf{v}\|, \quad (3.31)$$

$$|\mathcal{G}_2(\mathbf{u}, \mathbf{v})| \lesssim h \|\nabla \cdot \mathbf{u}\|_{H^1(\Omega)} \|\mathbf{v}\|. \quad (3.32)$$

We remark that if \mathbf{u} is the exact solution of (3.6), then $\mathcal{G}_2(\mathbf{u}, \mathbf{v})$ and $\mathcal{G}_2(\mathbf{u}, \mathbf{v})$ are indeed linear functionals defined on V_h . In general, they can also be viewed as nonsymmetric bilinear forms defined on $\mathbf{H}^1(\Omega) \times V_h$. This allows us to easily apply the above estimates in a duality argument to be presented later.

Proof. Consider a fixed $E \in \mathcal{E}_h$. By Lemma 3.1 and the approximation capacity of \mathbb{Q}_h , we have

$$\|(\nabla \mathbf{u} - \mathbb{Q}_h \nabla \mathbf{u}) \mathbf{n}\|_{E^\partial} \lesssim h_E^{-\frac{1}{2}} \|\nabla \mathbf{u} - \mathbb{Q}_h \nabla \mathbf{u}\|_E \lesssim h_E^{\frac{1}{2}} \|\mathbf{u}\|_{\mathbf{H}^2(E)}.$$

Applying the Cauchy-Schwarz and Young's inequalities, and the definition of semi-norm (3.16) gives

$$|\mathcal{G}_1(\mathbf{u}, \mathbf{v})| \lesssim \left(\sum_{E \in \mathcal{E}_h} h_E \|(\nabla \mathbf{u} - \mathbb{Q}_h \nabla \mathbf{u}) \mathbf{n}\|_{E^\partial}^2 \right)^{\frac{1}{2}} \left(\sum_{E \in \mathcal{E}_h} h_E^{-1} \|\mathbf{v}^\partial - \mathbf{v}^\circ\|_{E^\partial}^2 \right)^{\frac{1}{2}} \quad (3.33)$$

$$\lesssim \left(\sum_{E \in \mathcal{E}_h} h_E^2 \|\mathbf{u}\|_{\mathbf{H}(E)}^2 \right)^{\frac{1}{2}} \left(\sum_{E \in \mathcal{E}_h} h_E^{-1} \|\mathbf{v}^\partial - \mathbf{v}^\circ\|_{E^\partial}^2 \right)^{\frac{1}{2}} \quad (3.34)$$

$$\leq Ch \|\mathbf{u}\|_{\mathbf{H}^2(\Omega)} \|\mathbf{v}\|, \quad (3.35)$$

as desired. The second estimate can be proven in a similar way. \square

Theorem 3.1. Let \mathbf{u} be the exact solution of (3.6) with $\mathbf{H}^2(\Omega)$ regularity and \mathbf{u}_h be the numerical solution obtained from (3.12). There holds

$$\mu \sum_{E \in \mathcal{E}_h} \|\nabla \mathbf{u} - \nabla_w \mathbf{u}_h\|_E^2 + (\mu + \lambda) \sum_{E \in \mathcal{E}_h} \|\nabla \cdot \mathbf{u} - \nabla_w \cdot \mathbf{u}_h\|_E^2 \lesssim h^2 \|\mathbf{f}\|_{\mathbf{L}^2(\Omega)}^2. \quad (3.36)$$

Proof. We utilize Lemma 2.1 to split the elementwise errors into projection errors and discretization errors as shown below,

$$\|\nabla \mathbf{u} - \nabla_w \mathbf{u}_h\|_E^2 \lesssim \|\nabla \mathbf{u} - \mathbb{Q}_h \nabla \mathbf{u}\|_E^2 + \|\mathbb{Q}_h \nabla \mathbf{u} - \nabla_w \mathbf{u}_h\|_E^2,$$

$$\|\nabla \cdot \mathbf{u} - \nabla_w \cdot \mathbf{u}_h\|_E^2 \lesssim \|\nabla \cdot \mathbf{u} - \mathbb{Q}_h(\nabla \cdot \mathbf{u})\|_E^2 + \|\mathbb{Q}_h(\nabla \cdot \mathbf{u}) - \nabla_w \cdot \mathbf{u}_h\|_E^2.$$

For the projection errors, we have first elementwise estimates

$$\|\nabla \mathbf{u} - \mathbb{Q}_h \nabla \mathbf{u}\|_E \lesssim h \|\mathbf{u}\|_{\mathbf{H}^2(E)},$$

$$\|\nabla \cdot \mathbf{u} - Q_h(\nabla \cdot \mathbf{u})\|_E \lesssim h \|\nabla \cdot \mathbf{u}\|_{H^1(E)},$$

and then a mesh-wise estimate

$$\begin{aligned} & \mu \sum_{E \in \mathcal{E}_h} \|\nabla \mathbf{u} - \mathbb{Q}_h \nabla \mathbf{u}\|_E^2 + (\mu + \lambda) \sum_{E \in \mathcal{E}_h} \|\nabla \cdot \mathbf{u} - Q_h(\nabla \cdot \mathbf{u})\|_E^2 \\ & \lesssim h^2 \left(\mu \|\mathbf{u}\|_{\mathbf{H}^2(\Omega)}^2 + (\mu + \lambda) \|\nabla \cdot \mathbf{u}\|_{H^1(\Omega)}^2 \right) \lesssim h^2 \|\mathbf{f}\|_{\mathbf{L}^2(\Omega)}^2. \end{aligned} \quad (3.37)$$

In the last step, we have used the fact that

$$\mu \|\mathbf{u}\|_{\mathbf{H}^2(\Omega)}^2 + (\mu + \lambda) \|\nabla \cdot \mathbf{u}\|_{H^1(\Omega)}^2 \lesssim \|\mathbf{f}\|_{\mathbf{L}^2(\Omega)}^2,$$

which can be derived from (3.5) using the techniques developed in [77].

For the discretization errors between the projection and the finite element solution, we combine Lemmas 3.3 and 3.4 to obtain

$$\begin{aligned} & \mu \sum_{E \in \mathcal{E}_h} \|\mathbb{Q}_h \nabla \mathbf{u} - \nabla_w \mathbf{u}_h\|_E^2 + (\mu + \lambda) \sum_{E \in \mathcal{E}_h} \|Q_h(\nabla \cdot \mathbf{u}) - \nabla_w \cdot \mathbf{u}_h\|_E^2, \\ & \lesssim h^2 \left(\mu \|\mathbf{u}\|_{\mathbf{H}^2(\Omega)}^2 + (\mu + \lambda) \|\nabla \cdot \mathbf{u}\|_{H^1(\Omega)}^2 \right) \lesssim h^2 \|\mathbf{f}\|_{\mathbf{L}^2(\Omega)}^2. \end{aligned} \quad (3.38)$$

The desired result follows from combining (3.37) and (3.38). \square

We now establish an L^2 -norm estimate using a standard duality argument.

Theorem 3.2. (L^2 -norm estimate for displacement) Let \mathbf{u} be the exact solution of (3.6) with $\mathbf{H}^2(\Omega)$ regularity and \mathbf{u}_h be the numerical solution obtained from (3.12). There holds

$$\|\mathbf{u} - \mathbf{u}_h^\circ\|_{L^2(\Omega)} \leq Ch \|\mathbf{f}\|_{\mathbf{L}^2(\Omega)}, \quad (3.39)$$

where C is a positive constant independent of λ, h .

Proof. Let Φ be the solution of the dual problem

$$\begin{cases} -\mu\Delta\Phi - (\mu + \lambda)\nabla(\nabla \cdot \Phi) = \mathbf{e}_h^\circ, \\ \Phi|_{\partial\Omega} = \mathbf{0}. \end{cases} \quad (3.40)$$

As usual, we assume the dual solution has full regularity as follows

$$\mu\|\Phi\|_{\mathbf{H}^2(\Omega)} + (\mu + \lambda)\|\nabla \cdot \Phi\|_{H^1(\Omega)} \leq C\|\mathbf{e}_h^\circ\|_{\mathbf{L}^2(\Omega)}. \quad (3.41)$$

We test the dual equation against $\mathbf{v} \in V_h$ on an arbitrary element $E \in \mathcal{E}_h$ and apply integration by parts to obtain

$$-\mu\langle(\nabla\Phi)\mathbf{n}, \mathbf{v}^\circ\rangle_{E^\partial} - (\mu + \lambda)\langle(\nabla \cdot \Phi)\mathbf{n}, \mathbf{v}^\circ\rangle_{E^\partial} = (\mathbf{e}_h^\circ, \mathbf{v}^\circ)_E. \quad (3.42)$$

The normal continuity and boundary conditions of the dual solution together imply

$$\sum_{E \in \mathcal{E}_h} \langle(\nabla\Phi)\mathbf{n}, \mathbf{v}^\circ\rangle_{E^\partial} = 0, \quad \sum_{E \in \mathcal{E}_h} \langle(\nabla \cdot \Phi)\mathbf{n}, \mathbf{v}^\circ\rangle_{E^\partial} = 0. \quad (3.43)$$

Combined these yield

$$\sum_{E \in \mathcal{E}_h} (\mathbf{e}_h^\circ, \mathbf{v}^\circ)_E = \mu \sum_{E \in \mathcal{E}_h} \langle(\nabla\Phi)\mathbf{n}, \mathbf{v}^\circ - \mathbf{v}^\partial\rangle_{E^\partial} + (\mu + \lambda) \sum_{E \in \mathcal{E}_h} \langle(\nabla \cdot \Phi)\mathbf{n}, \mathbf{v}^\circ - \mathbf{v}^\partial\rangle_{E^\partial}. \quad (3.44)$$

Alternatively, applying Lemma 2.1 and Lemma 2.2, we have elementwise

$$\begin{aligned} & \mu(\nabla_w(\mathbf{Q}_h\Phi), \nabla_w\mathbf{v})_E + (\mu + \lambda)(\nabla_w \cdot (\mathbf{Q}_h\Phi), \nabla_w \cdot \mathbf{v})_E \\ &= \mu(\mathbf{Q}_h\nabla\Phi, \nabla_w\mathbf{v})_E + (\mu + \lambda)(\mathbf{Q}_h(\nabla \cdot \Phi), \nabla_w \cdot \mathbf{v})_E \\ &= \mu\langle(\mathbf{Q}_h\nabla\Phi)\mathbf{n}, \mathbf{v}^\circ - \mathbf{v}^\partial\rangle_{E^\partial} + (\mu + \lambda)\langle\mathbf{Q}_h(\nabla \cdot \Phi)\mathbf{n}, \mathbf{v}^\circ - \mathbf{v}^\partial\rangle_{E^\partial}. \end{aligned}$$

Over the entire mesh, we have

$$\begin{aligned} \mathcal{A}_h^{GD}(\mathbf{Q}_h \Phi, \mathbf{v}) &= \mu \sum_{E \in \mathcal{E}_h} \langle (\mathbf{Q}_h \nabla \Phi) \mathbf{n}, \mathbf{v}^\partial - \mathbf{v}^\circ \rangle_{E^\partial} \\ &+ (\mu + \lambda) \sum_{E \in \mathcal{E}_h} \langle Q_h(\nabla \cdot \Phi) \mathbf{n}, \mathbf{v}^\partial - \mathbf{v}^\circ \rangle_{E^\partial}. \end{aligned} \quad (3.45)$$

We now set $\mathbf{v} = \mathbf{e}_h$ in both (3.44) and (3.45), and perform a subtraction on both sides to obtain

$$\|\mathbf{e}_h^\circ\|^2 - \mathcal{A}_h^{GD}(\mathbf{Q}_h \Phi, \mathbf{e}_h) = \mu \mathcal{G}_1(\Phi, \mathbf{e}_h) + (\mu + \lambda) \mathcal{G}_2(\Phi, \mathbf{e}_h).$$

The symmetry in $\mathcal{A}_h^{GD}(\cdot, \cdot)$ leads to

$$\|\mathbf{e}_h^\circ\|^2 = \mathcal{A}_h^{GD}(\mathbf{e}_h, \mathbf{Q}_h \Phi) + \mu \mathcal{G}_1(\Phi, \mathbf{e}_h) + (\mu + \lambda) \mathcal{G}_2(\Phi, \mathbf{e}_h). \quad (3.46)$$

Similar to Lemma 3.4, we have immediately

$$\begin{aligned} |\mathcal{G}_1(\Phi, \mathbf{e}_h)| &\leq Ch \|\Phi\|_{\mathbf{H}^2(\Omega)} \|\mathbf{e}_h\|, \\ |\mathcal{G}_2(\Phi, \mathbf{e}_h)| &\leq Ch \|\nabla \cdot \Phi\|_{H^1(\Omega)} \|\mathbf{e}_h\|. \end{aligned}$$

The above two estimates combined with the dual regularity (3.41) imply

$$|\mu \mathcal{G}_1(\Phi, \mathbf{e}_h) + (\mu + \lambda) \mathcal{G}_2(\Phi, \mathbf{e}_h)| \leq Ch \|\mathbf{e}_h^\circ\| \|\mathbf{e}_h\|. \quad (3.47)$$

To estimate $\|\mathbf{e}_h\|$, we first set $\mathbf{v} = \mathbf{e}_h$ in (3.21) and then apply Lemmas 2.3, 3.3, and 3.4 to obtain

$$\|\mathbf{e}_h\| \leq Ch \|\mathbf{f}\|_{\mathbf{L}^2(\Omega)}, \quad (3.48)$$

where $C > 0$ is a constant independent of h and λ .

Applying Lemmas 3.3 and 3.4, and the regularity of the exact solution (3.5) yields

$$|\mathcal{A}_h^{GD}(\mathbf{e}_h, \mathbf{Q}_h \Phi)| \leq Ch \|\mathbf{f}\|_{\mathbf{L}^2(\Omega)} \|\mathbf{Q}_h \Phi\|.$$

Applying Lemmas 2.3, 2.1, the stability of the projection \mathbf{Q}_h and dual regularity, we have

$$\|\mathbf{Q}_h \Phi\| \lesssim \|\nabla_w(\mathbf{Q}_h \Phi)\| = \|\mathbf{Q}_h \nabla \Phi\| \leq \|\nabla \Phi\| \leq \|\Phi\|_{\mathbf{H}^2(\Omega)} \lesssim \|\mathbf{e}_h^\circ\|.$$

Combining the above two estimates gives

$$|\mathcal{A}_h^{GD}(\mathbf{e}_h, \mathbf{Q}_h \Phi)| \leq Ch \|\mathbf{f}\|_{\mathbf{L}^2(\Omega)} \|\mathbf{e}_h^\circ\|. \quad (3.49)$$

Finally, combining (3.46), (3.47), (3.48), and (3.49) yields the desired result. \square

Theorem 1 and 2 combined imply that for elasticity problems on rectangular meshes, the lowest-order WG finite element scheme $(Q_0^2, Q_0^2; RT_{[0]}^2, Q_0)$ has the following two properties.

- First order convergence in displacement, stress, and dilation (given full regularity of the exact solution);
- The convergence order does not deteriorate as $\lambda \rightarrow \infty$, i.e, the method is locking-free.

For elasticity problems with low regularity (see Section 3.6, Example 3.2), say, $\mathbf{u} \in \mathbf{H}^{1+s}(\Omega)$ with $s \in (0, 1)$, the method produces 1st order convergence in displacement and order s convergence in stress and dilation.

Remarks on the extension to quadrilateral and hexahedral meshes. It can be observed that the commuting identities in Lemma 2.1 play important roles in the error analysis. These identities demonstrate that the discrete weak gradient and the discrete weak divergence provide a good approximation to their classical counterparts.

Recall the definition of the discrete weak gradient,

$$\int_E (\nabla_w \mathbf{v}) : W = \int_{E^\partial} \mathbf{v}^\partial \cdot (W \mathbf{n}) - \int_{E^\circ} \mathbf{v}^\circ \cdot (\nabla \cdot W), \quad \forall W \in RT_{[0]}^2(E),$$

and Lemma 2.1

$$\nabla_w(\mathbf{Q}_h \mathbf{u}) = \mathbb{Q}_h(\nabla \mathbf{u}).$$

The above two quantities are expected to be in the same finite dimensional space, say, the local Raviart-Thomas space $RT_{[0]}^2(E)$ on a rectangle E , from which we take a typical test function W . By the definition of discrete weak gradient, the definition of the projection $\mathbf{Q}_h = \{\mathbf{Q}_h^\circ, \mathbf{Q}_h^\partial\}$, the definition of the projection \mathbb{Q}_h , and Gauss Divergence Theorem, we should have

$$\begin{aligned} \int_E \nabla_w(\mathbf{Q}_h \mathbf{u}) : W &= \int_{E^\partial} (\mathbf{Q}_h^\partial \mathbf{u}) \cdot (W \mathbf{n}) - \int_{E^\circ} (\mathbf{Q}_h^\circ \mathbf{u}) \cdot (\nabla \cdot W) \\ &\parallel \\ \int_E \mathbb{Q}_h(\nabla \mathbf{u}) : W & \\ &\parallel \\ \int_E (\nabla \mathbf{u}) : W &= \int_{E^\partial} \mathbf{u} \cdot W \mathbf{n} - \int_{E^\circ} \mathbf{u} \cdot (\nabla \cdot W). \end{aligned} \tag{3.50}$$

The 1st vertical equal sign holds due to the commuting property (Lemma 2.1). The 2nd vertical equal sign holds by the definition of the L^2 -projection \mathbb{Q}_h . This leads to **Matching Condition I** for (2.7), namely

- (i) $W \mathbf{n}$ (trace) lies in the same space as \mathbf{v}^∂ or in a subspace of this space (applicable to $\mathbf{Q}_h^\partial \mathbf{u}$);
- (ii) $\nabla \cdot W$ (div) lies in the same space as \mathbf{v}° or in a subspace of this space (applicable to $\mathbf{Q}_h^\circ \mathbf{u}$).

A similar analysis for Lemma 2.1 leads to **Matching Condition II** for (2.10), namely

- (i) The trace $w \mathbf{n}$ lies in the same space as \mathbf{v}^∂ or in a subspace of this space;
- (ii) The gradient ∇w lies in the same space as \mathbf{v}° or in a subspace of this space.

In this regard, for rectangles ($d = 2$) or bricks ($d = 3$), the $\mathbf{WG}(Q_0^d, Q_0^d; RT_{[0]}^d, Q_0)$ discretization is suitable.

The commuting identities in Lemma 2.1 while elegant, are not necessary conditions. Generally speaking, if the discrepancy between each pair of quantities is a higher order quantity of the mesh

size: $\mathcal{O}(h^{1+r})$ for some $r > 0$, then the error analysis in this section can still go through, although it will become more technically involved.

For the $\text{WG}(Q_0^2, Q_0^2)$ discrete weak functions on quadrilaterals, there are two ways for constructing a space for their discrete weak gradients:

- (i) Using the unmapped $RT_{[0]}^2$ space, for which the divergence $\nabla \cdot W$ is a constant vector, but the trace $W\mathbf{n}$ is not a constant vector;
- (ii) Using the mapped $RT_{[0]}^2$ space based on the Piola transform, for which $W\mathbf{n}$ (trace) is a constant vector, but $\nabla \cdot W$ (div) is not a constant vector [78].

A similar discussion applies to hexahedra. When the quadrilaterals are asymptotically parallelogram or the hexahedra are asymptotically parallelepiped, the aforementioned discrepancy will be a higher order quantity of the mesh size. Thus our finite element schemes can be extended to these types of quadrilateral and hexahedral meshes, see Section 6, Examples 3.3 and 3.5 for numerical results.

3.4 Implementation

We have implemented $\text{WG}(Q_0^2, Q_0^2; RT_{[0]}^2, Q_0)$ on quadrilateral meshes (including rectangular meshes as a special case) in our Matlab code package `DarcyLite`; and $\text{WG}(Q_0^3, Q_0^3; RT_{[0]}^3, Q_0)$ on hexahedral meshes (including brick meshes as a special case) in our code package `Darcy+`. For convenience, we use the normalized coordinates [68]

$$X = x - x_c, \quad Y = y - y_c, \quad Z = z - z_c,$$

since $\int_E X = 0, \int_E Y = 0, \int_E Z = 0$ on a rectangle or brick E .

3.4.1 Calculation of Numerical Stress on a Quadrilateral

Recall the eight basis functions $W_j (1 \leq j \leq 8)$ defined in (2.26). We now finish our discussion of discrete weak strain from Chapter 2, as we need the averages

$$\bar{W}_j = \frac{1}{2}(W_j + W_j^T)$$

for strain and stress calculations. Specifically, we have

$$\bar{W}_1 = \begin{bmatrix} 1 & 0 \\ 0 & 0 \end{bmatrix}, \quad \bar{W}_2 = \begin{bmatrix} 0 & \frac{1}{2} \\ \frac{1}{2} & 0 \end{bmatrix}, \quad \bar{W}_3 = \begin{bmatrix} X & 0 \\ 0 & 0 \end{bmatrix}, \quad \bar{W}_4 = \begin{bmatrix} 0 & \frac{Y}{2} \\ \frac{Y}{2} & 0 \end{bmatrix}, \quad (3.51)$$

$$\bar{W}_5 = \begin{bmatrix} 0 & \frac{1}{2} \\ \frac{1}{2} & 0 \end{bmatrix}, \quad \bar{W}_6 = \begin{bmatrix} 0 & 0 \\ 0 & 1 \end{bmatrix}, \quad \bar{W}_7 = \begin{bmatrix} 0 & \frac{X}{2} \\ \frac{X}{2} & 0 \end{bmatrix}, \quad \bar{W}_8 = \begin{bmatrix} 0 & 0 \\ 0 & Y \end{bmatrix}. \quad (3.52)$$

Let $\phi_i (1 \leq i \leq 10)$ be one of the ten $\text{WG}(Q_0^2, Q_0^2)$ basis functions on a quadrilateral and its discrete weak gradient be

$$\nabla_w \phi_i = \sum_{j=1}^8 c_{i,j} W_j, \quad 1 \leq i \leq 10.$$

Clearly, its discrete weak strain is

$$\varepsilon_w(\phi_i) = \sum_{j=1}^8 c_{i,j} \bar{W}_j, \quad 1 \leq i \leq 10.$$

Its discrete weak divergence is just a constant,

$$\nabla_w \cdot \phi_i = d_i, \quad 1 \leq i \leq 10.$$

The definition for discrete weak stress gives

$$\sigma = 2\mu \varepsilon_w(\phi_i) + \lambda d_i \mathbb{I}_2, \quad 1 \leq i \leq 10,$$

where \mathbb{I}_2 is the order 2 identity matrix. By direct calculations, we obtain the numerical stress corresponding to a single WG basis function $\phi_i (1 \leq i \leq 10)$ as

$$\left\{ \begin{array}{l} \sigma_{xx} = \sigma_{11} = (2\mu c_{i,1} + \lambda d_i) + 2\mu c_{i,3}X, \\ \sigma_{yy} = \sigma_{22} = (2\mu c_{i,6} + \lambda d_i) + 2\mu c_{i,8}Y, \\ \sigma_{xy} = \sigma_{12} = \mu(c_{i,2} + c_{i,5}) + \mu c_{i,7}X + \mu c_{i,4}Y, \\ \sigma_{yx} = \sigma_{21} = \sigma_{12}. \end{array} \right. \quad (3.53)$$

This also states that the normal stress σ_{11} is a linear function of only the first coordinate, the normal stress σ_{22} is a linear function of only the second coordinate, whereas the shear stress σ_{12} is a linear function of both coordinates. In this regard, our numerical stress has the same form as that obtained from the simplest nonconforming finite element method investigated in [47].

For graphical results involving elementwise averages of the stress components, we use (3.53) and numerical integration.

3.4.2 Calculation of Numerical Stress on a Hexahedron

In the same spirit, we consider the eighteen normalized basis functions $W_j(1 \leq j \leq 18)$ for $RT_{[0]}^3$ on a hexahedron. Their averages are

$$\bar{W}_1 = \begin{bmatrix} 1 & 0 & 0 \\ 0 & 0 & 0 \\ 0 & 0 & 0 \end{bmatrix}, \quad \bar{W}_2 = \begin{bmatrix} 0 & \frac{1}{2} & 0 \\ \frac{1}{2} & 0 & 0 \\ 0 & 0 & 0 \end{bmatrix}, \quad \bar{W}_3 = \begin{bmatrix} 0 & 0 & \frac{1}{2} \\ 0 & 0 & 0 \\ \frac{1}{2} & 0 & 0 \end{bmatrix}, \quad (3.54)$$

$$\bar{W}_4 = \begin{bmatrix} X & 0 & 0 \\ 0 & 0 & 0 \\ 0 & 0 & 0 \end{bmatrix}, \quad \bar{W}_5 = \begin{bmatrix} 0 & \frac{Y}{2} & 0 \\ \frac{Y}{2} & 0 & 0 \\ 0 & 0 & 0 \end{bmatrix}, \quad \bar{W}_6 = \begin{bmatrix} 0 & 0 & \frac{Z}{2} \\ 0 & 0 & 0 \\ \frac{Z}{2} & 0 & 0 \end{bmatrix}, \quad (3.55)$$

$$\bar{W}_7 = \begin{bmatrix} 0 & \frac{1}{2} & 0 \\ \frac{1}{2} & 0 & 0 \\ 0 & 0 & 0 \end{bmatrix}, \quad \bar{W}_8 = \begin{bmatrix} 0 & 0 & 0 \\ 0 & 1 & 0 \\ 0 & 0 & 0 \end{bmatrix}, \quad \bar{W}_9 = \begin{bmatrix} 0 & 0 & 0 \\ 0 & 0 & \frac{1}{2} \\ 0 & \frac{1}{2} & 0 \end{bmatrix}, \quad (3.56)$$

$$\bar{W}_{10} = \begin{bmatrix} 0 & \frac{X}{2} & 0 \\ \frac{X}{2} & 0 & 0 \\ 0 & 0 & 0 \end{bmatrix}, \quad \bar{W}_{11} = \begin{bmatrix} 0 & 0 & 0 \\ 0 & Y & 0 \\ 0 & 0 & 0 \end{bmatrix}, \quad \bar{W}_{12} = \begin{bmatrix} 0 & 0 & 0 \\ 0 & 0 & \frac{Z}{2} \\ 0 & \frac{Z}{2} & 0 \end{bmatrix}, \quad (3.57)$$

$$\bar{W}_{13} = \begin{bmatrix} 0 & 0 & \frac{1}{2} \\ 0 & 0 & 0 \\ \frac{1}{2} & 0 & 0 \end{bmatrix}, \quad \bar{W}_{14} = \begin{bmatrix} 0 & 0 & 0 \\ 0 & 0 & \frac{1}{2} \\ 0 & \frac{1}{2} & 0 \end{bmatrix}, \quad \bar{W}_{15} = \begin{bmatrix} 0 & 0 & 0 \\ 0 & 0 & 0 \\ 0 & 0 & 1 \end{bmatrix}, \quad (3.58)$$

$$\bar{W}_{16} = \begin{bmatrix} 0 & 0 & \frac{X}{2} \\ 0 & 0 & 0 \\ \frac{X}{2} & 0 & 0 \end{bmatrix}, \quad \bar{W}_{17} = \begin{bmatrix} 0 & 0 & 0 \\ 0 & 0 & \frac{Y}{2} \\ 0 & \frac{Y}{2} & 0 \end{bmatrix}, \quad \bar{W}_{18} = \begin{bmatrix} 0 & 0 & 0 \\ 0 & 0 & 0 \\ 0 & 0 & Z \end{bmatrix}. \quad (3.59)$$

Similarly, let $\phi_i (1 \leq i \leq 21)$ be a $\text{WG}(Q_0^3, Q_0^3)$ basis function. Assume its discrete weak gradient and discrete weak divergence are respectively

$$\nabla_w \phi_i = \sum_{j=1}^{18} c_{i,j} W_j, \quad \nabla_w \cdot \phi_i = d_i, \quad 1 \leq i \leq 21.$$

Then its discrete weak stress is

$$\sigma_{w,d}(\phi_i) = 2\mu \sum_{j=1}^{18} c_{i,j} \bar{W}_j + \lambda d_i \mathbb{I}_3, \quad 1 \leq i \leq 21.$$

The components of the stress tensor are (see [47] also)

$$\left\{ \begin{array}{l} \sigma_{xx} = (2\mu c_{i,1} + \lambda d_i) + 2\mu c_{i,4} X, \\ \sigma_{yy} = (2\mu c_{i,8} + \lambda d_i) + 2\mu c_{i,11} Y, \\ \sigma_{zz} = (2\mu c_{i,15} + \lambda d_i) + 2\mu c_{i,18} Z, \\ \sigma_{xy} = \mu(c_{i,2} + c_{i,7}) + \mu c_{i,10} X + \mu c_{i,5} Y, \\ \sigma_{xz} = \mu(c_{i,3} + c_{i,13}) + \mu c_{i,16} X + \mu c_{i,6} Z, \\ \sigma_{yz} = \mu(c_{i,9} + c_{i,14}) + \mu c_{i,17} Y + \mu c_{i,12} Z. \end{array} \right. \quad (3.60)$$

3.4.3 Block Diagonal Schur Complement

A salient feature of WGFEMs is the non-interaction between the basis functions defined in the interiors of different elements in the mesh. This motivates the use of Schur complement when solving the discrete linear system resulting from (3.8) or (3.12).

For ease of presentation, we assume the aforementioned linear system is partitioned as follows

$$\begin{bmatrix} \mathbf{A}_{00} & \mathbf{A}_{01} \\ \mathbf{A}_{10} & \mathbf{A}_{11} \end{bmatrix} \begin{bmatrix} \mathbf{x}_0 \\ \mathbf{x}_1 \end{bmatrix} = \begin{bmatrix} \mathbf{b}_0 \\ \mathbf{b}_1 \end{bmatrix}, \quad (3.61)$$

where label 0 refers to the degrees of freedom (DOFs) in element interiors, and label 1 refers to the DOFs on element interfaces.

The first equation

$$\mathbf{A}_{00} \mathbf{x}_0 + \mathbf{A}_{01} \mathbf{x}_1 = \mathbf{b}_0$$

can be easily solved as

$$\mathbf{x}_0 = \mathbf{A}_{00}^{-1} (\mathbf{b}_0 - \mathbf{A}_{01} \mathbf{x}_1), \quad (3.62)$$

based on the assumption that \mathbf{A}_{00} is invertible and \mathbf{x}_1 is available.

Substituting the above solution into the 2nd equation in (3.61) produces

$$\left(\mathbf{A}_{11} - \mathbf{A}_{10}\mathbf{A}_{00}^{-1}\mathbf{A}_{01}\right) \mathbf{x}_1 = \mathbf{b}_1 - \mathbf{A}_{10}\mathbf{A}_{00}^{-1}\mathbf{b}_0, \quad (3.63)$$

which concerns only the unknown \mathbf{x}_1 and has a smaller size than the original linear system. Here $\widehat{\mathbf{A}}_{11} = \mathbf{A}_{11} - \mathbf{A}_{10}\mathbf{A}_{00}^{-1}\mathbf{A}_{01}$ is called the Schur complement (matrix) of the original partitioned coefficient matrix in (3.61).

Usually, the Schur complement matrix is not formed explicitly, since it can be expensive to compute. An iterative solver for (3.63) mainly requires the matrix-vector multiplication

$$\widehat{\mathbf{A}}_{11} \mathbf{v} = \mathbf{A}_{11}\mathbf{v} - \mathbf{A}_{10}\mathbf{A}_{00}^{-1}\mathbf{A}_{01}\mathbf{v}.$$

This corresponds to four matrix-vector multiplications and one vector subtraction. For WG FEMs, \mathbf{A}_{00} is a block diagonal matrix where each block is a small-size SPD matrix, hence \mathbf{A}_{00}^{-1} can be pre-computed. For an elasticity problem using the $\text{WG}(Q_0^3, Q_0^3; RT_{[0]}^3, Q_0)$ lowest-order method on a brick or hexahedral mesh, \mathbf{A}_{00} is a block diagonal matrix where each block is a 3×3 SPD matrix. Its inverse can be obtained using Cholesky factorization.

3.5 A Related Method: $\text{WG}(P_1^2, P_{rm}; P_0^{2 \times 2}, P_0)$ With Stabilization

In [20], a family of WG finite element schemes were developed for general polygonal and polyhedral meshes, from which we can derive a particular WG method on rectangular meshes: $\text{WG}(P_1^2, P_{rm}; P_0^{2 \times 2}, P_0)$, where P_1^2 means linear vector-valued polynomials are used for element interiors, and P_{rm} means the edgewise space of rigid motions ($\dim(P_{rm}) = 3$). Elementwise there are 18 degrees of freedom for each rectangle. For these WG basis functions, however, their

discrete weak gradients are just constant 2×2 matrices, and their discrete weak divergences are also constants.

Here is a brief list for comparison. Our method

- does not require stabilization,
- uses fewer degrees of freedom,
- achieves first-order convergence in displacement, stress, and dilation.

The $\text{WG}(P_1^2, P_{rm}; P_0^{2 \times 2}, P_0)$ method derived from [20]

- requires stabilization,
- has 2nd order convergence in displacement but only 1st order in stress and dilation,
- can be applied to general polygonal meshes.

Overall, our approach is simpler and more suited for a the specific quadrilateral/hexahedral case, but it does not obtain the 2nd order convergence in displacement seen in [20].

3.6 Numerical Results

In this section we present numerical experiments for these solvers for linear elasticity on rectangular and brick meshes. We include also numerical results on asymptotically parallelogram quadrilateral (parallelepiped hexahedral) meshes. We observe the expected locking-free property and optimal order convergence in displacement, stress, and dilation. The performance of the computational approach using the Schur complement is also examined. In addition to uniform rectangular and brick meshes, we use also graded rectangular meshes and asymptotically parallelogram trapezoidal meshes (Figure 1).

Example 3.1 (Locking-free). This example is a variant of Example 1 in [79]. Specifically, the domain is $\Omega = (0, 1)^2$, a Neumann condition is posed on the right boundary of the domain, whereas

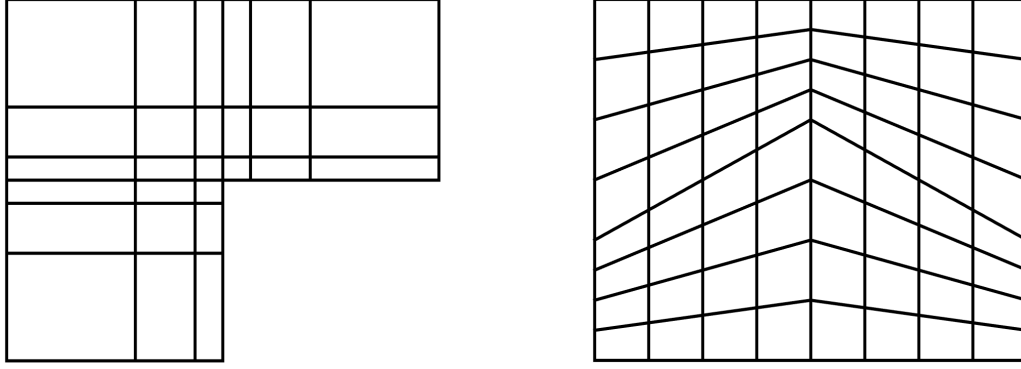


Figure 3.1: Some meshes used in numerical experiments: *Left:* An initial graded mesh used in Example 3.2 Case II; *Right:* An initial trapezoidal mesh used in Example 3.3 (see [1] also).

Table 3.1: Example 3.1 Case I ($\lambda = 1.6644 \times 10^2$): $\text{WG}(Q_0^2, Q_0^2; RT_{[0]}, Q_0)$ on rectangular meshes

$1/h$	$\ \mathbf{u} - \mathbf{u}_h^o\ $	$\ \sigma - \sigma_h\ $	$\ \nabla \cdot \mathbf{u} - \nabla_w \cdot \mathbf{u}_h\ $
8	2.5288e-01	6.6770e-01	2.1689e-03
16	1.2609e-01	3.2291e-01	1.0745e-03
32	6.2981e-02	1.6009e-01	5.3561e-04
64	3.1482e-02	8.0209e-02	2.6756e-04
Conv.rate	1st order	1st order	1st order

the other three sides have Dirichlet conditions. The known exact solution for displacement is

$$\mathbf{u}(x, y) = \begin{bmatrix} (\pi/2) \sin^2(\pi x) \sin(2\pi y) \\ -(\pi/2) \sin(2\pi x) \sin^2(\pi y) \end{bmatrix} + \frac{1}{\lambda} \begin{bmatrix} \sin(\pi x) \sin(\pi y) \\ \sin(\pi x) \sin(\pi y) \end{bmatrix},$$

and hence

$$\nabla \cdot \mathbf{u} = \frac{\pi}{\lambda} \cos(\pi(x+y)) = \frac{(1+\nu)(1-2\nu)}{E\nu} \pi \cos(\pi(x+y)).$$

It is clear that $\nabla \cdot \mathbf{u} \neq 0$ if $\nu \in (0, \frac{1}{2})$, and $\nabla \cdot \mathbf{u} = 0$ if $\nu = \frac{1}{2}$.

Numerical results for $\text{WG}(Q_0^2, Q_0^2; RT_{[0]}, Q_0)$ on rectangular meshes are shown in Tables 3.1 & 3.2. The convergence rates in displacement, stress, and dilation are demonstrably first order for two different values of λ that are six orders of magnitude apart.

Table 3.2: Example 3.1 Case II ($\lambda = 1.667 \times 10^8$): $\text{WG}(Q_0^2, Q_0^2; RT_{[0]}, Q_0)$ on rectangular meshes

$1/h$	$\ \mathbf{u} - \mathbf{u}_h^\circ\ $	$\ \sigma - \sigma_h\ $	$\ \nabla \cdot \mathbf{u} - \nabla_w \cdot \mathbf{u}_h\ $
8	2.5289e-01	6.6702e-01	2.1665e-09
16	1.2609e-01	3.2245e-01	1.0731e-09
32	6.2981e-02	1.5967e-01	5.3491e-10
64	3.1482e-02	7.9625e-02	2.6721e-10
Conv.rate	1st order	1st order	1st order

Example 3.2 (Low-regularity). This example is derived from [80]. The problem is posed on a Γ -shaped domain $\Omega = (-1, 1)^2 \setminus ([0, 1] \times [-1, 0])$ with a body force $\mathbf{f} = \mathbf{0}$. The known analytical solution for displacement in Cartesian coordinates is

$$\mathbf{u} = \left[A \cos \theta - B \sin \theta, A \sin \theta + B \cos \theta \right]^T =: [C, D]^T, \quad (3.64)$$

where (r, θ) are the polar coordinates and

$$\begin{cases} A = \frac{r^\alpha}{2\mu} \left(-(1 + \alpha) \cos((1 + \alpha)\theta) + C_1(C_2 - 1 - \alpha) \cos((1 - \alpha)\theta) \right), \\ B = \frac{r^\alpha}{2\mu} \left((1 + \alpha) \sin((1 + \alpha)\theta) - C_1(C_2 - 1 + \alpha) \sin((1 - \alpha)\theta) \right). \end{cases} \quad (3.65)$$

Here $\alpha \approx 0.544483737$ is the so-called *critical exponent*.

We present further details about the exact solution that were not provided in the original paper [80]. The dilation is

$$\nabla \cdot \mathbf{u} = \partial_r A + (\partial_\theta B)/r + A/r, \quad (3.66)$$

where

$$\begin{cases} \partial_r A = A \frac{\alpha}{r}, & \partial_r B = B \frac{\alpha}{r}, \\ \partial_\theta A = \frac{r^\alpha}{2\mu} \left((1 + \alpha)^2 \sin((1 + \alpha)\theta) - C_1(C_2 - 1 - \alpha)(1 - \alpha) \sin((1 - \alpha)\theta) \right), \\ \partial_\theta B = \frac{1}{2\mu} r^\alpha \left((1 + \alpha)^2 \cos((1 + \alpha)\theta) - C_1(C_2 - 1 + \alpha)(1 - \alpha) \cos((1 - \alpha)\theta) \right). \end{cases} \quad (3.67)$$

Table 3.3: Example 3.2 Case I ($\nu = 0.3$): Lowest-order WG on uniform rectangular meshes

$1/h$	$\ \mathbf{u} - \mathbf{u}_h^\circ\ $	$\ \sigma - \sigma_h\ $	$\ \nabla \cdot \mathbf{u} - \nabla_w \cdot \mathbf{u}_h\ $
8	3.5814e-06	7.4745e-01	4.0348e-06
16	1.7968e-06	5.1626e-01	2.7822e-06
32	8.9935e-07	3.5529e-01	1.9134e-06
64	4.4972e-07	2.4407e-01	1.3141e-06
128	2.2480e-07	1.6751e-01	9.0181e-07
Conv.rate	0.998	0.539	0.540

The stress is

$$\sigma = \begin{bmatrix} 2\mu(\partial_x C) + \lambda(\nabla \cdot \mathbf{u}) & \mu(\partial_y C + \partial_x D) \\ \mu(\partial_y C + \partial_x D) & 2\mu(\partial_y D) + \lambda(\nabla \cdot \mathbf{u}) \end{bmatrix}, \quad (3.68)$$

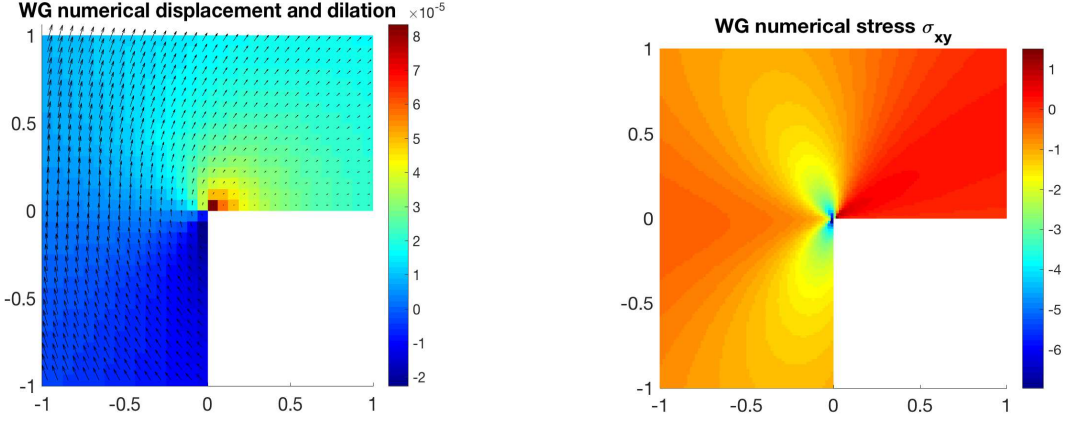
where

$$\left\{ \begin{array}{l} \partial_x C = (\partial_r A) \cos^2 \theta - (\partial_\theta A) \frac{\cos \theta \sin \theta}{r} + A \frac{\sin^2 \theta}{r} \\ \quad - (\partial_r B) \cos \theta \sin \theta + (\partial_\theta B) \frac{\sin^2 \theta}{r} + B \frac{\cos \theta \sin \theta}{r}, \\ \partial_y D = (\partial_r A) \sin^2 \theta + (\partial_\theta A) \frac{\cos \theta \sin \theta}{r} + A \frac{\cos^2 \theta}{r} \\ \quad + (\partial_r B) \cos \theta \sin \theta + (\partial_\theta B) \frac{\cos^2 \theta}{r} - B \frac{\cos \theta \sin \theta}{r}, \\ \partial_y C + \partial_x D = (\partial_r A) \sin(2\theta) + (\partial_\theta A) \frac{\cos(2\theta)}{r} - A \frac{\sin(2\theta)}{r} \\ \quad + (\partial_r B) \cos(2\theta) - (\partial_\theta B) \frac{\sin(2\theta)}{r} - B \frac{\cos(2\theta)}{r}. \end{array} \right. \quad (3.69)$$

We choose $E = 10^5$, $\nu = 0.3$ (Case I) or $\nu = 0.49999$ (Case II).

For Case I ($\nu = 0.3$), Table 3.3 shows the numerical results of the $\text{WG}(Q_0, Q_0; RT_{[0]}^2, Q_0)$ lowest-order method applied to a family of rectangular meshes. The displacement error has first order convergence, whereas the stress and dilation errors have convergence rates of approximately 0.54, close to the critical exponent α . The singularity at the origin is also clearly reflected in the profiles of the numerical dilation and stress shown in Figure 3.2.

For Case II ($\nu = 0.49999$), we utilize graded meshes [81]. An initial mesh is shown in Figure 1 left panel, which has three partitions for the boundary segments connecting $(0, 0)$ to $(1, 0)$ or $(0, 0)$ to $(0, -1)$. Successive regular refinements are performed. The results in Table 4 indicate that our



Numerical displacement and dilation for $h = \frac{1}{16}$ Numerical shear stress σ_{xy} for $h = \frac{1}{64}$

Figure 3.2: Example 3.2 Case I ($\nu = 0.3$): Low-regularity captured by the lowest-order WG method on rectangular meshes

Table 3.4: Example 3.2 Case II ($\nu = 0.49999$): Lowest-order WG on graded rectangular meshes

refinements	$\ \mathbf{u} - \mathbf{u}_h^\circ\ $	rate	$\ \sigma - \sigma_h\ $	rate	$\ \nabla \cdot \mathbf{u} - \nabla_w \cdot \mathbf{u}_h\ $	rate
2	2.5254e-06	—	4.0880e-01	—	1.3870e-10	—
3	1.2630e-06	0.99	2.6754e-01	0.61	8.8424e-11	0.64
4	6.3149e-07	1.00	1.7960e-01	0.57	5.8522e-11	0.59
5	3.1571e-07	1.00	1.2189e-01	0.55	3.9426e-11	0.56
6	1.5784e-07	1.00	8.3149e-02	0.55	2.6792e-11	0.55

WG method handles the dual challenges of a corner singularity and near-incompressibility very well, since the convergence rates for displacement, stress and dilation are essentially unchanged from the case when $\nu = 0.3$.

Example 3.3. For this example adopted from [47], the domain is $\Omega = (0, 1)^2$, and the Lamé constants are $\lambda = 1$ and $\mu = 0.5$. A homogeneous Dirichlet boundary condition is specified on the entire boundary. The known analytical solution for displacement is $\mathbf{u} = [4x(1 - x)y(1 - y), -4x(1 - x)y(1 - y)]^T$.

Numerical results using $\text{WG}(Q_0^2, Q_0^2; RT_{[0]}^2, Q_0)$ on rectangular meshes and asymptotically parallelogram trapezoidal meshes adopted from [1] are shown in Table 3.5. These demonstrate first order convergence in displacement, stress, and dilation for both types of meshes.

Example 3.4 (Comparison with $\text{WG}(P_1^2, P_{rm}; P_0^{2 \times 2}, P_0)$ method). This example is directly taken from [20] p. 359 testcase 9.3. In particular, $\Omega = (0, 1)^2$, $\lambda = 1$, $\mu = 0.5$.

Table 3.5: Example 3.3: Results of $\text{WG}(Q_0^2, Q_0^2; RT_{[0]}^2, Q_0)$ on rectangular meshes and asymptotically parallelogram trapezoidal meshes adopted from [1]

Rectangular meshes			
$1/h$	$\ \mathbf{u} - \mathbf{u}_h^\circ\ $	$\ \sigma - \sigma_h\ $	$\ \nabla \cdot \mathbf{u} - \nabla_w \cdot \mathbf{u}_h\ $
2^3	3.032e-02	1.547e-01	1.002e-01
2^4	1.520e-02	7.752e-02	5.038e-02
2^5	7.605e-03	3.878e-02	2.522e-02
2^6	3.803e-03	1.939e-02	1.261e-02
Rate	1st order	1st order	1st order
Asymp. parallelogram trapezoidal meshes			
$1/h$	$\ \mathbf{u} - \mathbf{u}_h^\circ\ $	$\ \sigma - \sigma_h\ $	$\ \nabla \cdot \mathbf{u} - \nabla_w \cdot \mathbf{u}_h\ $
2^3	3.106e-02	1.762e-01	1.046e-01
2^4	1.556e-02	8.756e-02	5.248e-02
2^5	7.784e-03	4.368e-02	2.625e-02
2^6	3.892e-03	2.182e-02	1.312e-02
Rate	1st order	1st order	1st order

Numerical results for the $\text{WG}(Q_0^2, Q_0^2; RT_{[0]}^2, Q_0)$ method developed in this chapter and for the $\text{WG}(P_1^2, P_{rm}; P_0^{2 \times 2}, P_0)$ method with $\rho = 1$ derived from [20] are shown in Table 3.6 for a sequence of rectangular meshes. As expected, the lowest-order WG method derived in this chapter exhibits first order convergence in displacement and stress. For the WG method derived in [20], the displacement has 2nd order convergence, since linear polynomials are used for approximation. However, its stress has only 1st order convergence, since the discrete weak gradient is in $P_0^{2 \times 2}$ and the discrete weak divergence is in P_0 . For both WG methods, numerical dilation exhibit superconvergence. However, this phenomena is specific to this example and the theoretical convergence rates are just one.

Example 3.5 (Schur complement). For this three-dimensional example, $\Omega = (0, 1)^3$, $\lambda = \mu = 1$, the known exact solution for displacement is

$$\mathbf{u} = \frac{1}{3\pi} \begin{bmatrix} \sin(\pi x) \cos(\pi y) \cos(\pi z) \\ \cos(\pi x) \sin(\pi y) \cos(\pi z) \\ \cos(\pi x) \cos(\pi y) \sin(\pi z) \end{bmatrix}. \quad (3.70)$$

Accordingly, the dilation is

Table 3.6: Example 3.4: Results of two WG methods on rectangular meshes

WG ($Q_0^2, Q_0^2; RT_{[0]}^2, Q_0$)			
$1/h$	$\ \mathbf{u} - \mathbf{u}_h^\circ\ $	$\ \sigma - \sigma_h\ $	$\ \nabla \cdot \mathbf{u} - \nabla_w \cdot \mathbf{u}_h\ $
2^3	6.029e-02	2.823e-02	1.104e-03
2^4	3.015e-02	1.404e-02	3.132e-04
2^5	1.507e-02	7.011e-03	8.648e-05
2^6	7.538e-03	3.504e-03	2.347e-05
Rate	1st order	1st order	≈ 1.85
WG ($P_1^2, P_{rm}; P_0^{2 \times 2}, P_0$) with $\rho = 1$			
$1/h$	$\ \mathbf{u} - \mathbf{u}_h^\circ\ $	$\ \sigma - \sigma_h\ $	$\ \nabla \cdot \mathbf{u} - \nabla_w \cdot \mathbf{u}_h\ $
2^3	5.750e-03	4.489e-02	6.621e-03
2^4	1.483e-03	2.082e-02	2.087e-03
2^5	3.746e-04	1.007e-02	6.093e-04
2^6	9.394e-05	4.980e-03	1.711e-04
Rate	2nd order	1st order	≈ 1.75

Table 3.7: Example 3.5: Lowest-order WG solver on hexahedral meshes: Single-matrix approach

$1/h$	$\ \mathbf{u} - \mathbf{u}_h^\circ\ $	$\ \sigma - \sigma_h\ $	$\ \nabla \cdot \mathbf{u} - \nabla_w \cdot \mathbf{u}_h\ $	DOFs	#ltr
4	2.488e-02	3.557e-01	1.361e-01	912	116
8	1.289e-02	1.875e-01	7.034e-02	6720	312
16	6.552e-03	9.564e-02	3.574e-02	51456	706
32	3.291e-03	4.795e-02	1.793e-02	402432	1415
64	1.648e-03	2.398e-02	8.968e-03	3182592	2748
Rate	0.97	0.97	0.98		

$$\nabla \cdot \mathbf{u} = \cos(\pi x) \cos(\pi y) \cos(\pi z). \quad (3.71)$$

The body force is $\mathbf{f} = 6\pi^2(\lambda + 2\mu)\mathbf{u}$ and the exact stress is

$$\sigma = \begin{bmatrix} \sigma_{xx} & \sigma_{xy} & \sigma_{xz} \\ \sigma_{yx} & \sigma_{yy} & \sigma_{yz} \\ \sigma_{zx} & \sigma_{zy} & \sigma_{zz} \end{bmatrix},$$

where

Table 3.8: Example 3.5: Lowest-order WG on hexahedral meshes: Schur-complement approach

$1/h$	$\ \mathbf{u} - \mathbf{u}_h^\circ\ $	$\ \sigma - \sigma_h\ $	$\ \nabla \cdot \mathbf{u} - \nabla_w \cdot \mathbf{u}_h\ $	DOFs	#Itr
4	2.488e-02	3.557e-01	1.361e-01	720	69
8	1.289e-02	1.875e-01	7.034e-02	5184	168
16	6.552e-03	9.564e-02	3.574e-02	39168	352
32	3.291e-03	4.795e-02	1.793e-02	304128	659
64	1.648e-03	2.398e-02	8.968e-03	2396160	1292
Rate	0.97	0.97	0.98		

$$\left\{ \begin{array}{l} \sigma_{xx} = \sigma_{yy} = \sigma_{zz} = (3\lambda + 2\mu)/3 \cos(\pi x) \cos(\pi y) \cos(\pi z), \\ \sigma_{xy} = (-2\mu/3) \sin(\pi x) \sin(\pi y) \cos(\pi z), \\ \sigma_{xz} = (-2\mu/3) \sin(\pi x) \cos(\pi y) \sin(\pi z), \\ \sigma_{yz} = (-2\mu/3) \cos(\pi x) \sin(\pi y) \sin(\pi z). \end{array} \right. \quad (3.72)$$

This problem is solved using $\text{WG}(Q_0^3, Q_0^3; RT_{[0]}^3, Q_0)$ on a sequence of hexahedral meshes adopted from [82], which are smooth perturbations of brick meshes. Specifically, the hexahedral mesh nodes are

$$\left\{ \begin{array}{l} x = \hat{x} + 0.03 \sin(3\pi\hat{x}) \cos(3\pi\hat{y}) \cos(3\pi\hat{z}), \\ y = \hat{y} - 0.04 \cos(3\pi\hat{x}) \sin(3\pi\hat{y}) \cos(3\pi\hat{z}), \\ z = \hat{z} + 0.05 \sin(3\pi\hat{x}) \cos(3\pi\hat{y}) \sin(3\pi\hat{z}), \end{array} \right.$$

where $(\hat{x}, \hat{y}, \hat{z})$ are the brick mesh nodes. Both single-matrix and Schur-complement approaches are tested. As shown in Tables 3.7 and 3.8, the errors in displacement, stress, and dilation are the same, since two equivalent discrete linear systems are solved. However, it can be observed that the numbers of iterations for the Schur-complement approach are about half of those for the single-matrix approach. Additionally, the Schur-complement approach has the advantage that there are approaches to compute it without forming the block matrix first, which makes it beneficial for large problems which may be memory-bound on some machines.

Example 3.6 (A nearly incompressible block under compression). This example is taken from [83]. An elastic body has elasticity modulus $E = 240.56595979$ and Poisson's ratio $\nu = 0.499899987$, respectively. Accordingly, its Lamé constants are $\lambda = 4.00837688 * 10^5$ and $\mu =$

8.0194×10^1 . This brick-shaped body is under compression on the middle part of its two opposite surfaces. Utilizing symmetry, we consider the top-upper-right octant of the brick domain and set the origin at the center to give an elasticity problem posed on the unit cube $\Omega = (0, 1)^3$, see Figure 3.3 left panel. The symmetry implies that for the displacement $\mathbf{u} = [u_1, u_2, u_3]^T$, we have $u_1 = 0$ on the left face $x = 0$, $u_2 = 0$ on the back face $y = 0$, $u_3 = 0$ on the bottom face $z = 0$. A constant downward traction $[0, 0, -1]^T$ (point-wise) is posed on $(0, \frac{1}{2})^2 \times \{z = 1\}$. No analytical solution is available for this problem.

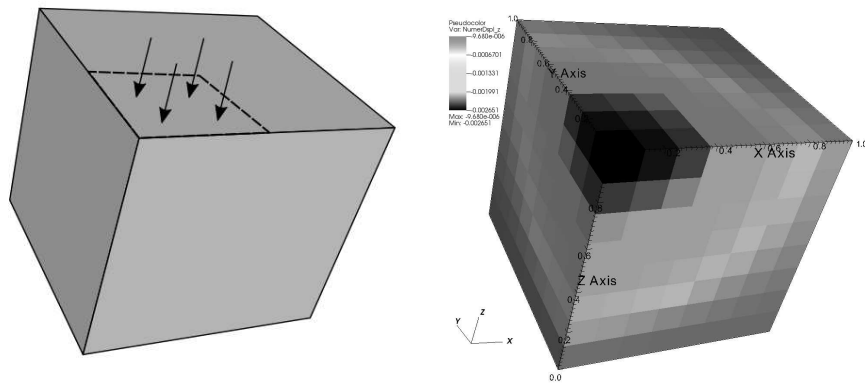


Figure 3.3: Example 3.6: A nearly incompressible block under compression. *Left:* An illustration for the problem; *Right:* A profile of the vertical displacement (z -component) obtained from using $\text{WG}(Q_0^3, Q_0^3; RT_{[0]}^3, Q_0)$ with $h = 1/8$.

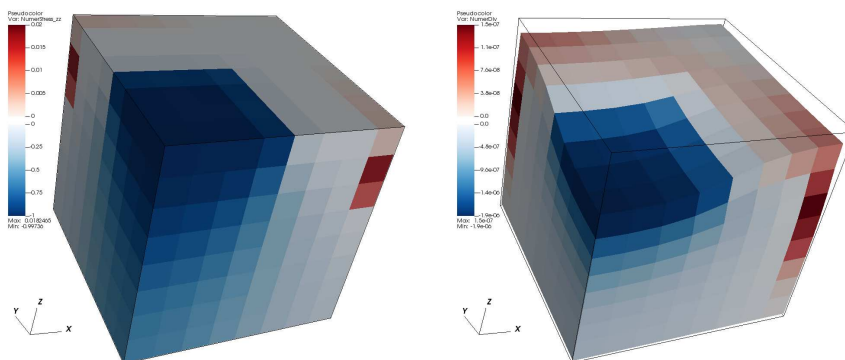


Figure 3.4: Example 3.6: $\text{WG}(Q_0^3, Q_0^3; RT_{[0]}^3, Q_0)$ applied with $h = 1/8$. *Left:* Profile of elementwise normal stress σ_{zz} ; *Right:* Elementwise dilation and deformation magnified 100 times. Plots were produced using `visit` [2]. Note the positive and negative scales are not equal.

We apply the lowest-order $\text{WG}(Q_0^3, Q_0^3; RT_{[0]}^3, Q_0)$ finite element method on a uniform $8 \times 8 \times 8$ brick mesh. The normal stress σ_{zz} is shown Figure 3.4 left panel. The numerical dilation and deformation using the displacement values in element interiors is shown in the right panel of Figure 3.4. The deformation was magnified by 100 times for better visual effect. It can be clearly observed that the external faces $\{x = 1\}$ and $\{y = 1\}$ are deformed inwards, while the top face (lower-left part) is being deformed downwards. The lowest-order weak Galerkin method is therefore able to capture the main features of this problem on even a very coarse mesh.

3.7 Summary

Our work is closely related to that in [47] in terms of seeking a simple method. Here is a brief comparison. The method in [47]:

- is in the mixed formulation and results in a saddle-point problem,
- has fewer DOFs per element: 9 in two dimensions and 18 in three dimensions,
- is 1st order accurate in displacement and stress.

Our methods

- are in primal formulation for displacement, resulting in SPD linear systems,
- have slightly more DOFs per element: 10 in two dimensions and 21 in three dimensions,
- are 1st order accurate in displacement, stress, and dilation,
- are extendable to quadrilateral and hexahedral meshes.

Our methods apply to asymptotically parallelogram (parallelepiped) quadrilateral (hexahedral) meshes. This assumption on mesh quality is not really a severe restriction, since a polygonal domain can be partitioned into a family of asymptotically parallelogram quadrilateral meshes [1]. Similarly, a polyhedral domain can be partitioned into a family of asymptotically parallelepiped hexahedral meshes by nested refinement [84]. We additionally discuss potential extensions and higher-order methods for this chapter's finite element methods in Chapter 5.

Chapter 4

Stokes-Darcy Coupling

4.1 Introduction and Notation

Let $\Omega^{\mathcal{D}}, \Omega^{\mathcal{S}} \in \mathbb{R}^d$ ($d = 2, 3$) be two open domains of Darcy and Stokes flow, respectively, which share a $(d - 1)$ dimensional interface $\Gamma^{\mathcal{I}} := \overline{\Omega^{\mathcal{D}}} \cup \overline{\Omega^{\mathcal{S}}}$. To tie back the application of flow over a riverbed, we will often depict the Stokes domain above the Darcy domain as in Figure 4.1.

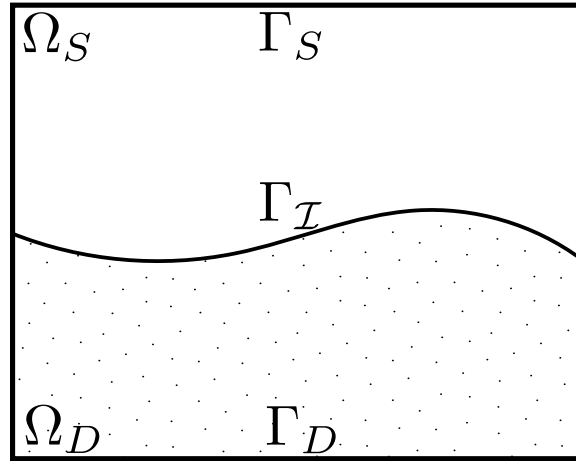


Figure 4.1: An example of the Stokes-Darcy configuration for $d = 2$.

Suppose that each domain has its own respective Dirichlet and Neumann conditions so furthermore $\partial\Omega^{\mathcal{D}}$ may be partitioned as $\partial\Omega^{\mathcal{D}} = \Gamma_D^{\mathcal{D}} \cup \Gamma_N^{\mathcal{D}} \cup \Gamma^{\mathcal{I}}$ and similarly, $\partial\Omega^{\mathcal{S}}$ may be partitioned as $\partial\Omega^{\mathcal{S}} = \Gamma_D^{\mathcal{S}} \cup \Gamma_N^{\mathcal{S}} \cup \Gamma^{\mathcal{I}}$. Given a permeability tensor \mathbf{K} which is uniformly SPD on $\Omega^{\mathcal{D}}$, a source term $f^{\mathcal{D}} \in L^2(\Omega^{\mathcal{D}})$, and boundary conditions $p_D^{\mathcal{D}}, \mathbf{u}_N^{\mathcal{D}}$, the goal of the Darcy equation is to find pressure $p^{\mathcal{D}} \in H^2(\Omega_D)$ so that

$$\begin{cases} \nabla \cdot (-\mathbf{K}\nabla p^{\mathcal{D}}) = f^{\mathcal{D}} & \text{in } \Omega^{\mathcal{D}}, \\ p^{\mathcal{D}} = p_D^{\mathcal{D}} & \text{on } \Gamma_D^{\mathcal{D}}, \\ (-\mathbf{K}\nabla p^{\mathcal{D}}) \cdot \mathbf{n} = u_N^{\mathcal{D}} & \text{on } \Gamma_N^{\mathcal{D}}. \end{cases}$$

We refer to the Darcy velocity as $\mathbf{u}^{\mathcal{D}} = -\mathbf{K}\nabla p^{\mathcal{D}}$. To be dimensionally consistent, this definition should also incorporate the dynamic viscosity μ for the fluid; however, we may think of it as just another constant factor incorporated in the permeability.

Given a body force $\mathbf{f}^{\mathcal{S}}$ on a region of incompressible laminar flow and boundary conditions $\mathbf{t}_N^{\mathcal{S}}, \mathbf{u}_D^{\mathcal{S}}$, the goal of the incompressible Stokes equations is to find velocity $\mathbf{u}^{\mathcal{S}} \in (H^2(\Omega^{\mathcal{S}}))^d$ and pressure $p^{\mathcal{S}} \in H^1(\Omega^{\mathcal{S}})$ satisfying

$$\left\{ \begin{array}{ll} -\nabla \cdot \sigma = \mathbf{f}^{\mathcal{S}} & \text{in } \Omega^{\mathcal{S}}, \\ \sigma = 2\mu\varepsilon(\mathbf{u}^{\mathcal{S}}) - p^{\mathcal{S}}\mathbf{I} & \text{in } \Omega^{\mathcal{S}}, \\ \varepsilon(\mathbf{u}^{\mathcal{S}}) = (\nabla\mathbf{u}^{\mathcal{S}} + (\nabla\mathbf{u}^{\mathcal{S}})^T)/2 & \text{in } \Omega^{\mathcal{S}}, \\ \nabla \cdot \mathbf{u}^{\mathcal{S}} = 0 & \text{in } \Omega^{\mathcal{S}}, \\ \mathbf{u}^{\mathcal{S}} = \mathbf{u}_D^{\mathcal{S}} & \text{on } \Gamma_D^{\mathcal{S}}, \\ \sigma\mathbf{n} = \mathbf{t}_N^{\mathcal{S}} & \text{on } \Gamma_N^{\mathcal{S}}. \end{array} \right.$$

We will refer to σ as the stress tensor and ε as the strain rate tensor. Along the interface $\Gamma^{\mathcal{I}}$, the fluids interact. Hence, three conditions are imposed: mass conservation, normal stress continuity, and the Beavers-Joseph-Saffman boundary condition. The first two conditions state, roughly speaking, that matter is neither created nor destroyed and for every action there is an equal and opposite reaction. The Beavers-Joseph-Saffman boundary condition was developed empirically by the work of Beavers and Joseph in [35] and then improved by the work of Saffman in [36] and it may be thought of as a friction term for the interface as the combined effect of the Darcy permeability and a dimensionless friction coefficient α . Let \mathbf{n} be the outward unit normal vector on a domain when the meaning is unambiguous, let $\mathbf{n}^{\mathcal{D}}$ and $\mathbf{n}^{\mathcal{S}}$ be the outward unit normals for the domains $\Omega^{\mathcal{D}}$ and $\Omega^{\mathcal{S}}$, respectively, and let \mathbf{t} be the unit tangent along the interface $\Gamma^{\mathcal{I}}$. The interface equations are

$$\begin{aligned}
-\mathbf{u}^S \cdot \mathbf{n}^S &= \mathbf{u}^D \cdot \mathbf{n}^D, \\
\mathbf{n}^T \sigma \mathbf{n} &= -p^D, \\
\mathbf{t}^T \sigma \mathbf{n} &= -\frac{\mu^{1/2} \alpha}{\sqrt{\mathbf{t}^T \mathbf{K} \mathbf{t}}} \mathbf{u}^S \cdot \mathbf{t}.
\end{aligned} \tag{4.1}$$

We will substitute $\beta := \frac{\mu^{1/2} \alpha}{\sqrt{\mathbf{t}^T \mathbf{K} \mathbf{t}}}$ for simplicity of notation. Combined, these equations yield the single system seeking (p^D, \mathbf{u}^S, p^S) satisfying

$$\left\{ \begin{array}{ll}
\nabla \cdot (-\mathbf{K} \nabla p^D) = f^D & \text{in } \Omega^D, \\
p^D = p_D^D & \text{on } \Gamma_D^D, \\
(-\mathbf{K} \nabla p^D) \cdot \mathbf{n} = u_N^D & \text{on } \Gamma_N^D, \\
-\nabla \cdot (2\mu \varepsilon(\mathbf{u}^S) - p^S \mathbf{I}) = \mathbf{f}^S & \text{in } \Omega^S, \\
\nabla \cdot \mathbf{u}^S = 0 & \text{in } \Omega^S, \\
\mathbf{u}^S = \mathbf{u}_D^S & \text{on } \Gamma_D^S, \\
\sigma \mathbf{n} = \mathbf{t}_N^S & \text{on } \Gamma_N^S, \\
\mathbf{u}^D \cdot \mathbf{n}^D = -\mathbf{u}^S \cdot \mathbf{n}^S & \text{on } \Gamma^I, \\
\mathbf{n}^T \sigma \mathbf{n} = -p^D & \text{on } \Gamma^I, \\
\mathbf{t}^T \sigma \mathbf{n} = -\beta \mathbf{u}^S \cdot \mathbf{t} & \text{on } \Gamma^I.
\end{array} \right. \tag{4.2}$$

4.2 Dimensional Analysis

Due to the conflicting use of coefficients and units in existing literature, we briefly perform some dimensional analysis and discuss the units of the constants shown in Equation 4.2 for clarity.

The easiest variable to approach first is the fluid velocity \mathbf{u} , which has units $[\mathbf{u}] = \text{L}^1 \text{T}^{-1}$. The symmetric gradient is a first-order differential operator in space and therefore has units $[\varepsilon] = \text{L}^{-1}$. This is why the $\varepsilon(\mathbf{u})$ is referred to as the strain rate tensor, as it has units $[\varepsilon(\mathbf{u})] = \text{T}^{-1}$. The relation $\sigma = 2\mu \varepsilon(\mathbf{u}^S) - p^S \mathbf{I}$ implies that stress has the same units as pressure, i.e., $[\sigma] = [p] = \text{M}^1 \text{L}^{-1} \text{T}^{-2}$. Based on that, and the relation between strain rate and stress, we have $[\mu] = \text{M}^1 \text{L}^{-1} \text{T}^{-1}$.

Returning to the permeability tensor and recalling that we absorbed the dynamic viscosity, the units for \mathbf{K} are $[\mathbf{K}] = \text{M}^{-1} \text{L}^3 \text{T}^1$. Based on the BJS condition, we may deduce the units for the

Beavers-Joseph-Saffman constant by observing

$$[\sigma] = [\mu]^{1/2}[\alpha][\mathbf{K}]^{-1/2}[\mathbf{u}^S].$$

Substituting in the known values yields

$$\mathbf{M}^1\mathbf{L}^{-1}\mathbf{T}^{-2} = (\mathbf{M}^1\mathbf{L}^{-1}\mathbf{T}^{-1})^{1/2}[\alpha](\mathbf{M}^{-1}\mathbf{L}^3\mathbf{T}^1)^{1/2}(\mathbf{L}^1\mathbf{T}^{-1}).$$

Hence, the constant α we refer to in the BJS condition is dimensionless.

4.3 Weak Formulation

In order to develop a weak formulation for the finite element scheme to rely on, we begin by testing the Darcy equation by a test function $q \in H_{0,\Gamma_D^D}^1(\Omega^D)$ then integrating over Ω^D , followed by integration by parts, the Gauss divergence theorem, $\partial\Omega^D = \Gamma_D^D \cup \Gamma_N^D \cup \Gamma^I$, and $q|_{\Gamma_D^D} = 0$ yields

$$\begin{aligned} \int_{\Omega^D} f^D q &= \int_{\Omega^D} -\nabla \cdot (\mathbf{K}\nabla p^D) q \\ &= \int_{\Omega^D} \mathbf{K}\nabla p^D \cdot \nabla q - \int_{\partial\Omega^D} (\mathbf{K}\nabla p^D) \cdot \mathbf{n} q \\ &= \int_{\Omega^D} \mathbf{K}\nabla p^D \cdot \nabla q + \int_{\Gamma_D^D} \mathbf{u}^D \cdot \mathbf{n} q + \int_{\Gamma_N^D} \mathbf{u}^D \cdot \mathbf{n} q + \int_{\Gamma^I} \mathbf{u}^D \cdot \mathbf{n}^D q \\ &= \int_{\Omega^D} \mathbf{K}\nabla p^D \cdot \nabla q + \int_{\Gamma_N^D} u_N^D q - \int_{\Gamma^I} \mathbf{u}^S \cdot \mathbf{n}^S q. \end{aligned}$$

Since the quantity u_N^D is known, it may be moved to the opposite side, yielding

$$\int_{\Omega^D} \mathbf{K}\nabla p^D \cdot \nabla q - \int_{\Gamma^I} \mathbf{u}^S \cdot \mathbf{n}^S q = \int_{\Omega^D} f^D q - \int_{\Gamma_N^D} u_N^D q.$$

Testing the first Stokes equation by a test function $\mathbf{v} \in X^{\mathcal{S},0}$ and integrating over Ω^S yields

$$\begin{aligned}
\int_{\Omega^S} \mathbf{f}^S \cdot \mathbf{v} &= \int_{\Omega^S} (-\nabla \cdot (2\mu\varepsilon(\mathbf{u}^S) - p^S \mathbf{I})) \cdot \mathbf{v} \\
&= \int_{\Omega^S} (2\mu\varepsilon(\mathbf{u}^S) - p^S \mathbf{I}) : \nabla \mathbf{v} - \int_{\partial\Omega^S} (2\mu\varepsilon(\mathbf{u}^S) - p^S \mathbf{I}) \mathbf{n} \cdot \mathbf{v} \\
&= \int_{\Omega^S} 2\mu\varepsilon(\mathbf{u}^S) : \varepsilon(\mathbf{v}) - \int_{\Omega^S} p^S \mathbf{I} : \nabla \mathbf{v} - \int_{\Gamma_N^S} \sigma \mathbf{n} \cdot \mathbf{v} - \int_{\Gamma^{\mathcal{I}}} \sigma \mathbf{n} \cdot \mathbf{v} \\
&= \int_{\Omega^S} 2\mu\varepsilon(\mathbf{u}^S) : \varepsilon(\mathbf{v}) - \int_{\Omega^S} p^S \nabla \cdot \mathbf{v} - \int_{\Gamma_N^S} \mathbf{t}_N^S \cdot \mathbf{v} - \int_{\Gamma^{\mathcal{I}}} \sigma \mathbf{n} \cdot \mathbf{v}.
\end{aligned}$$

We have used $:$ to represent the matrix colon product, also known as the dot product or Frobenius inner product of matrices. We also used the fact from Chapter 3 that $\varepsilon(\mathbf{u}) : \nabla \mathbf{v} = \varepsilon(\mathbf{u}) : \varepsilon(\mathbf{v})$. For the Stokes equation, the traction condition \mathbf{t}_N^S is a known quantity, so it may be moved to the right-hand side. Along the interface $\Gamma^{\mathcal{I}}$, the vector $\sigma \mathbf{n}$ can be decomposed as normal and tangential components. That is, in two dimensions, $\sigma \mathbf{n} = (\mathbf{n}^T \sigma \mathbf{n}) \mathbf{n} + (\mathbf{t}^T \sigma \mathbf{n}) \mathbf{t}$. This allows the integral along $\Gamma^{\mathcal{I}}$ to be simplified further as

$$\begin{aligned}
- \int_{\Gamma^{\mathcal{I}}} \sigma \mathbf{n} \cdot \mathbf{v} &= - \int_{\Gamma^{\mathcal{I}}} ((\mathbf{n}^T \sigma \mathbf{n}) \mathbf{n} + (\mathbf{t}^T \sigma \mathbf{n}) \mathbf{t}) \cdot \mathbf{v} \\
&= - \int_{\Gamma^{\mathcal{I}}} (\mathbf{n}^T \sigma \mathbf{n})(\mathbf{n} \cdot \mathbf{v}) + (\mathbf{t}^T \sigma \mathbf{n})(\mathbf{t} \cdot \mathbf{v}) \\
&= \int_{\Gamma^{\mathcal{I}}} p^{\mathcal{D}}(\mathbf{n}^S \cdot \mathbf{v}) + \beta(\mathbf{u}^S \cdot \mathbf{t})(\mathbf{v} \cdot \mathbf{t}).
\end{aligned}$$

We remark that in three dimensions, there are two orthogonal tangential directions, meaning that $\sigma \mathbf{n}$ must instead be decomposed as $\sigma \mathbf{n} = (\mathbf{n}^T \sigma \mathbf{n}) \mathbf{n} + (\mathbf{t}_1^T \sigma \mathbf{n}) \mathbf{t}_1 + (\mathbf{t}_2^T \sigma \mathbf{n}) \mathbf{t}_2$.

This changes the previous integral for a three-dimensional problem to

$$- \int_{\Gamma^{\mathcal{I}}} \sigma \mathbf{n} \cdot \mathbf{v} = \int_{\Gamma^{\mathcal{I}}} p^{\mathcal{D}}(\mathbf{n}^S \cdot \mathbf{v}) + \beta_1(\mathbf{u}^S \cdot \mathbf{t}_1)(\mathbf{v} \cdot \mathbf{t}_1) + \beta_2(\mathbf{u}^S \cdot \mathbf{t}_2)(\mathbf{v} \cdot \mathbf{t}_2),$$

where β_i represents the constant β corresponding to permeability in tangential direction i . More concisely, one may write

$$- \int_{\Gamma^{\mathcal{I}}} \sigma \mathbf{n} \cdot \mathbf{v} = \int_{\Gamma^{\mathcal{I}}} p^{\mathcal{D}}(\mathbf{n}^S \cdot \mathbf{v}) + \sum_{i=1}^{d-1} \beta_i(\mathbf{u}^S \cdot \mathbf{t}_i)(\mathbf{v} \cdot \mathbf{t}_i);$$

however, to ease the burden of notation, we will write the integrals as we did for the $d = 2$ case, but remain mindful of this fact. The resulting weak form of the first Stokes equation is

$$\begin{aligned} \int_{\Gamma^{\mathcal{I}}} p^{\mathcal{D}}(\mathbf{v} \cdot \mathbf{n}^{\mathcal{S}}) + \int_{\Omega^{\mathcal{S}}} 2\mu\varepsilon(\mathbf{u}^{\mathcal{S}}) : \varepsilon(\mathbf{v}) + \int_{\Gamma^{\mathcal{I}}} \beta(\mathbf{u}^{\mathcal{S}} \cdot \mathbf{t})(\mathbf{v} \cdot \mathbf{t}) - \int_{\Omega^{\mathcal{S}}} p^{\mathcal{S}}\nabla \cdot \mathbf{v} \\ = \int_{\Omega^{\mathcal{S}}} \mathbf{f}^{\mathcal{S}} \cdot \mathbf{v} + \int_{\Gamma_N^{\mathcal{S}}} \mathbf{t}_N^{\mathcal{S}} \cdot \mathbf{v}. \end{aligned}$$

Testing the incompressibility equation with a function $r \in Y$ yields

$$- \int_{\Omega^{\mathcal{S}}} (\nabla \cdot \mathbf{u}^{\mathcal{S}})r = 0.$$

For these weak forms, define the bilinear operators

$$\begin{aligned} \mathcal{A}^{\mathcal{D}}(p^{\mathcal{D}}, q) &= \int_{\Omega^{\mathcal{D}}} \mathbf{K}\nabla p^{\mathcal{D}} \cdot \nabla q, \\ \mathcal{C}^{\mathcal{I}}(p^{\mathcal{D}}, \mathbf{v}) &= \int_{\Gamma^{\mathcal{I}}} p^{\mathcal{D}}(\mathbf{v} \cdot \mathbf{n}^{\mathcal{S}}), \\ \mathcal{A}^{\mathcal{S}}(\mathbf{u}^{\mathcal{S}}, \mathbf{v}) &= \int_{\Omega^{\mathcal{S}}} \varepsilon(\mathbf{u}^{\mathcal{S}}) : \varepsilon(\mathbf{v}) + \int_{\Gamma^{\mathcal{I}}} \beta(\mathbf{u}^{\mathcal{S}} \cdot \mathbf{t})(\mathbf{v} \cdot \mathbf{t}), \\ \mathcal{B}^{\mathcal{S}}(p^{\mathcal{S}}, \mathbf{v}) &= \int_{\Omega^{\mathcal{S}}} p^{\mathcal{S}}\nabla \cdot \mathbf{v}, \end{aligned}$$

and define the linear operators

$$\begin{aligned} \mathcal{F}^{\mathcal{D}}(q) &= \int_{\Omega^{\mathcal{D}}} f^{\mathcal{D}}q + \int_{\Gamma_N^{\mathcal{D}}} u_N^{\mathcal{D}}q, \\ \mathcal{F}^{\mathcal{S}}(\mathbf{v}) &= \int_{\Omega^{\mathcal{S}}} \mathbf{f}^{\mathcal{S}} \cdot \mathbf{v} + \int_{\Gamma_N^{\mathcal{S}}} \mathbf{t}_N^{\mathcal{S}} \cdot \mathbf{v}. \end{aligned}$$

Then the weak form of the system of equations may be written with these operators as

$$\begin{cases} \mathcal{A}^{\mathcal{S}}(\mathbf{u}^{\mathcal{S}}, \mathbf{v}) - \mathcal{B}^{\mathcal{S}}(p^{\mathcal{S}}, \mathbf{v}) + \mathcal{C}^{\mathcal{I}}(p^{\mathcal{D}}, \mathbf{v}) &= \mathcal{F}^{\mathcal{S}}(\mathbf{v}), \\ \mathcal{B}^{\mathcal{S}}(r, \mathbf{u}^{\mathcal{S}}) &= 0, \\ -\mathcal{C}^{\mathcal{I}}(q, \mathbf{u}^{\mathcal{S}}) + \mathcal{A}^{\mathcal{D}}(p^{\mathcal{D}}, q) &= \mathcal{F}^{\mathcal{D}}(q). \end{cases} \quad (4.3)$$

4.4 The Bernardi-Raugel Space on Quadrilateral Meshes

Before we proceed to the finite element scheme, we will briefly discuss the Bernardi-Raugel space, which we refer to by BR_1 . The Bernardi-Raugel space is another classical finite element space presented in [61] for Stokes flow. The BR_1 space is an enrichment of Q_1^d by edge-based bubble functions motivated by the fact that the pair (Q_1^d, Q_0) is not an LBB stable combination for Stokes flow. Indeed, the pair (BR_1, Q_0) is an LBB stable combination for Stokes flow on quadrilateral meshes, so this motivates its use for our Stokes domain discretization.

Let E be a quadrilateral with vertices $P_i(x_i, y_i)$ ($i = 1, 2, 3, 4$) starting at the lower-left corner and going counterclockwise. Let e_i ($i = 1, 2, 3, 4$) be the edge connecting P_i to P_{i+1} with the modulo convention $P_5 = P_1$. Let \mathbf{n}_i ($i = 1, 2, 3, 4$) be the outward unit normal vector on edge e_i . A bilinear mapping from (\hat{x}, \hat{y}) in the reference element $\hat{E} = [0, 1]^2$ to (x, y) in a general quadrilateral is established as follows

$$\begin{cases} x = x_1 + (x_2 - x_1)\hat{x} + (x_4 - x_1)\hat{y} + ((x_1 + x_3) - (x_2 + x_4))\hat{x}\hat{y}, \\ y = y_1 + (y_2 - y_1)\hat{x} + (y_4 - y_1)\hat{y} + ((y_1 + y_3) - (y_2 + y_4))\hat{x}\hat{y}. \end{cases} \quad (4.4)$$

On the reference element \hat{E} , we have four standard bilinear functions

$$\begin{aligned} \hat{\phi}_4(\hat{x}, \hat{y}) &= (1 - \hat{x})\hat{y}, & \hat{\phi}_3(\hat{x}, \hat{y}) &= \hat{x}\hat{y}, \\ \hat{\phi}_1(\hat{x}, \hat{y}) &= (1 - \hat{x})(1 - \hat{y}), & \hat{\phi}_2(\hat{x}, \hat{y}) &= \hat{x}(1 - \hat{y}). \end{aligned} \quad (4.5)$$

After the bilinear mapping defined by (4.4), we obtain four scalar basis functions on E :

$$\phi_i(x, y) = \hat{\phi}_i(\hat{x}, \hat{y}), \quad i = 1, 2, 3, 4. \quad (4.6)$$

These are used to define eight node-based local basis functions for $Q_1(E)^2$:

$$\begin{bmatrix} \phi_1 \\ 0 \end{bmatrix}, \begin{bmatrix} 0 \\ \phi_1 \end{bmatrix}, \begin{bmatrix} \phi_2 \\ 0 \end{bmatrix}, \begin{bmatrix} 0 \\ \phi_2 \end{bmatrix}, \begin{bmatrix} \phi_3 \\ 0 \end{bmatrix}, \begin{bmatrix} 0 \\ \phi_3 \end{bmatrix}, \begin{bmatrix} \phi_4 \\ 0 \end{bmatrix}, \begin{bmatrix} 0 \\ \phi_4 \end{bmatrix}. \quad (4.7)$$

Furthermore, we define four edge-based scalar functions on \hat{E} :

$$\begin{aligned} \hat{\psi}_1(\hat{x}, \hat{y}) &= (1 - \hat{x})\hat{x}(1 - \hat{y}), & \hat{\psi}_2(\hat{x}, \hat{y}) &= \hat{x}(1 - \hat{y})\hat{y}, \\ \hat{\psi}_3(\hat{x}, \hat{y}) &= (1 - \hat{x})\hat{x}\hat{y}, & \hat{\psi}_4(\hat{x}, \hat{y}) &= (1 - \hat{x})(1 - \hat{y})\hat{y}. \end{aligned} \quad (4.8)$$

They become univariate quadratic functions on respective edges of \hat{E} , and for that reason they are sometimes referred to as edge-based “bubble functions.” For a generic convex quadrilateral E , we utilize the bilinear mapping to define

$$\psi_i(x, y) = \hat{\psi}_i(\hat{x}, \hat{y}), \quad i = 1, 2, 3, 4. \quad (4.9)$$

Then we have four edge-based local basis functions on E as shown in Figure 4.2:

$$\mathbf{b}_i(x, y) = \mathbf{n}_i \psi_i(x, y), \quad i = 1, 2, 3, 4. \quad (4.10)$$

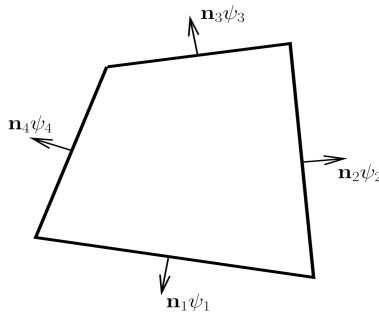


Figure 4.2: Four edge-based bubble functions used in the BR_1 space.

Let $Q_1(E)^2$ be the set of vector-valued mapped bilinear functions on a quadrilateral E . Combining the $Q_1(E)^2$ functions and the bubble functions, the $BR_1(E)$ space on the quadrilateral is

defined as

$$BR_1(E) = Q_1(E)^2 + \text{span}(\mathbf{b}_1, \mathbf{b}_3, \mathbf{b}_3, \mathbf{b}_4). \quad (4.11)$$

The global finite element space is defined by combining all local spaces, but care must be taken to define the global bubble functions in a consistent manner. This may be done by defining an orientation for each edge and using that to assign a consistent direction to each bubble function's normal vector.

4.4.1 Properties of the (BR_1, Q_0) Element Pair for Stokes Flow

The (BR_1, Q_0) pair satisfies several appealing properties which will be beneficial for the approximation of Stokes flow. First, the addition of bubble functions allows for enrichment of interpolation. In [61], the global interpolation operator, denoted here as \mathbf{P}_h , is specified as the piecewise bilinear interpolant at mesh nodes and the bubble function coefficients are so defined that the bulk flux is captured on each edge e_i ,

$$\int_{e_i} (\mathbf{P}_h \mathbf{v} - \mathbf{v}) \cdot \mathbf{n} = 0, \quad \forall \mathbf{v} \in \mathbf{H}_0^1(\Omega). \quad (4.12)$$

For a polygonal domain Ω^S and a shape-regular mesh \mathcal{E}_h^S consisting of convex quadrilaterals, this implies that for all $E \in \mathcal{E}_h^S$,

$$(w_h, \nabla \cdot (\mathbf{P}_h \mathbf{v} - \mathbf{v}))_E = 0, \quad \forall \mathbf{v} \in \mathbf{H}_0^1(\Omega), \quad \forall w_h \in Q_0(E). \quad (4.13)$$

Another property described in [61] is the inf-sup condition. Let \mathbf{V}_h be the global BR_1 finite element space on the mesh \mathcal{E}_h^S and let \mathbf{V}_h^0 be the space of functions in \mathbf{V}_h that vanish on all boundaries. Then the discretization satisfies the inf-sup condition

$$\gamma \|w_h\|_{L^2(\Omega^S)} \leq \sup_{\mathbf{v} \in \mathbf{V}_h^0} \frac{(w_h, \nabla \cdot \mathbf{v}_h)_{\Omega^S}}{\|\varepsilon(\mathbf{v}_h)\|_{L^2(\Omega^S)}}, \quad \forall w_h \in Q_0(\mathcal{E}_h^S), \quad (4.14)$$

where $\gamma > 0$ is a constant independent of mesh size h .

4.4.2 Implementation Details

This section presents the finite element scheme for the coupled problem, but first we will introduce appropriate notations and spaces.

Let $\mathcal{E}_h^S, \mathcal{E}_h^D$ be shape-regular quadrilateral meshes of Ω^S, Ω^D , respectively, with size h , and let Γ_h^I be a mesh of Γ^I , which is conforming with \mathcal{E}_h^S and \mathcal{E}_h^D . Let \mathbf{V}_h^S, W_h^S be the global BR_1 and piecewise constant spaces on \mathcal{E}_h^S for the unknowns (\mathbf{u}_h^S, p_h^S) , respectively. Then let V_h^D be the $WG(Q_0, Q_0)$ space on \mathcal{E}_h^D for the unknowns $\{p_h^{D,\circ}, p_h^{D,\theta}\}$. Furthermore, we use $\mathbf{V}_h^{S,0}, V_h^{D,0}$ to denote the subspaces of \mathbf{V}_h^S, V_h^D consisting of functions that vanish on Dirichlet boundaries, respectively. Figure 4.3 shows where the degrees of freedom for this multinumerics coupling are located.

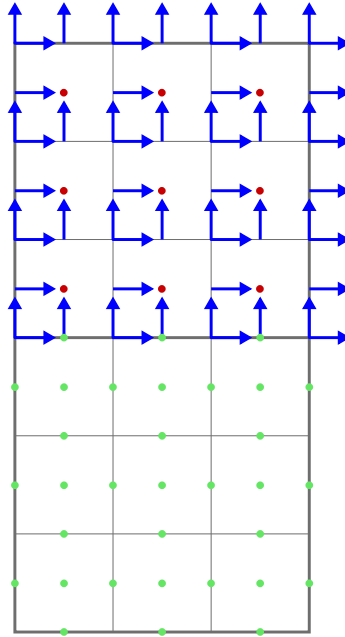


Figure 4.3: Degrees of freedom for the coupled $WG(Q_0, Q_0; AC_0)$ (light green), BR_1 (blue), Q_0 (dark red) method for Stokes-Darcy flow.

The Stokes discretization requires $2(\#\text{nodes}) + (\#\text{edges}) + (\#\text{elements})$ variables for the discretization and the Darcy discretization requires $(\#\text{edges}) + (\#\text{elements})$ variables for the $WG(Q_0, Q_0)$, making this a very economic combination of finite element methods.

Now we have four discrete bilinear forms defined on these finite element spaces:

$$\mathcal{A}_h^S(\mathbf{u}_h^S, \mathbf{v}_h) = \sum_{E \in \mathcal{E}_h^S} 2\mu \int_E \varepsilon(\mathbf{u}_h^S) : \varepsilon(\mathbf{v}_h) + \sum_{e \in \Gamma_h^I} \int_e \beta(\mathbf{u}_h^S \cdot \mathbf{t}_e^S)(\mathbf{v}_h \cdot \mathbf{t}_e^S), \quad (4.15)$$

$$\mathcal{B}_h^S(p_h^S, \mathbf{v}_h) = \sum_{E \in \mathcal{E}_h^S} \int_E p_h^S (\nabla \cdot \mathbf{v}_h), \quad (4.16)$$

$$\mathcal{C}_h^I(p_h^D, \mathbf{v}_h) = \sum_{e \in \Gamma_h^I} \int_e p_h^{D,\partial} (\mathbf{v}_h \cdot \mathbf{n}^S), \quad (4.17)$$

$$\mathcal{A}_h^D(p_h^D, q_h) = \sum_{E \in \mathcal{E}_h^D} \int_E (\mathbf{K} \nabla_w p_h^D) \cdot \nabla_w q_h, \quad (4.18)$$

and two discrete linear forms

$$\mathcal{F}_h^S(\mathbf{v}_h) = \sum_{E \in \mathcal{E}_h^S} \int_E \mathbf{f} \cdot \mathbf{v}_h + \sum_{e \in \Gamma_{N,h}^S} \int_e \mathbf{t}_N^S \cdot \mathbf{v}_h, \quad (4.19)$$

$$\mathcal{F}_h^D(q_h) = \sum_{E \in \mathcal{E}_h^D} \int_{E^\circ} s q_h^\circ - \sum_{e \in \Gamma_{N,h}^D} \int_e u_N^D q_h^\partial - \sum_{E \in \mathcal{E}_h^D} \int_E \mathbf{Q}_h(-\mathbf{K} \mathbf{f}^D) \cdot \nabla_w q_h, \quad (4.20)$$

where \mathbf{Q}_h is the local projection from $L^2(\Omega^D)^2$ to the broken AC_0 space.

Our finite element scheme for the coupled Stokes-Darcy flow problem is: Seek $\mathbf{u}_h^S \in \mathbf{V}_h^S$, $p_h^S \in W_h^S$, and $p_h^D \in V_h^D$ such that $\mathbf{u}_h^S|_{\Gamma_D^S} = \mathbf{P}_h(\mathbf{u}_D^S)$, $p_h^D|_{\Gamma_D^D} = Q_h^\partial(p_D^D)$, and for any $\mathbf{v}_h \in \mathbf{V}_h^{S,0}$, $r_h \in W_h^S$, and $q_h \in V_h^{D,0}$, there holds

$$\begin{cases} \mathcal{A}_h^S(\mathbf{u}_h^S, \mathbf{v}_h) - \mathcal{B}_h^S(p_h^S, \mathbf{v}_h) + \mathcal{C}_h^I(p_h^D, \mathbf{v}_h) &= \mathcal{F}_h^S(\mathbf{v}_h), \\ \mathcal{B}_h^S(r_h, \mathbf{u}_h^S) &= 0, \\ -\mathcal{C}_h^I(q_h, \mathbf{u}_h^S) + \mathcal{A}_h^D(p_h^D, q_h) &= \mathcal{F}_h^D(q_h). \end{cases} \quad (4.21)$$

Note that the assembly for each of the discrete bilinear forms \mathcal{A}_h^S , \mathcal{B}_h^S and \mathcal{A}_h^D is handled almost as with the independent Stokes or Darcy problem. An important part of this implementation is the handling of the interface term \mathcal{C}_h^I and the BJS condition within the \mathcal{A}_h^S term.

After a numerical Darcy pressure p_h^D is obtained from solving the sparse monolithic system, we define the numerical Darcy velocity by postprocessing the numerical Darcy pressure by

$$\mathbf{u}_h^{\mathcal{D}} = \mathbf{Q}_h(-\mathbf{K}(\nabla_w p_h^{\mathcal{D}} - \mathbf{f}^{\mathcal{D}})). \quad (4.22)$$

The numerical Darcy velocity is used in the upcoming section to show the weak Galerkin discretization provides conservation properties for the flow in the Darcy domain.

4.5 A Priori Error Analysis

This section presents a rigorous analysis for the new finite element scheme. For ease of presentation, we adopt the following assumptions.

- (i) $\mathbf{K} = \kappa \mathbf{I}$. For analysis on Darcy solvers with a general permeability, see [23].
- (ii) $\mathbf{f}^{\mathcal{D}} = \mathbf{0}$. Then $\mathbf{u}^{\mathcal{D}} = -\kappa \nabla p^{\mathcal{D}}$ and $\mathbf{u}_h^{\mathcal{D}} = -\kappa \nabla_w p_h^{\mathcal{D}}$ due to (i) and (4.22).
- (iii) Homogeneous pure Dirichlet boundary conditions are posed for both Stokes and Darcy parts.

We define the following energy semi-norms for $\mathbf{v}_h \in \mathbf{V}_h^{\mathcal{S}}$ and $q_h \in V_h^{\mathcal{D}}$:

$$\|\|\mathbf{v}_h\|\|_h^2 = \mathcal{A}_h^{\mathcal{S}}(\mathbf{v}_h, \mathbf{v}_h), \quad \|\|q_h\|\|_h^2 = \mathcal{A}_h^{\mathcal{D}}(q_h, q_h), \quad (4.23)$$

which induce an energy semi-norm on the space $\mathbf{V}_h^{\mathcal{S}} \times V_h^{\mathcal{D}}$:

$$\|\|(\mathbf{v}_h, q_h)\|\|_h^2 = \|\|\mathbf{v}_h\|\|_h^2 + \|\|q_h\|\|_h^2. \quad (4.24)$$

4.5.1 Properties of Operators and Subspaces

For the Stokes part, let π_h as the local L^2 -projection operator from $L_0^2(\Omega)$ to $W_h^{\mathcal{S}}$. We start our analysis by observing that Lemmas 2.1, 2.2, 2.3, 2.4 all apply to this choice of finite element space per the discussion in Chapter 2.

Under the assumption $\mathbf{K} = \kappa \mathbf{I}$, Lemma 2.1 implies that

$$\mathbf{Q}_h(\mathbf{K} \nabla p^{\mathcal{D}}) = \mathbf{K}(\mathbf{Q}_h \nabla p^{\mathcal{D}}) = \mathbf{K} \nabla_w (Q_h p^{\mathcal{D}}).$$

Lemma 4.1. (Conservation of mass for Darcy flow) For any $E \in \mathcal{E}_h^{\mathcal{D}}$, there holds

$$\int_{E^\partial} \mathbf{u}_h^{\mathcal{D}} \cdot \mathbf{n} = \int_E f. \quad (4.25)$$

Proof. This statement is common in the literature for weak Galerkin methods for Darcy flow, but the only difference here is we choose $\mathbf{v}_h = 0$, $r_h = 0$, and $q_h = \{\chi_{E^\circ}, 0\}$ in (4.21). The remainder of the proof follows from applying the conversion to trace and definition of the Darcy velocity (see also [4, 62]). \square

Lemma 4.2. (Bulk flux continuity for Darcy flow) For any two elements $E_1, E_2 \in \mathcal{E}_h^{\mathcal{D}}$ which share an interior edge e , their respective local velocities $\mathbf{u}_{h,1}^{\mathcal{D}}, \mathbf{u}_{h,2}^{\mathcal{D}}$ satisfy

$$\int_e \mathbf{u}_{h,1}^{\mathcal{D}} \cdot \mathbf{n}_1 + \int_e \mathbf{u}_{h,2}^{\mathcal{D}} \cdot \mathbf{n}_2 = 0. \quad (4.26)$$

Proof. This is another common statement for weak Galerkin methods for Darcy flow, and just as in Lemma 4.1, we choose $\mathbf{v}_h = 0$, $r_h = 0$, but $q_h = \{0, \chi_e\}$. The remainder of the proof may be obtained by applying a conversion to trace and definition of numerical Darcy velocity (see also [4, 62]). \square

4.5.2 Existence and Uniqueness

In this subsection, we prove the existence and uniqueness of the finite element scheme (4.21). It suffices to show the uniqueness, since the discrete linear system is finite-dimensional and square. This will be accomplished by setting the source terms to zero and then showing that all parts of the discrete solution are zero. Thus, we consider the special system

$$\begin{cases} \mathcal{A}_h^{\mathcal{S}}(\mathbf{u}_h^{\mathcal{S}}, \mathbf{v}_h) - \mathcal{B}_h^{\mathcal{S}}(p_h^{\mathcal{S}}, \mathbf{v}_h) + \mathcal{C}_h^{\mathcal{I}}(p_h^{\mathcal{D}}, \mathbf{v}_h) = 0, \\ \mathcal{B}_h^{\mathcal{S}}(r_h, \mathbf{u}_h^{\mathcal{S}}) = 0, \\ -\mathcal{C}_h^{\mathcal{I}}(q_h, \mathbf{u}_h^{\mathcal{S}}) + \mathcal{A}_h^{\mathcal{D}}(p_h^{\mathcal{D}}, q_h) = 0. \end{cases} \quad (4.27)$$

We set $\mathbf{v}_h = \mathbf{u}_h^{\mathcal{S}}$, $r_h = p_h^{\mathcal{S}}$, and $q_h = p_h^{\mathcal{D}}$, and sum the equations to obtain

$$\|(\mathbf{u}_h^S, p_h^D)\|_h^2 = \mathcal{A}_h^S(\mathbf{u}_h^S, \mathbf{u}_h^S) + \mathcal{A}_h^D(p_h^D, p_h^D) = 0.$$

This immediately implies $\varepsilon(\mathbf{u}_h^S) = \mathbf{0}$, $\mathbf{u}_h^S \cdot \mathbf{t} = 0$, and $\nabla_w p_h^D = \mathbf{0}$. The fact that the Dirichlet boundary in the Stokes domain is nonempty implies $\mathbf{u}_h^S = \mathbf{0}$. The discrete inf-sup condition (4.14) then implies $p_h^S = 0$. Finally, the norm property of discrete weak gradient from Lemma 2.4 implies $p_h^D \equiv 0$. Furthermore, from this we conclude $\|(\cdot, \cdot)\|_h$ is a norm on $\mathbf{V}_h^{S,0} \times V_h^{D,0}$.

4.5.3 Error Equations

We split the errors of finite element solutions as discrete errors and projection errors. The discrete errors are defined as

$$\mathbf{e}_h^S = \mathbf{P}_h \mathbf{u}^S - \mathbf{u}_h^S, \quad e_h^S = \pi_h p^S - p_h^S, \quad e_h^D = Q_h p^D - p_h^D, \quad (4.28)$$

The projection errors are defined as

$$\mathbf{u}^S - \mathbf{P}_h \mathbf{u}^S, \quad p^S - \pi_h p^S, \quad p^D - Q_h p^D.$$

In this subsection, we establish error equations to express the above discrete errors in terms of the projection errors, which are known to be controlled by the regularity of the exact solutions and the approximation capacity of the finite element subspaces constructed.

Lemma 4.3. (Error equations) Let (\mathbf{u}^S, p^S, p^D) be the exact solutions to the coupled Stokes-Darcy flow problem (4.2) with homogeneous Dirichlet boundary conditions on the whole boundary (except the interface). Let $(\mathbf{u}_h^S, p_h^S, p_h^D)$ be the numerical solutions obtained from the finite element scheme (4.21). Then for any $\mathbf{v}_h \in \mathbf{V}_h^{S,0}$, $r_h \in W_h^{S,0}$, and $q_h \in V_h^{D,0}$, there holds

$$\begin{cases} \mathcal{A}_h^S(\mathbf{e}_h^S, \mathbf{v}_h) - \mathcal{B}_h^S(e_h^S, \mathbf{v}_h) + \mathcal{C}_h^I(e_h^D, \mathbf{v}_h) = \mathcal{G}^S(\mathbf{u}^S, p^S, p^D, \mathbf{v}_h), \\ \mathcal{B}_h^S(r_h, \mathbf{e}_h^S) = 0, \\ -\mathcal{C}_h^I(q_h, \mathbf{e}_h^S) + \mathcal{A}_h^D(e_h^D, q_h) = \mathcal{G}^D(\mathbf{u}^D, q_h), \end{cases} \quad (4.29)$$

where

$$\left\{ \begin{array}{l} \mathcal{G}^S(\mathbf{u}^S, p^S, p^D, \mathbf{v}_h) = \mathcal{A}_h^S(\mathbf{P}_h \mathbf{u}^S - \mathbf{u}^S, \mathbf{v}_h) \\ \quad - \mathcal{B}_h^S(\pi_h p^S - p^S, \mathbf{v}_h) + \mathcal{C}_h^I(Q_h p^D - p^D, \mathbf{v}_h), \\ \mathcal{G}^D(\mathbf{u}^D, q_h) = \sum_{E \in \mathcal{E}_h^D} (\mathbf{\Pi}_h \mathbf{u}^D - \mathbf{Q}_h \mathbf{u}^D, \nabla_w q_h)_E. \end{array} \right. \quad (4.30)$$

Proof. To handle Darcy pressure error, we use the 3rd equation in the finite element scheme (4.21) to obtain

$$\begin{aligned} \mathcal{A}_h^D(e_h^D, q_h) &= \mathcal{A}_h^D(Q_h p^D, q_h) - \mathcal{A}_h^D(p_h^D, q_h) \\ &= \mathcal{A}_h^D(Q_h p^D, q_h) - \mathcal{F}_h^D(q_h) - \mathcal{C}_h^I(q_h, \mathbf{u}_h^S). \end{aligned}$$

By Lemma 2.1, the first term in the last line is converted to

$$\begin{aligned} \mathcal{A}_h^D(Q_h p^D, q_h) &= \sum_{E \in \mathcal{E}_h^D} (\mathbf{K} \nabla_w(Q_h p^D), \nabla_w q_h)_E \\ &= \sum_{E \in \mathcal{E}_h^D} (\mathbf{Q}_h(\mathbf{K} \nabla p^D), \nabla_w q_h)_E \\ &= - \sum_{E \in \mathcal{E}_h^D} (\mathbf{Q}_h \mathbf{u}^D, \nabla_w q_h)_E. \end{aligned} \quad (4.31)$$

To deal with Darcy source term $s = \nabla \cdot (-\mathbf{K} \nabla p^D)$, we consider $q_h \in V_h^{D,0}$. Then

$$\begin{aligned} \mathcal{F}_h^D(q_h) &= \sum_{E \in \mathcal{E}_h^D} (s, q_h^\circ)_{E^\circ} = \sum_{E \in \mathcal{E}_h^D} (\nabla \cdot (-\mathbf{K} \nabla p^D), q_h^\circ)_{E^\circ} \\ &= \sum_{E \in \mathcal{E}_h^D} (\nabla \cdot \mathbf{u}^D, q_h^\circ)_{E^\circ} = \sum_{E \in \mathcal{E}_h^D} (\nabla \cdot (\mathbf{\Pi}_h \mathbf{u}^D), q_h^\circ)_{E^\circ}. \end{aligned}$$

Note that $\mathbf{\Pi}_h \mathbf{u}^D$ is in the global AC_0 space. By the definition of discrete weak gradient, we have

$$\mathcal{F}_h^D(q_h) = \sum_{E \in \mathcal{E}_h^D} \langle (\mathbf{\Pi}_h \mathbf{u}^D) \cdot \mathbf{n}, q_h^\partial \rangle_{E^\partial} - \sum_{E \in \mathcal{E}_h^D} (\mathbf{\Pi}_h \mathbf{u}^D, \nabla_w q_h)_E.$$

The interpolant in the global AC_0 space is continuous. Therefore, the terms for the interior edges vanish, and the terms for Dirichlet edges satisfy $q_h^\partial = 0$, so the only surviving terms lie on the

interface edges. Thus we have

$$\mathcal{F}_h^{\mathcal{D}}(q_h) = \sum_{e \in \Gamma_h^{\mathcal{I}}} \langle (\mathbf{\Pi}_h \mathbf{u}^{\mathcal{D}}) \cdot \mathbf{n}^{\mathcal{D}}, q_h^{\partial} \rangle_e - \sum_{E \in \mathcal{E}_h^{\mathcal{D}}} (\mathbf{\Pi}_h \mathbf{u}^{\mathcal{D}}, \nabla_w q_h)_E. \quad (4.32)$$

Combining the above results yields

$$\begin{aligned} \mathcal{A}_h^{\mathcal{D}}(e_h^{\mathcal{D}}, q_h) &= \sum_{E \in \mathcal{E}_h^{\mathcal{D}}} (\mathbf{\Pi}_h \mathbf{u}^{\mathcal{D}} - \mathbf{Q}_h \mathbf{u}^{\mathcal{D}}, \nabla_w q_h)_E \\ &\quad - \sum_{e \in \Gamma_h^{\mathcal{I}}} \langle (\mathbf{\Pi}_h \mathbf{u}^{\mathcal{D}}) \cdot \mathbf{n}^{\mathcal{D}}, q_h^{\partial} \rangle_e - C_h^{\mathcal{I}}(q_h, \mathbf{u}_h^{\mathcal{S}}). \end{aligned} \quad (4.33)$$

Therefore, subtracting $C_h^{\mathcal{I}}(q_h, \mathbf{e}_h^{\mathcal{S}})$ from $\mathcal{A}_h^{\mathcal{D}}(e_h^{\mathcal{D}}, q_h)$ yields

$$\begin{aligned} \mathcal{A}_h^{\mathcal{D}}(e_h^{\mathcal{D}}, q_h) - C_h^{\mathcal{I}}(q_h, \mathbf{e}_h^{\mathcal{S}}) &= \mathcal{A}_h^{\mathcal{D}}(e_h^{\mathcal{D}}, q_h) - C_h^{\mathcal{I}}(q_h, \mathbf{P}_h \mathbf{u}^{\mathcal{S}} - \mathbf{u}_h^{\mathcal{S}}) \\ &= \mathcal{A}_h^{\mathcal{D}}(e_h^{\mathcal{D}}, q_h) + C_h^{\mathcal{I}}(q_h, \mathbf{u}_h^{\mathcal{S}}) - C_h^{\mathcal{I}}(q_h, \mathbf{P}_h \mathbf{u}^{\mathcal{S}}) \\ &= \sum_{E \in \mathcal{E}_h^{\mathcal{D}}} (\mathbf{\Pi}_h \mathbf{u}^{\mathcal{D}} - \mathbf{Q}_h \mathbf{u}^{\mathcal{D}}, \nabla_w q_h)_E - \sum_{e \in \Gamma_h^{\mathcal{I}}} \langle (\mathbf{\Pi}_h \mathbf{u}^{\mathcal{D}}) \cdot \mathbf{n}^{\mathcal{D}}, q_h^{\partial} \rangle_e \\ &\quad - \sum_{e \in \Gamma_h^{\mathcal{I}}} \langle (\mathbf{P}_h \mathbf{u}^{\mathcal{S}}) \cdot \mathbf{n}^{\mathcal{S}}, q_h^{\partial} \rangle_e \\ &= \sum_{E \in \mathcal{E}_h^{\mathcal{D}}} (\mathbf{\Pi}_h \mathbf{u}^{\mathcal{D}} - \mathbf{Q}_h \mathbf{u}^{\mathcal{D}}, \nabla_w q_h)_E + \sum_{e \in \Gamma_h^{\mathcal{I}}} \langle (\mathbf{P}_h \mathbf{u}^{\mathcal{S}} - \mathbf{\Pi}_h \mathbf{u}^{\mathcal{D}}) \cdot \mathbf{n}^{\mathcal{D}}, q_h^{\partial} \rangle_e. \end{aligned} \quad (4.34)$$

By the flux-capturing property of the BR_1 interpolation operator (4.12), the flux capturing property of the AC_0 interpolation operator (2.33), and the first interface condition, the second sum vanishes, and one is led to the 3rd error equation in (4.29)

$$\begin{aligned}
\mathcal{A}_h^{\mathcal{D}}(e_h^{\mathcal{D}}, q_h) - C_h^{\mathcal{I}}(q_h, \mathbf{e}_h^{\mathcal{S}}) &= \mathcal{A}_h^{\mathcal{D}}(e_h^{\mathcal{D}}, q_h) - C_h^{\mathcal{I}}(q_h, \mathbf{P}_h \mathbf{u}^{\mathcal{S}} - \mathbf{u}_h^{\mathcal{S}}) \\
&= \sum_{E \in \mathcal{E}_h^{\mathcal{D}}} (\mathbf{\Pi}_h \mathbf{u}^{\mathcal{D}} - \mathbf{Q}_h \mathbf{u}^{\mathcal{D}}, \nabla_w q_h)_E + \sum_{e \in \Gamma_h^{\mathcal{I}}} \langle (\mathbf{u}^{\mathcal{D}} - \mathbf{\Pi}_h \mathbf{u}^{\mathcal{D}}) \cdot \mathbf{n}^{\mathcal{D}}, q_h^{\partial} \rangle_e \\
&= \sum_{E \in \mathcal{E}_h^{\mathcal{D}}} (\mathbf{\Pi}_h \mathbf{u}^{\mathcal{D}} - \mathbf{Q}_h \mathbf{u}^{\mathcal{D}}, \nabla_w q_h)_E \\
&= \mathcal{G}^{\mathcal{D}}(\mathbf{u}^{\mathcal{D}}, q_h).
\end{aligned} \tag{4.35}$$

To handle the Stokes velocity error, we use the 1st equation in the finite element scheme (4.21). We remark that while the Stokes discretization is conforming, we proceed carefully due to the $C_h^{\mathcal{I}}$ term to obtain

$$\begin{aligned}
\mathcal{A}_h^{\mathcal{S}}(\mathbf{e}_h^{\mathcal{S}}, \mathbf{v}_h) &= \mathcal{A}_h^{\mathcal{S}}(\mathbf{P}_h \mathbf{u}^{\mathcal{S}}, \mathbf{v}_h) - \mathcal{A}_h^{\mathcal{S}}(\mathbf{u}_h^{\mathcal{S}}, \mathbf{v}_h) \\
&= \mathcal{A}_h^{\mathcal{S}}(\mathbf{P}_h \mathbf{u}^{\mathcal{S}}, \mathbf{v}_h) - \mathcal{F}_h^{\mathcal{S}}(\mathbf{v}_h) - \mathcal{B}_h^{\mathcal{S}}(p_h^{\mathcal{S}}, \mathbf{v}_h) + C_h^{\mathcal{I}}(p_h^{\mathcal{D}}, \mathbf{v}_h).
\end{aligned} \tag{4.36}$$

Similarly, we utilize Stokes 1st equation to rewrite the forcing term and obtain

$$\begin{aligned}
\mathcal{F}_h^{\mathcal{S}}(\mathbf{v}_h) &= \sum_{E \in \mathcal{E}_h^{\mathcal{S}}} (\mathbf{f}, \mathbf{v}_h)_E = \sum_{E \in \mathcal{E}_h^{\mathcal{S}}} (-\nabla \cdot \sigma, \mathbf{v}_h)_E \\
&= \sum_{E \in \mathcal{E}_h^{\mathcal{S}}} (\sigma, \nabla \mathbf{v}_h)_E - \langle \sigma \mathbf{n}, \mathbf{v}_h \rangle_{E^{\partial}} \\
&= \sum_{E \in \mathcal{E}_h^{\mathcal{S}}} 2\mu(\varepsilon(\mathbf{u}^{\mathcal{S}}), \varepsilon(\mathbf{v}_h))_E - (p^{\mathcal{S}}, \nabla \cdot \mathbf{v}_h)_E - \langle \sigma \mathbf{n}, \mathbf{v}_h \rangle_{E^{\partial}}.
\end{aligned} \tag{4.37}$$

All normal contributions of stress cancel across the interior edges, leaving only the interface edges, where $\sigma \mathbf{n}^{\mathcal{S}}$ is once again decomposed into normal and tangential components, yielding

$$\begin{aligned}
\mathcal{F}_h^{\mathcal{S}}(\mathbf{v}_h) &= \sum_{E \in \mathcal{E}_h^{\mathcal{S}}} 2\mu(\varepsilon(\mathbf{u}^{\mathcal{S}}), \varepsilon(\mathbf{v}_h))_E - (p^{\mathcal{S}}, \nabla \cdot \mathbf{v}_h)_E \\
&\quad + \sum_{e \in \mathcal{E}_h^{\mathcal{I}}} \langle \beta \mathbf{u}^{\mathcal{S}} \cdot \mathbf{t}^{\mathcal{S}}, \mathbf{v}_h \cdot \mathbf{t}^{\mathcal{S}} \rangle_e + \langle p^{\mathcal{D}}, \mathbf{v}_h \cdot \mathbf{n}^{\mathcal{S}} \rangle_e.
\end{aligned} \tag{4.38}$$

So we have

$$\begin{aligned}
\mathcal{F}_h^S(\mathbf{v}_h) &= \sum_{E \in \mathcal{E}_h^S} 2\mu(\varepsilon(\mathbf{u}^S), \varepsilon(\mathbf{v}_h))_E + \sum_{e \in \mathcal{E}_h^I} \langle \beta \mathbf{u}^S \cdot \mathbf{t}^S, \mathbf{v}_h \cdot \mathbf{t}^S \rangle_e \\
&\quad - \mathcal{B}_h^S(p^S, \mathbf{v}_h) + \mathcal{C}_h^I(p^D, \mathbf{v}_h).
\end{aligned} \tag{4.39}$$

Therefore,

$$\begin{aligned}
\mathcal{A}_h^S(\mathbf{e}_h^S, \mathbf{v}_h) &= \mathcal{A}_h^S(\mathbf{P}_h \mathbf{u}^S, \mathbf{v}_h) - \sum_{E \in \mathcal{E}_h^S} 2\mu(\varepsilon(\mathbf{u}^S), \varepsilon(\mathbf{v}_h))_E \\
&\quad - \sum_{e \in \mathcal{E}_h^I} \langle \beta \mathbf{u}^S \cdot \mathbf{t}^S, \mathbf{v}_h \cdot \mathbf{t}^S \rangle_e + \mathcal{B}_h^S(p^S - p_h^S, \mathbf{v}_h) - \mathcal{C}_h^I(p^D - p_h^D, \mathbf{v}_h) \\
&= \mathcal{A}_h^S(\mathbf{P}_h \mathbf{u}^S - \mathbf{u}^S, \mathbf{v}_h) + \mathcal{B}_h^S(p^S - \pi_h p^S + \pi_h p^S - p_h^S, \mathbf{v}_h) \\
&\quad - \mathcal{C}_h^I(p^D - Q_h p^D + Q_h p^D - p_h^D, \mathbf{v}_h) \\
&= \mathcal{A}_h^S(\mathbf{P}_h \mathbf{u}^S - \mathbf{u}^S, \mathbf{v}_h) + \mathcal{B}_h^S(e_h^S, \mathbf{v}_h) - \mathcal{C}_h^I(e_h^D, \mathbf{v}_h) \\
&\quad - \mathcal{B}_h^S(\pi_h p^S - p^S, \mathbf{v}_h) + \mathcal{C}_h^I(Q_h p^D - p^D, \mathbf{v}_h) \\
&= \mathcal{G}^S(\mathbf{u}^S, p^S, p^D, \mathbf{v}_h) + \mathcal{B}_h^S(e_h^S, \mathbf{v}_h) - \mathcal{C}_h^I(e_h^D, \mathbf{v}_h),
\end{aligned} \tag{4.40}$$

which yields the 1st error equation in (4.29).

4.5.4 Error Estimation

For the approximation capacity of the finite element spaces used for the scheme in this dissertation, one has the following results. For any quadrilateral element E , there holds

$$\begin{aligned}
\|\mathbf{u}^S - \mathbf{P}_h \mathbf{u}^S\|_k &\lesssim h^{2-k} \|\mathbf{u}^S\|_{\mathbf{H}^2(E)}, \quad k = 0, 1; \\
\|p^S - \pi_h p^S\|_0 &\lesssim h \|p^S\|_{H^1(E)}.
\end{aligned} \tag{4.41}$$

Additionally, we shall frequently use the following standard trace inequality for any scalar- or vector-valued H^1 -function

$$h_E \|\phi\|_e^2 \lesssim \|\phi\|_0^2 + h_E^2 \|\phi\|_1^2. \quad (4.42)$$

Based on these facts, we have

$$\|(\mathbf{u}^S - \mathbf{P}_h \mathbf{u}^S) \cdot \mathbf{t}\|_e \lesssim h_E^{\frac{3}{2}} \|\mathbf{u}^S\|_{\mathbf{H}^2(E)}. \quad (4.43)$$

We shall also use the following bounds for norms of a function $\mathbf{v} \in \mathbf{H}^1(\Omega^S)$:

$$\|\nabla \cdot \mathbf{v}\|_{L^2(\Omega^S)} \lesssim \|\varepsilon(\mathbf{v})\|_{\mathbf{L}^2(\Omega^S)} \leq \|\nabla \mathbf{v}\|_{\mathbf{L}^2(\Omega^S)} \leq \|\mathbf{v}\|_{\mathbf{H}^1(\Omega^S)}. \quad (4.44)$$

Theorem 4.1 (Energy norm error estimate). Let $(\mathbf{u}^S, p^S, p^D) \in \mathbf{H}^2(\Omega^S) \times H^1(\Omega^S) \times H^2(\Omega^D)$ be the full-regularity solutions to (1–5) under the assumptions from the beginning of this section. Let $(\mathbf{u}_h^S, p_h^S, p_h^D) \in \mathbf{V}_h^{S,0} \times W_h^S \times V_h^{D,0}$ be the numerical solutions of (4.21). Then

$$\begin{aligned} \|\|(\mathbf{e}_h^S, e_h^D)\|\|_h &\lesssim h (\|\mathbf{u}^S\|_{\mathbf{H}^2(\Omega^S)} + \|p^S\|_{H^1(\Omega^S)} + \|p^D\|_{H^2(\Omega^D)}), \\ \|e_h^S\| &\lesssim h (\|\mathbf{u}^S\|_{\mathbf{H}^2(\Omega^S)} + \|p^S\|_{H^1(\Omega^S)} + \|p^D\|_{H^2(\Omega^D)}). \end{aligned} \quad (4.45)$$

Proof. Taking $\mathbf{v}_h = \mathbf{e}_h^S$, $r_h = e_h^S$, and $q_h = e_h^D$ in the error equations (4.29) and summing them yields

$$\begin{aligned} \|\|(\mathbf{e}_h^S, e_h^D)\|\|_h^2 &= \|\|\mathbf{e}_h^S\|\|_h^2 + \|\|e_h^D\|\|_h^2 = \mathcal{A}_h^S(\mathbf{e}_h^S, \mathbf{e}_h^S) + \mathcal{A}_h^D(e_h^D, e_h^D) \\ &= \mathcal{G}^S(\mathbf{u}^S, p^S, p^D, \mathbf{e}_h^S) + \mathcal{G}^D(\mathbf{u}^D, e_h^D). \end{aligned} \quad (4.46)$$

Part (1) Handling $\mathcal{G}^S(\mathbf{u}^S, p^S, p^D, \mathbf{e}_h^S)$. Recall that

$$\mathcal{G}^S(\mathbf{u}^S, p^S, p^D, \mathbf{v}_h) = \mathcal{A}_h^S(\mathbf{P}_h \mathbf{u}^S - \mathbf{u}^S, \mathbf{v}_h) - \mathcal{B}_h^S(\pi_h p^S - p^S, \mathbf{v}_h) + \mathcal{C}_h^I(Q_h p^D - p^D, \mathbf{v}_h).$$

The three terms on the right-hand side of \mathcal{G}^S will be estimated individually.

(i) For $\mathcal{A}_h^S(\mathbf{P}_h \mathbf{u}^S - \mathbf{u}^S, \mathbf{v}_h)$, by applying triangle inequalities, Cauchy-Schwarz inequalities, trace inequalities, and the following fact that is derived from (4.44):

$$\|\varepsilon(\mathbf{P}_h \mathbf{u}^S - \mathbf{u}^S)\|_{\mathbf{L}^2(\Omega^S)} \lesssim \|\mathbf{P}_h \mathbf{u}^S - \mathbf{u}^S\|_{\mathbf{H}^1(\Omega^S)},$$

we obtain

$$\begin{aligned} & |\mathcal{A}_h^S(\mathbf{P}_h \mathbf{u}^S - \mathbf{u}^S, \mathbf{e}_h^S)| \\ &= \left| \sum_{E \in \mathcal{E}_h^S} 2\mu(\varepsilon(\mathbf{P}_h \mathbf{u}^S - \mathbf{u}^S), \varepsilon(\mathbf{e}_h^S))_E + \sum_{e \in \mathcal{E}_h^I} \langle \beta(\mathbf{P}_h \mathbf{u}^S - \mathbf{u}^S) \cdot \mathbf{t}^S, \mathbf{e}_h^S \cdot \mathbf{t}^S \rangle_e \right| \\ &\leq 2\mu \left(\sum_{E \in \mathcal{E}_h^S} \|\varepsilon(\mathbf{P}_h \mathbf{u}^S - \mathbf{u}^S)\|_E^2 \right)^{\frac{1}{2}} \left(\sum_{E \in \mathcal{E}_h^S} \|\varepsilon(\mathbf{e}_h^S)\|_E^2 \right)^{\frac{1}{2}} \\ &\quad + \left(\sum_{e \in \mathcal{E}_h^I} \|(\mathbf{P}_h \mathbf{u}^S - \mathbf{u}^S) \cdot \mathbf{t}^S\|_e^2 \right)^{\frac{1}{2}} \left(\sum_{e \in \mathcal{E}_h^I} \|\beta^{\frac{1}{2}} \mathbf{e}_h^S \cdot \mathbf{t}^S\|_e^2 \right)^{\frac{1}{2}} \\ &\lesssim h \|\mathbf{u}^S\|_{\mathbf{H}^2(\Omega^S)} \|\mathbf{e}_h^S\|_h + h^{\frac{3}{2}} \|\mathbf{u}^S\|_{\mathbf{H}^2(\Omega^S)} \|\mathbf{e}_h^S\|_h. \end{aligned} \tag{4.47}$$

For $\mathcal{B}_h^S(p^S - \pi_h p^S, \mathbf{e}_h^S)$, we apply similar techniques to obtain

$$\begin{aligned} & |\mathcal{B}_h^S(p^S - \pi_h p^S, \mathbf{e}_h^S)| = \left| \sum_{E \in \mathcal{E}_h^S} (p^S - \pi_h p^S, \nabla \cdot \mathbf{e}_h^S)_E \right| \\ &\leq \left(\sum_{E \in \mathcal{E}_h^S} \|p^S - \pi_h p^S\|_E^2 \right)^{\frac{1}{2}} \left(\sum_{E \in \mathcal{E}_h^S} \|\nabla \cdot \mathbf{e}_h^S\|_E^2 \right)^{\frac{1}{2}} \\ &\leq \|p^S - \pi_h p^S\|_{L^2(\Omega^S)} \|\nabla \cdot \mathbf{e}_h^S\|_{L^2(\Omega^S)} \\ &\lesssim h \|p^S\|_{H^1(\Omega^S)} \|\varepsilon(\mathbf{e}_h^S)\|_{L^2(\Omega^S)} \\ &\leq h \|p^S\|_{H^1(\Omega^S)} \|\mathbf{e}_h^S\|_h. \end{aligned} \tag{4.48}$$

Finally, for $C_h^I(p^D - Q_h p^D, \mathbf{e}_h^S)$, we estimate its interface terms by using the techniques for duality pairing in [64]. This yields

$$\begin{aligned}
|\mathcal{C}_h^{\mathcal{I}}(p^{\mathcal{D}} - Q_h p^{\mathcal{D}}, \mathbf{e}_h^S)| &= \left| \sum_{e \in \mathcal{E}_h^{\mathcal{I}}} \langle p^{\mathcal{D}} - Q_h p^{\mathcal{D}}, \mathbf{e}_h^S \cdot \mathbf{n} \rangle_e \right| \\
&\leq \|p^{\mathcal{D}} - Q_h p^{\mathcal{D}}\|_{H^{-\frac{1}{2}}(\Gamma_h^{\mathcal{I}})} \|\mathbf{e}_h^S \cdot \mathbf{n}\|_{H^{\frac{1}{2}}(\Gamma_h^{\mathcal{I}})} \\
&\leq h \|p^{\mathcal{D}}\|_{H^{\frac{1}{2}}(\Gamma^{\mathcal{I}})} \|\mathbf{e}_h^S\|_{\mathbf{H}^1(\Omega_h^S)} \\
&\leq h \|p^{\mathcal{D}}\|_{H^1(\Omega^{\mathcal{D}})} \|\mathbf{e}_h^S\|_h,
\end{aligned} \tag{4.49}$$

where the inequalities for \mathbf{e}_h^S are due to a trace inequality and then the Korn's inequality.

Part (2) Handling $\mathcal{G}^{\mathcal{D}}(\mathbf{u}^{\mathcal{D}}, e_h^{\mathcal{D}})$. Recall that

$$\mathcal{G}^{\mathcal{D}}(\mathbf{u}^{\mathcal{D}}, q_h) = \sum_{E \in \mathcal{E}_h^{\mathcal{D}}} (\mathbf{\Pi}_h \mathbf{u}^{\mathcal{D}} - \mathbf{Q}_h \mathbf{u}^{\mathcal{D}}, \nabla_w q_h)_E.$$

This involves two approximations to $\mathbf{u}^{\mathcal{D}}$. Each converges with first order. Based on the approximation capacity of $\mathbf{\Pi}_h, \mathbf{Q}_h$ (and triangle inequalities), we have, for each element E ,

$$\|\mathbf{\Pi}_h \mathbf{u}^{\mathcal{D}} - \mathbf{Q}_h \mathbf{u}^{\mathcal{D}}\|_E \leq \|\mathbf{\Pi}_h \mathbf{u}^{\mathcal{D}} - \mathbf{u}^{\mathcal{D}}\|_E + \|\mathbf{u}^{\mathcal{D}} - \mathbf{Q}_h \mathbf{u}^{\mathcal{D}}\|_E \lesssim h \|\mathbf{u}^{\mathcal{D}}\|_{\mathbf{H}^1(E)}.$$

Then by the Cauchy-Schwarz inequality, we have

$$\begin{aligned}
\mathcal{G}^{\mathcal{D}}(\mathbf{u}^{\mathcal{D}}, e_h^{\mathcal{D}}) &= \sum_{E \in \mathcal{E}_h^{\mathcal{D}}} (\mathbf{\Pi}_h \mathbf{u}^{\mathcal{D}} - \mathbf{Q}_h \mathbf{u}^{\mathcal{D}}, \nabla_w e_h^{\mathcal{D}})_E \\
&\leq \left(\sum_{E \in \mathcal{E}_h^{\mathcal{D}}} \|\mathbf{\Pi}_h \mathbf{u}^{\mathcal{D}} - \mathbf{Q}_h \mathbf{u}^{\mathcal{D}}\|_E^2 \right)^{\frac{1}{2}} \left(\sum_{E \in \mathcal{E}_h^{\mathcal{D}}} \|\nabla_w e_h^{\mathcal{D}}\|_E^2 \right)^{\frac{1}{2}} \\
&\lesssim h \|\mathbf{u}^{\mathcal{D}}\|_{\mathbf{H}^1(\Omega^{\mathcal{D}})} \frac{1}{\sqrt{\kappa}} \|\mathbf{e}_h^{\mathcal{D}}\|_h,
\end{aligned} \tag{4.50}$$

where in the last step we have used the fact $\|\mathbf{e}_h^{\mathcal{D}}\|_h^2 \geq \kappa \sum_{E \in \mathcal{E}_h^{\mathcal{D}}} \|\nabla_w e_h^{\mathcal{D}}\|_E^2$.

Combining these results, noting that $\|\mathbf{u}^{\mathcal{D}}\|_1 \lesssim \|p^{\mathcal{D}}\|_2$ and dividing both sides by $\|\mathbf{e}_h^S, e_h^{\mathcal{D}}\|_h$ yields the first inequality in (4.45).

Part (3) Handling $\|e_h^S\|$. First, we remark that solving the first error equation (4.29) for \mathcal{B}_h^S yields

$$|\mathcal{B}_h^S(e_h^S, \mathbf{v}_h)| = |\mathcal{A}_h^S(\mathbf{e}_h^S, \mathbf{v}_h) + \mathcal{C}_h^I(e_h^D, \mathbf{v}_h) - \mathcal{G}^S(\mathbf{u}^S, p^S, p^D, \mathbf{v}_h)|.$$

This holds true for each $\mathbf{v}_h \in \mathbf{V}_h^{S,0}$, so we may additionally restrict $\mathbf{v}|_{\Gamma^I} \equiv 0$, for which we denote by $\mathbf{v} \in \mathbf{V}_h^0 \subset \mathbf{V}_h^{S,0}$ to obtain

$$\begin{aligned} |\mathcal{B}_h^S(e_h^S, \mathbf{v}_h)| &= |\mathcal{A}_h^S(\mathbf{e}_h^S, \mathbf{v}_h) - \mathcal{G}^S(\mathbf{u}^S, p^S, p^D, \mathbf{v}_h)| \\ &\lesssim \|\|\mathbf{e}_h^S\|\|_h \|\|\mathbf{v}_h\|\|_h + h (\|\mathbf{u}^S\|_{\mathbf{H}^2(\Omega^S)} + \|p^S\|_{H^1(\Omega^S)} + \|p^D\|_{H^2(\Omega^D)}) \|\|\mathbf{v}_h\|\|_h \\ &\lesssim h (\|\mathbf{u}^S\|_{\mathbf{H}^2(\Omega^S)} + \|p^S\|_{H^1(\Omega^S)} + \|p^D\|_{H^2(\Omega^D)}) \|\|\mathbf{v}_h\|\|_h. \end{aligned} \quad (4.51)$$

The inf-sup condition for \mathcal{B}_h^S is well-known in the case of Stokes flow [61], and it applies to $\mathbf{v}_h \in \mathbf{V}_h^0$. Therefore, we have

$$\begin{aligned} \|e_h^S\|_{L^2(\Omega^S)} &\lesssim \sup_{\mathbf{v} \in \mathbf{V}_h^0} \frac{|\mathcal{B}_h^S(e_h^S, \mathbf{v}_h)|}{\|\|\mathbf{v}_h\|\|_h} \\ &\lesssim h (\|\mathbf{u}^S\|_{\mathbf{H}^2(\Omega^S)} + \|p^S\|_{H^1(\Omega^S)} + \|p^D\|_{H^2(\Omega^D)}), \end{aligned} \quad (4.52)$$

which concludes the proof.

Later on in numerical experiments, we shall also observe that

- L^2 -norm of Stokes velocity errors exhibits 2nd order convergence;
- L^2 -norm of Darcy pressure errors exhibits 1st order convergence.

4.6 Numerical Results

This section presents numerical experiments to demonstrate accuracy and efficiency of our new finite element solver for coupled Stokes-Darcy flow problems.

Example 4.1 (Known analytical solutions). First we consider an example that has a known analytical solution. The example is taken from [55]. Specifically, the domain for Stokes flow is

$\Omega^S = (0, \pi) \times (0, 1)$, the domain for Darcy flow is $\Omega^D = (0, \pi) \times (-1, 0)$, and the interface is $\Gamma^I = (0, \pi) \times \{y = 0\}$. Fluid viscosity is set as $\mu = 1$, the permeability matrix is $\mathbf{K} = \mathbf{I}$, and $\mathbf{f}^D = \mathbf{0}$.

For the Stokes part, the exact solutions for velocity and pressure are

$$\mathbf{u}^S(x, y) = \begin{bmatrix} \cos(x)v'(y) \\ \sin(x)v(y) \end{bmatrix}, \quad p^S(x, y) = \sin(x) \sin(y),$$

where $v(y) = \frac{1}{\pi^2} \sin^2(\pi y) - 2$. Clearly, $\nabla \cdot \mathbf{u}^S = 0$. For the Darcy part, one has

$$p^D(x, y) = \sin(x)(e^y - e^{-y}), \quad \mathbf{u}^D(x, y) = - \begin{bmatrix} \cos(x)(e^y - e^{-y}) \\ \sin(x)(e^y + e^{-y}) \end{bmatrix}.$$

We verify that the divergences satisfy

$$\nabla \cdot \mathbf{u}^D = 0, \quad \nabla \cdot \mathbf{u}^S = 0.$$

The strain and stress tensors for the Stokes domain are

$$\begin{aligned} \nabla \mathbf{u}^S &= \begin{bmatrix} -\sin(x)v'(y) & \cos(x)v''(y) \\ \cos(x)v(y) & \sin(x)v'(y) \end{bmatrix}, \\ \varepsilon(\mathbf{u}^S) &= \begin{bmatrix} -\sin(x)v'(y) & \frac{1}{2} \cos(x)(v(y) + v''(y)) \\ \frac{1}{2} \cos(x)(v(y) + v''(y)) & \sin(x)v'(y) \end{bmatrix}, \\ \sigma &= \begin{bmatrix} \sin(x)(-2\mu v'(y) - \sin(y)) & \mu \cos(x)(v(y) + v''(y)) \\ \mu \cos(x)(v(y) + v''(y)) & \sin(x)(2\mu v'(y) - \sin(y)) \end{bmatrix}. \end{aligned}$$

Therefore, the resulting source term and body force are

$$f^{\mathcal{D}} = \nabla \cdot \mathbf{u}^{\mathcal{D}} = 0,$$

$$\mathbf{f}^{\mathcal{S}} = \begin{bmatrix} (-2\mu v'(y) - \sin(y)) \cos(x) + \mu \cos(x)(v'(y) + v'''(y)) \\ (-\mu \sin(x)(v(y) + v''(y)) + (2\mu v''(y) - \cos(y)) \sin(x) \end{bmatrix},$$

where $v'(y) = \frac{1}{\pi} \sin(2\pi y)$, $v''(y) = 2 \cos(2\pi y)$, $v'''(y) = -4\pi \sin(2\pi y)$. To verify the interface conditions, conservation of mass along $\Gamma^{\mathcal{I}}$ requires

$$\mathbf{u}^{\mathcal{D}} \cdot \mathbf{n}^{\mathcal{D}} = -\mathbf{u}^{\mathcal{S}} \cdot \mathbf{n}^{\mathcal{S}}$$

$$- \begin{bmatrix} \cos(x)(e^y - e^{-y}) \\ \sin(x)(e^y + e^{-y}) \end{bmatrix} \cdot \mathbf{n}^{\mathcal{D}} = - \begin{bmatrix} \cos(x)v'(y) \\ \sin(x)v(y) \end{bmatrix} \cdot \mathbf{n}^{\mathcal{S}}$$

$$- \begin{bmatrix} 0 \\ 2 \sin(x) \end{bmatrix} \cdot \mathbf{n}^{\mathcal{D}} = - \begin{bmatrix} 0 \\ -2 \sin(x) \end{bmatrix} \cdot \mathbf{n}^{\mathcal{S}},$$

which is satisfied since $\mathbf{n}^{\mathcal{D}} = -\mathbf{n}^{\mathcal{S}}$ along $\Gamma^{\mathcal{I}}$. Along the interface, $\sigma = 0$, so the continuity of normal stress equation is satisfied because

$$\mathbf{n}^T \sigma \mathbf{n} = 0 = -p^{\mathcal{D}}.$$

The BJS condition behaves similarly. Because $\mathbf{u}^{\mathcal{S}}$ is perpendicular to the interface, the BJS condition yields

$$\mathbf{t}^T \sigma \mathbf{n}^{\mathcal{S}} = 0 = - \left(\frac{\alpha}{2\sqrt{\mathbf{K}}} \right) \mathbf{u}^{\mathcal{S}} \cdot \mathbf{t}^{\mathcal{S}}.$$

Example 4.1 is tested on a sequence of uniform rectangular meshes that have n partitions in each of x, y -directions. In this case, the local AC_0 space is the same as the classical $RT_{[0]}$ space. The numerical results in Table 4.1 demonstrate the proved first order convergence in the discrete error energy norm, in addition to the Stokes pressure error L^2 -norm. We remark that although it

Table 4.1: Example 4.1: Errors and convergence rates

n	$\ (\mathbf{e}_h^S, e_h^D)\ _h$	Rate	$\ \mathbf{u}^S - \mathbf{u}_h^S\ _{L^2}$	Rate	$\ p^S - p_h^S\ _{L^2}$	Rate	$\ p^D - p_h^D\ _{L^2}$	Rate
8	7.8459e-01	–	1.2081e-02	–	1.0693e-01	–	2.7925e-01	–
16	4.0554e-01	0.95	2.7332e-03	2.14	5.3511e-02	0.99	1.4022e-01	0.99
32	2.0445e-01	0.99	6.6254e-04	2.04	2.6757e-02	0.99	7.0187e-02	0.99
64	1.0244e-01	0.97	1.6429e-04	2.01	1.3378e-02	1.00	3.5103e-02	0.99
128	5.1250e-02	0.99	4.0987e-05	2.00	6.6892e-03	0.99	1.7553e-02	0.99

was not proved, for this numerical example, we observe second order convergence in the Stokes velocity error L^2 -norm and first order convergence in the Darcy pressure error L^2 -norm.

Example 4.2 (Lid-driven cavity + heterogeneous permeability). This example couples the well-known lid-driven cavity problem for Stokes flow and Darcy flow in a heterogeneous permeability field. Here the Stokes domain is $\Omega^S = (0, 2) \times (0, 1)$ whereas the Darcy domain is $\Omega^D = (0, 2) \times (-1, 0)$.

For the Stokes part, $\mu = 1$. There is no body force. Dirichlet boundary conditions are posed. Specifically, for the top-side ($y = 1$), one has $\mathbf{u}_D^S = [1, 0]^T$; for the left- and right-sides, a no-slip boundary condition ($\mathbf{u} = \mathbf{0}$) is posed.

For the Darcy part, a heterogeneous permeability $\mathbf{K} = \kappa \mathbf{I}$ is given. Specifically, Ω^D is divided uniformly into 10×5 blocks. Labeling from left to right and top to bottom, these six blocks have a very low permeability value $\kappa = 10^{-6}$: (2, 2), (2, 4), (2, 7), (2, 9), (3, 2), (3, 5). For the remaining blocks, $\kappa = 1$ instead. There is no source, and $\mathbf{f}^D = \mathbf{0}$. A no-flow boundary condition ($\mathbf{u}^D \cdot \mathbf{n} = 0$) is posed on the left-, right-, and bottom- sides of the domain.

There is no known analytical solution for comparison, but our new finite element scheme can capture the main physics features. Shown in Figure 4.4 are the velocity and pressure profiles obtained on a uniform rectangular mesh with $h = 1/20$. Here are some qualitative observations.

- (i) Smooth flow exchange between the free flow (Stokes) and the porous-medium flow (Darcy) across the known interface ($y = 0$): for $x > 1$, flow travels from the Stokes domain to the Darcy domain; for $x < 1$, flow travels from the Darcy domain to the Stokes domain;
- (ii) Pressure singularity at the two corners (0, 1), (2, 1) for Stokes flow;

(iii) Detours of flow path around the six low permeability blocks for Darcy flow.

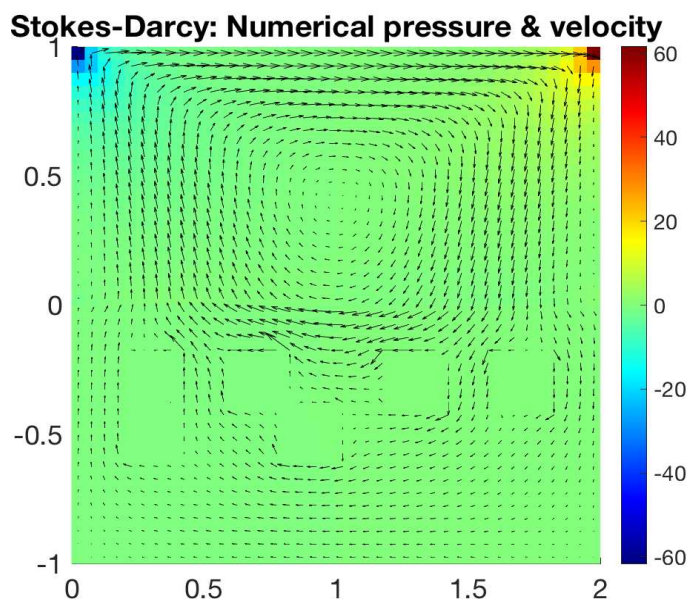


Figure 4.4: Example 4.2: Numerical velocity and pressure obtained from using $CG(BR_1, Q_0) + WG(P_0, P_0; AC_0)$ on a rectangular mesh with $h = 1/20$. (Velocity is plotted at element centers and the magnitude is doubled for better visual effect.)

4.7 Summary

There are several noteworthy takeaways from this method. This method

- uses a primal formulation for Darcy flow with a mixed formulation for Stokes flow,
- satisfies an inf-sup condition for the energy norm in Equation (4.24),
- satisfies continuity of mass and bulk flux in the Darcy domain,
- has first-order convergence of \mathbf{u}^S and p^D in the energy norm,
- has first-order convergence of p^S in the L^2 norm,
- uses 5 degrees of freedom per element in the Darcy domain and 13 degrees of freedom per element in the Stokes domain.

We also observe second-order convergence for Stokes velocity in the L^2 norm, although it was not proven.

Chapter 5

Conclusion

We have presented rigorous analysis and numerical results for two FEMs based on WG discretizations. Each of the presented methods satisfies physically meaningful properties while maintaining a relatively cheap computational cost.

5.1 Locking-Free WGFEMs for Linear Elasticity

This method presented in Chapter 3 is a locking-free stabilizer-free approach to solving linear elasticity in the displacement formulation on quadrilateral and hexahedral meshes. It uses piecewise constants on element interiors and the mesh skeleton, and it additionally avoids direct discretization of other variables such as stress, therefore requiring very few variables in the global linear system compared to other methods. This method uses the Schur complement to remove the element interior degrees of freedom from the global system, reducing the number of variables even further.

Building off the general analysis performed in Chapter 2, locking-free first-order convergence in the L^2 norm of displacement is proven for this method, and a comparison with another WGFEM for linear elasticity is provided. Many numerical examples are provided to verify the robustness of the solver in two and three dimensions. A low regularity example is tested as an attempt to stress the method, and the computational advantage from the Schur complement reduction is verified in another example.

Computational details are provided throughout the chapter and the software implementation is publicly available in the `DarcyLite` and `Darcy+` software packages.

5.2 Efficient Quadrilateral Solver for Stokes-Darcy Coupling

This method presented in Chapter 4 is an extensible stabilizer-free multinumerics approach to a coupled interface problem on quadrilateral meshes. It combines the classical Bernardi-Raugel

pair (BR_1, Q_0) for Stokes flow on quadrilaterals with the $WG(Q_0, Q_0; AC_0)$ element for to yield a computationally cheap discretization that satisfies the satisfies the inf-sup condition on the Stokes domain and mass conservation and bulk flux continuity on the Darcy domain.

First-order convergence in the energy norm for Stokes velocity and Darcy pressure is proven, and first-order convergence in the L^2 norm of Stokes pressure is proven. Some numerical examples are tested to verify the method behaves as expected, and first-order convergence in the L^2 norm is also observed for the Stokes velocity and Darcy pressure variables.

This software implementation is publicly available in the `DarcyLite` software package.

5.3 Extensions and Future Work

We expect the work in Chapter 3 extends to $WG(Q_k^d, Q_k^d; RT_{[k]}^d, Q_k)$ ($d = 2$ or 3) methods ($k \geq 1$) for linear elasticity on asymptotically parallelogram quadrilateral meshes or asymptotically parallelepiped hexahedral meshes. This extension would involve more technical analysis, but it would still contain many of the same ideas. One of the things that changes the analysis is that Lemma 2.2 no longer holds. Instead, there is an additional term that appears and requires the classical gradient, which then causes these additional terms to proliferate in the analysis, but otherwise the analysis is similar.

In Chapter 4 we prove analysis for the case of homogeneous Dirichlet boundary conditions on both domains with a constant permeability tensor for analysis purposes, but arguments to make these more general are technicalities. We expect this work generalizes to hexahedral meshes by instead taking W_{grad} as the Arbogast-Tao (AT_k) space. Higher order methods may be constructed by using the Taylor-Hood pair in the Stokes domain combined with higher polynomial order WG spaces in the Darcy domain. Another possible extension for this method involves using $WG(Q_k, Q_k; AC_k)$ discretizations for quadrilaterals on both domains since the AC_k offers divergence-free supplements. As with Chapter 3, the higher order extension of this work would suffer from a proliferation of additional terms since Lemma 2.2 has additional terms for higher order methods, but would otherwise remain similar.

While we presented one use of WGFEMs for a multiphysics problem coupled across an interface in Chapter 4, there are plenty more interesting multiphysics applications that are worth studying. We believe that the methodology for the analysis of Stokes-Darcy coupling extends to a larger class of domain decomposition methods and different physics for WGFEMs. Multiscale FEMs may be viewed as domain decomposition methods as well, and thus similar extensions may apply.

There are plenty of opportunities for implementation of WGFEMs in parallel programming models like Message Passing Interface (MPI), Open Multi-Processing (OpenMP), and Compute Unified Device Architecture (CUDA). This may be done in dedicated WGFEMs software like `DarcyLite` and `Darcy+` or in larger more general packages like `deal.II`. While the current implementation in `deal.II` does not showcase these models, `deal.II` contains many inherent capabilities for handling these computations and is therefore another good choice for future work.

Bibliography

- [1] D.N. Arnold, D. Boffi, and R.S. Falk. Approximation by quadrilateral finite elements. *Math. Comput.*, 71:909–922, 2002.
- [2] Lawrence Livermore National Laboratory. *VisIt User’s Manual*, 1.5 edition, October 2005.
- [3] Junping Wang and Xiu Ye. A weak Galerkin finite element method for second-order elliptic problems. *Journal of Computational and Applied Mathematics*, 241:103–115, 2013.
- [4] Guang Lin, Jianguo Liu, Lin Mu, and Xiu Ye. Weak Galerkin finite element methods for Darcy flow: Anisotropy and heterogeneity. *Journal of Computational Physics*, 276:422–437, 2014.
- [5] Junping Wang and Xiu Ye. A weak Galerkin finite element method for the Stokes equations. *Advances in Computational Mathematics*, 42(1):155–174, 2016.
- [6] Qilong Zhai, Ran Zhang, and Lin Mu. A new weak Galerkin finite element scheme for the brinkman model. *Communications in Computational Physics*, 19(5):1409–1434, 2016.
- [7] Ming Sun and Hongxing Rui. A coupling of weak Galerkin and mixed finite element methods for poroelasticity. *Computers & Mathematics with Applications*, 73(5):804–823, 2017.
- [8] Yanli Chen and Tie Zhang. A weak Galerkin finite element method for Burgers’ equation. *Journal of Computational and Applied Mathematics*, 348:103–119, 2019.
- [9] Junping Wang, Qilong Zhai, Ran Zhang, and Shangyou Zhang. A weak Galerkin finite element scheme for the Cahn-Hilliard equation. *Mathematics of Computation*, 88(315):211–235, 2019.
- [10] Graham Harper, Jianguo Liu, Simon Tavener, and Bin Zheng. Lowest-order weak Galerkin finite element methods for linear elasticity on rectangular and brick meshes. *Journal of Scientific Computing*, 78(3):1917–1941, 2019.

- [11] Chunmei Wang, Junping Wang, Ruishu Wang, and Ran Zhang. A locking-free weak Galerkin finite element method for elasticity problems in the primal formulation. *Journal of Computational and Applied Mathematics*, 307:346–366, 2016.
- [12] Lin Mu, Junping Wang, Yanqiu Wang, and Xiu Ye. A weak Galerkin mixed finite element method for biharmonic equations. In *Numerical Solution of Partial Differential Equations: Theory, Algorithms, and Their Applications*, pages 247–277. Springer, 2013.
- [13] Lin Mu, Junping Wang, and Xiu Ye. Weak Galerkin finite element methods for the biharmonic equation on polytopal meshes. *Numerical Methods for Partial Differential Equations*, 30(3):1003–1029, 2014.
- [14] Ran Zhang and Qilong Zhai. A weak Galerkin finite element scheme for the biharmonic equations by using polynomials of reduced order. *Journal of Scientific Computing*, 64(2):559–585, 2015.
- [15] Chunmei Wang and Junping Wang. A primal-dual weak Galerkin finite element method for Fokker-Planck type equations. *arXiv preprint arXiv:1704.05606*, 2017.
- [16] Lin Mu, Junping Wang, Xiu Ye, and Shangyou Zhang. A weak Galerkin finite element method for the maxwell equations. *Journal of Scientific Computing*, 65(1):363–386, 2015.
- [17] Lin Mu, Junping Wang, Guowei Wei, Xiu Ye, and Shan Zhao. Weak Galerkin methods for second order elliptic interface problems. *Journal of computational physics*, 250:106–125, 2013.
- [18] Ran Zhang, Haiming Song, and Nana Luan. Weak Galerkin finite element method for valuation of American options. *Frontiers of Mathematics in China*, 9(2):455–476, 2014.
- [19] Lin Mu, Junping Wang, Yanqiu Wang, and Xiu Ye. A computational study of the weak Galerkin method for second-order elliptic equations. *Numerical Algorithms*, 63(4):753–777, 2013.

- [20] Chunmei Wang, Junping Wang, Ruishu Wang, and Ran Zhang. A locking-free weak Galerkin finite element method for elasticity problems in the primal formulation. *J. Comput. Appl. Math.*, 307:346–366, 2016.
- [21] Jianguo Liu, Graham Harper, Nolisa Malluwawadu, and Simon Tavener. A lowest-order weak Galerkin finite element method for Stokes flow on polygonal meshes. *Journal of Computational and Applied Mathematics*, 368:112479, 2020.
- [22] Jianguo Liu, Simon Tavener, and Zhuoran Wang. Lowest-order weak Galerkin finite element method for Darcy flow on convex polygonal meshes. *SIAM J. Sci. Comput.*, 40:B1229–B1252, 2018.
- [23] Jianguo Liu, Simon Tavener, and Zhuoran Wang. The lowest order weak Galerkin finite element methods for the Darcy equation on quadrilateral and hybrid meshes. *J. Comput. Phys.*, 359:312–330, 2018.
- [24] Graham Harper, Jianguo Liu, Simon Tavener, and Zhuoran Wang. A two-field finite element solver for poroelasticity on quadrilateral meshes. In *International Conference on Computational Science*, pages 76–88. Springer, 2018.
- [25] Yujie Liu and Junping Wang. A simplified weak Galerkin finite element method: Algorithm and error estimates. *arXiv preprint arXiv:1808.08667*, 2018.
- [26] Ivo Babuška. The finite element method with lagrangian multipliers. *Numerische Mathematik*, 20(3):179–192, 1973.
- [27] Franco Brezzi. On the existence, uniqueness and approximation of saddle-point problems arising from lagrangian multipliers. *Publications mathématiques et informatique de Rennes*, (S4):1–26, 1974.
- [28] F. Brezzi and M. Fortin. *Mixed and hybrid finite element methods*. Springer-Verlag, 1991.

- [29] Christine Bernardi and Ajmia Y. Orfi. A posteriori error analysis of the fully discretized time-dependent coupled Darcy and Stokes equations. *Comput. Math. Appl.*, 76:340–360, 2018.
- [30] Wenbin Chen, Max Gunzburger, Dong Sun, and Xiaoming Wang. An efficient and long-time accurate third-order algorithm for the Stokes–Darcy system. *Numer. Math.*, 134:857–879, 2016.
- [31] Marco Discacciati, Edie Miglio, and Alfio Quarteroni. Mathematical and numerical models for coupling surface and groundwater flows. *Applied Numerical Mathematics*, 43(1-2):57–74, 2002.
- [32] Marco Discacciati and Alfio Quarteroni. Navier-Stokes/Darcy coupling: modeling, analysis, and numerical approximation. *Rev. Mat. Complut.*, 22:315–426, 2009.
- [33] Max Gunzburger, Xiaoming He, and Buyang Li. On Stokes-Ritz projection and multistep backward differentiation schemes in decoupling the Stokes-Darcy model. *SIAM J. Numer. Anal.*, 56:397–427, 2018.
- [34] Oleg Iliev and Vsevolod Laptev. On numerical simulation of flow through oil filters. *Computing and Visualization in Science*, 6(2-3):139–146, 2004.
- [35] Gordon S Beavers and Daniel D Joseph. Boundary conditions at a naturally permeable wall. *Journal of fluid mechanics*, 30(1):197–207, 1967.
- [36] Philip Geoffrey Saffman. On the boundary condition at the surface of a porous medium. *Studies in applied mathematics*, 50(2):93–101, 1971.
- [37] E. Burman and P. Hansbo. A unified stabilized method for Stokes and Darcy’s equations. *J. Comput. Appl. Math.*, 198:35–51, 2007.
- [38] Gabriel N Gatica and Filánder A Sequeira. Analysis of the HDG method for the Stokes–Darcy coupling. *Numerical Methods for Partial Differential Equations*, 33(3):885–917, 2017.

- [39] Guido Kanschat and Beatrice Rivière. A strongly conservative finite element method for the coupling of Stokes and Darcy flow. *J. Comput. Phys.*, 229:5933–5943, 2010.
- [40] Rui Li, Jian Li, Xiaoming He, and Zhangxin Chen. A stabilized finite volume element method for a coupled Stokes-Darcy problem. *Appl. Numer. Math.*, 133:2–24, 2018.
- [41] Beatrice Rivière and Ivan Yotov. Locally conservative coupling of Stokes and Darcy flows. *SIAM J. Numer. Anal.*, 42:1959–1977, 2005.
- [42] Hongxin Rui and R. Zhang. A unified stabilized mixed finite element method for coupling Stokes and Darcy flows. *Comput. Meth. Appl. Mech. Engrg.*, 198:2692–2699, 2009.
- [43] Tong Pin and THH Pian. The convergence of finite element method in solving linear elastic problems. *International Journal of Solids and Structures*, 3(5):865–879, 1967.
- [44] Leone Corradi Dell’Acqua and Giulio Maier. A matrix theory of elastic-locking structures. *Meccanica*, 4(4):298–313, 1969.
- [45] Son-Young Yi. Nonconforming mixed finite element methods for linear elasticity using rectangular elements in two and three dimensions. *Calcolo*, 42:115–133, 2005.
- [46] Son-Young Yi. A new nonconforming mixed finite element method for linear elasticity. *Math. Model. Meth. Appl. Sci.*, 16:979–999, 2006.
- [47] Jun Hu, Hongying Man, Jianye Wang, and Shangyou Zhang. The simplest nonconforming mixed finite element method for linear elasticity in the symmetric formulation on n-rectangular grids. *Comput Math. Appl.*, 71:1317–1336, 2016.
- [48] Shipeng Mao and Shaochun Chen. A quadrilateral nonconforming finite element for linear elasticity problem. *Adv. Comput. Math.*, 28:81–100, 2008.
- [49] Zhimin Zhang. Analysis of some quadrilateral nonconforming elements for incompressible elasticity. *SIAM J. Numer. Anal.*, 34:640–663, 1997.

- [50] Douglas Arnold, Gerard Awanou, and Weifeng Qiu. Mixed finite elements for elasticity on quadrilateral meshes. *Adv. Comput. Math.*, 41:553–572., 2015.
- [51] Yanping Chen, Xin Zhao, and Yunqing Huang. Mortar element method for the time dependent coupling of Stokes and Darcy flows. *J. Sci. Comput.*, 80:1310–1329, 2019.
- [52] Benjamin Ganis, Danail Vassilev, ChangQing Wang, and Ivan Yotov. A multiscale flux basis for mortar mixed discretizations of Stokes–Darcy flows. *Comput. Meth. Appl. Mech. Engrg.*, 313:259–278, 2017.
- [53] Vivette Girault, Danail Vassilev, and Ivan Yotov. Mortar multiscale finite element methods for Stokes-Darcy flows. *Numer. Math.*, 127:93–165, 2014.
- [54] Rui Li, Yali Gao, Jian Li, and Zhangxin Chen. A weak Galerkin finite element method for a coupled Stokes-Darcy problem on general meshes. *J. Comput. Appl. Math.*, 334:111–127, 2018.
- [55] Wenbin Chen, Fang Wang, and Yanqiu Wang. Weak Galerkin method for the coupled Darcy-Stokes flow. *IMA J. Numer. Anal.*, 36:897–921, 2016.
- [56] Marco Discacciati and Ricardo Oyarzúa. A conforming mixed finite element method for the Navier–Stokes/Darcy coupled problem. *Numer. Math.*, 135:571–606, 2017.
- [57] Gabriel N. Gatica, S. Meddahi, and R. Oyarzua. A conforming mixed finite element method for the coupling of fluid flow with porous media flow. *IMA J. Numer. Anal.*, 29:86–108, 2009.
- [58] Gang Wang, Feng Wang, Long Chen, and Yinnian He. A divergence free weak virtual element method for the Stokes-Darcy problem on general meshes. *Comput. Meth. Appl. Mech. Engrg.*, 344:998–1020, 2019.
- [59] Alfonso Caiazzo, Volker John, and Ulrich Wilbrandt. On classical iterative subdomain methods for the Stokes-Darcy problem. *Comput. Geosci.*, 18:711–728, 2014.

- [60] Guosheng Fu and Christoph Lehrenfeld. A strongly conservative hybrid DG/mixed FEM for the coupling of Stokes and Darcy flow. *J. Sci. Comput.*, 77:1605–1620, 2018.
- [61] Christine Bernardi and Geneviève Raugel. Analysis of some finite elements for the Stokes problem. *Math. Comput.*, 44:71–79, 1985.
- [62] Jiangguo Liu, Simon Tavener, and Zhuoran Wang. Penalty-free any-order weak Galerkin FEMs for elliptic problems on quadrilateral meshes. *J. Sci. Comput.*, page Revision submitted, 2020.
- [63] Todd Arbogast and Maicon Correa. Two families of mixed finite elements on quadrilaterals of minimal dimension. *SIAM J. Numer. Anal.*, 54:3332–3356, 2016.
- [64] Todd Arbogast, Gergina Pencheva, Mary F. Wheeler, and Ivan Yotov. A multiscale mortar mixed finite element method. *Multiscale Modeling & Simulation*, 6(1):319–346, 2007.
- [65] Susanne Brenner and Ridgway Scott. *The mathematical theory of finite element methods*, volume 15. Springer Science & Business Media, 2007.
- [66] Charles R Johnson and Roger A Horn. *Matrix analysis*. Cambridge University Press Cambridge, 1985.
- [67] Junping Wang and Xiu Ye. A weak Galerkin finite element method for second order elliptic problems. *J. Comput. Appl. Math.*, 241:103–115, 2013.
- [68] Jiangguo Liu and R.Cali. A note on the approximation properties of the locally divergence-free finite elements. *Int. J. Numer. Anal. Model.*, 5:693–703, 2008.
- [69] P Raviart and J Thomas. A mixed finite element method for 2-nd order elliptic problems. *Mathematical aspects of finite element methods*, pages 292–315, 1977.
- [70] D.N.Arnold, D.Boffi, and R.S.Falk. Quadratic $H(\text{div})$ finite elements. *SIAM J. Numer. Anal.*, 42:2429–2451, 2005.

- [71] Jiangguo Liu, Farrah Sadre-Marandi, and Zhuoran Wang. Darcylite: A Matlab toolbox for Darcy flow computation. *Procedia Computer Science*, 80:1301–1312, 2016.
- [72] D. Arndt, W. Bangerth, T. C. Clevenger, D. Davydov, M. Fehling, D. Garcia-Sanchez, G. Harper, T. Heister, L. Heltai, M. Kronbichler, R. M. Kynch, M. Maier, J.-P. Pelteret, B. Turcksin, and D. Wells. The deal.II library, version 9.1. *Journal of Numerical Mathematics*, 2019. accepted.
- [73] Knut-Andreas Lie. *An introduction to reservoir simulation using MATLAB/GNU Octave: User guide for the MATLAB Reservoir Simulation Toolbox (MRST)*. Cambridge University Press, 2019.
- [74] Zhuoran Wang, Graham Harper, Patrick O’Leary, Jiangguo Liu, and Simon Tavener. deal.ii implementation of a weak Galerkin finite element solver for Darcy flow. In *International Conference on Computational Science*, pages 495–509. Springer, 2019.
- [75] Junping Wang and Xiu Ye. A weak Galerkin mixed finite element method for second order elliptic problems. *Mathematics of Computation*, 83(289):2101–2126, 2014.
- [76] Ivo Babuska and Barna Szabo. On the rates of convergence of the finite element method. *International Journal for Numerical Methods in Engineering*, 18(3):323–341, 1982.
- [77] Susanne Brenner and Li-Yeng Sung. Linear finite element methods for planar linear elasticity. *Math. Comput.*, 59:321–338, 1992.
- [78] F. Brezzi and M. Fortin. *Mixed and hybrid finite element methods*. Springer-Verlag, 1991.
- [79] C. Carstensen and M. Schedensack. Medius analysis and comparison results for first-order finite element methods in linear elasticity. *IMA J. Numer. Anal.*, 35:1591–1621, 2015.
- [80] J. Albery, C. Carstensen, S.A. Funken, and R. Klose. Matlab implementation of the finite element method in elasticity. *Computing*, 69:239–263, 2002.

- [81] Hengguang Li and Victor Nistor. LNG FEM: Graded meshes on domains of polygonal structures. *Contemp. Math.*, 586:239–246, 2013.
- [82] Mary Wheeler, Guangri Xue, and Ivan Yotov. A multipoint flux mixed finite element method on distorted quadrilaterals and hexahedra. *Numer. Math.*, 121:165–204, 2012.
- [83] D. Mijuca. On hexahedral finite element $hc8/27$ in elasticity. *Comput. Mech.*, 33:466–480, 2004.
- [84] Shangyou Zhang. On the nested refinement of quadrilateral and hexahedral finite elements and the affine approximation. *Numer. Math.*, 98:559–579, 2004.